An *in vitro* and *in vivo* Assessment of the Effects of Alpha-MSH on Skeletal Muscle Glucose Uptake in Healthy Human Volunteers

The thesis is submitted to University College Dublin in fulfilment of the requirements for the degree of Doctor of Philosophy

Patrick Swan

BSc Food Science

Student number: 14522703

Diabetes Complications Research Centre, Conway Institute.

Principal Investigator: Dr. Neil Docherty

Co Supervisor: Professor Carel le Roux

Head of School: Professor Michael Keane

March 2022

Table of Contents

List of Figures

List of Tables

Abstract

Diabetes mellitus is the fastest growing chronic condition globally. In 2021 the International Diabetes Federation estimated that 1 in 10 (537 million) adults are living with diabetes, with diabetes-related healthcare expenditure increasing by 316% over the last 15 years. Postprandial hyperglycaemic excursions are a key target for most therapeutic strategies, due to glucotoxicity being a major risk factor for the development of diabetic complications. Progression of disease states in both T1DM and T2DM can result in the need for intensive insulin therapy to manage hyperglycaemia. This can result in an increased incidence of hypoglycaemic episodes and chronic weight gain. Consequently, there is a rationale and need for novel pharmacological approaches which may compliment the glucose-lowering response of insulin, thus providing an insulin-sparing effect and may hold promise as use for a future adjunct therapy. Our collaborator, Prof. Michael Cowley (Monash University, Melbourne) has published pre-clinical data demonstrating that through melanocortin receptor 5 agonism, pituitary derived alpha-melanocyte stimulatory hormone (α-MSH), improves post-prandial glucose tolerance by inducing glucose uptake into skeletal muscle via an insulin-independent pathway. This thesis aimed to take the first steps in translating these findings to human biology and assess whether targeting of this novel mechanism may hold therapeutic potential in the pharmacological management of glucose homeostasis.

In vitro studies

Healthy adult volunteers (n=6) were recruited to donate *vastus lateralis* muscle biopsies, which were processed to isolate myogenic satellite cells that were used to establish primary human myoblast cell lines. These cells lines were characterized and found to be free from fibroblast contamination, capable of differentiating into myotubes, and were insulin responsive. Additionally, an insulin-resistant myotube model was developed in which ectopic lipid accumulation was induced by chronic incubation with palmitic acid. The melanocortin receptor (MCR) profile of the six established cell lines was characterized. MCR1, MCR3, and MCR4 were found to be expressed at stable levels, whilst low levels of MCR5 was also found. Incubation of myotubes with α-MSH significantly increased glucose uptake over basal conditions, with a similar effect size

to insulin. In insulin resistant myotubes, the glucose uptake response to α-MSH was ablated. Incubation of α-MSH with insulin resulted in an additive effect on glucose uptake in myotubes. Specific agonism of MCR5 with the peptidomimetic PG-901 increased glucose uptake over control, suggesting that the effect may be in part MCR5 mediated. In commercially obtained primary human adipocytes, MCR1 and MCR3 were both expressed but α-MSH had no impact on glucose uptake.

In vivo studies

Fifteen healthy volunteers were recruited into a study investigating whether α-MSH infusion could improve post-prandial glucose tolerance during an oral glucose tolerance test (OGTT) and whole-body glucose uptake during a hyperinsulinaemic-euglycaemic clamp. Participants first underwent four OGTT visits, in which they were infused with placebo or one of three doses of α-MSH in a randomized, double-blind, crossover manner. The highest dose (1500 ng/kg/hr) of α-MSH reduced 0-120 minute glucose incremental area under the curve (iAUC) in concert with a concomitant reduction in plasma insulin AUC. Exploratory analysis revealed this effect was most pronounced during the hyperglycaemic peak of the OGTT (30-60 minutes). The same cohort of participants then underwent hyperinsulinaemic-euglycaemic clamp studies while being infused with either saline or 150 ng/kg/hr α-MSH in a randomized, double-blind, crossover manner. Glucose infusion rate was consistently increased in the presence of α-MSH. No adverse events were recorded during OGTT or clamp experiments.

These studies thus document for the first time in humans, that exogenous α-MSH acts directly on skeletal muscle to induce glucose uptake and can lead to improvements in glucose tolerance. Manifestation of this physiological effect in healthy humans appears to have a promising safety profile, with no hypoglycaemic episodes or other adverse events recorded. This thesis lays the groundwork for further investigation of the therapeutic potential of skeletal muscle melanocortin receptor activation in diabetes.

Statement of Original Authorship

I hereby certify that the submitted work is my own work, was completed while registered as a candidate for the degree of Doctor of Philosophy, and I have not obtained a degree elsewhere on the basis of the research presented in this submitted work

Patrick Swan

Awards, Publications, and Presentations

Awards:

EFSD Albert Renold Travel Fellowship Award (2019)

Publications:

Wilkinson M, Sinclair P, Dellatorre-Teixeira L, **Swan P**, Brennan E, Moran B, Wedekind D, Downey P, Sheahan K, Conroy E, Gallagher WM, Docherty N, Roux CL, Brennan DJ. The Molecular Effects of a High Fat Diet on Endometrial Tumour Biology. Life (Basel). 2020 Sep 10;10(9):188. doi: 10.3390/life10090188. PMID: 32927694; PMCID: PMC7554710.

Conference Presentations:

Alpha-melanocyte Stimulatory Hormone: A Novel Player in Post-prandial Glucose Disposal in Skeletal Muscle in Humans- 15th International Conference on Advanced Technologies and Treatments for Diabetes (Barcelona, April 2022)

Manuscripts in Preparation

Patrick Swan, Brett Johnson, Suhaniya Samarasinghe, Ludmilla Pessanha, Giuseppe de Vito, Michael A. Cowley, Carel W. le Roux, Alexander D. Miras, Neil G. Docherty. Alpha-Melanocyte Stimulatory Hormone Improves Post-Prandial Glucose Tolerance in Healthy Humans.

Acknowledgements

The first acknowledgement of course goes to my primary supervisor Dr. Neil Docherty. I could not have asked for a better supervisor and mentor at such an early stage in my research career. Without your ever-present patience and cool head, I would still to this day be taking pieces out of peoples legs in an effort to grow a few muscle cells. I will forever appreciate you taking a chance on me with such a complex project spanning several clinical and laboratory-based research environments. I would also like to thank my co-supervisor Prof. Carel le Roux. I was spoiled for choice with all the projects that you allowed me the opportunity to collaborate on. Your annual summer braai and Christmas party were a constant motivator to generate some data to casually present over some good wine and food! Prof. Michael Cowley and Carissa Greenough, it was a pleasure collaborating with you and your team over the course of the study. My thanks to the other members of my doctoral studies panel, Prof. Fionnuala McAuliffe and Dr. Fiona McGillicuddy. Thank you to Prof. Catherine Godson and the rest of the members of the DCRC for being such a welcoming, helpful, and intelligent network of likeminded scientists.

A massive thanks to the real heroes, my wing manager Dr. Tracy Mullen and her rival Éimear Ryan. I'll dispose of my radioactive waste one day. Many thanks to Emer Bonham, Mark Crowley, and the rest of the Conway directorate for making everything run so smoothly and of course the staff in stores; Luke, Nicola, and Annette. None of the experiments would have been possible without the Core facilities staff, specifically Eugene, Janet, Catherine, and Dimitri.

Alex Miras, Suhaniya Samarasinghe and Brett Johnson, the saviours of the clinical study, thank you! I will forever appreciate the effort you took in taking me under your wings and teaching me how to conduct clinical research. I'm happy I gained your trust enough to graduate from making tea to collecting blood samples. Of course, thank you to Mr. Remy Long for the constant motivation.

Lud and James, thanking you adequately here will look a bit ridiculous, so I'll save it for when I see you! This thesis wouldn't have been written without the huge motivation to celebrate with everyone I'm lucky enough to call my friends in Conway and those who has passed through the Metabolic Medicine Lab over the years, thank you!

Abbreviations

ACACA	Acetyl-CoA Carboxylase
ACTH	Adrenocorticotrophic Hormone
ADA	American Diabetes Association
AGRP	Agouti-related Peptide
AMK	AMPK-activated Protein Kinase
AMP	Adenosine Monophosphate
α-MSH	Alpha-melanocyte Stimulatory Hormone
AMPK	Adenosine Monophosphate Kinase
ANOVA	Analysis of Variance
ANS	Autonomic Nervous System
ASP	Agouti Signaling Protein
ATP	Adenosine Triphosphate
AUC	Area Under the Curve
BCA	Bradford Coomassie Assay
BMI	Body Mass Index
BSA	Bovine Serum Albumin
CPE	Carboxypeptidase E
CPM	Counts Per Minute
CREB	cAMP Response Element Binding
DAG	Diacylglycerol
DAPI	4’,6-diamidino-2-phenylindole
DCCT	Diabetes Complications and Control Trial
DEPC	Diethylpyrocarbonate
DHAP	Dihydroxyacetone Phosphate
DIO	Diet-induced Obesity
DM	Diabetes Mellitus
DMEM	Dulbecco’s Modified Eagles Medium
DMSO	Dimethylsulphoxide
DNL	De novo Lipogenesis
DPP4	Dipeptidyl-peptidase 4
EC_{50}	Dose producing 50% maximal response

ECG	Electrocardiogram
EDIC	Epidemiology of Diabetes and its Complications
ELISA	Enzyme-linked Immunoassay
EMA	European Medicines Agency
FFA	Free Fatty Acid
FOXO1	Forkhead Box O1
G3P	Glucose-3-phosphate
G6P	Glucose-6-phosphate
GAPDH	Glyceraldehyde-3-phosphate dehydrogenase
GHSR	Growth Hormone Secretagogue Receptor
GIP	Gastric Inhibitory Polypeptide
GIR	Glucose Infusion Rate
GLP	Glucagon Like Peptide
GMP	Good Manufacturing Practice
GPCR	G-Protein Coupled Receptor
GRPP	Glucagon-related Polypeptide
GS1	Glycogen Synthase 1
GS2	Glycogen Synthase 2
GTP	Guanine Triphosphate
GTT	Glucose Tolerance Test
HAAF	Hypoglycaemic-associated Autonomic Failure
HDL	High-density Lipoprotein
HPRA	Health Products Regulatory Authority
ICL	Imperial College London
IDDM	Insulin-dependent Diabetes Mellitus
INSR	Insulin Receptor
IRS	Insulin Receptor Substrate
ISPK	Insulin-stimulated Protein Kinase
LEPR	Leptin Receptor
LPH	Lipotropic Hormone
MCR	Melanocortin Receptor
MCR1	Melanocortin Receptor 1
MCR2	Melanocortin Receptor 2

MCR3	Melanocortin Receptor 3
MCR4	Melanocortin Receptor 4
MCR5	Melanocortin Receptor 5
MHC3	Myosin Heavy Chain 3
NADH	Nicotinamide Adenine Dinucleotide
NAFLD	Non-alcoholic Fatty Liver Disease
NHS	National Health Service
NIDDM	Non-Insulin Dependent Diabetes Mellitus
NPH	Neural Protamine Hagedorn
NPY	Neuropeptide Y
OAA	Oxaloacetate
OGTT	Oral Glucose Tolerance Test
PC1	Prohormone Convertase 1
PC2	Prohormone Convertase 2
PCR	Polymerase Chain Reaction
PDH	Pyruvate Dehydrogenase
PDPK1	PIP3-Dependant Kinase 1
PDPK2,	PIP3-Dependant Kinase 2
PEP	Phosphoenolpyruvate
PEPCK	Phosphoenolpyruvate Carboxykinase
PFK	Phosphofructokinase
PI3K	Phosphoinositide 3-kinase
PIP3	Phosphatidylinositol 3,4,5-triphosphate
PKA	Protein Kinase A
PKB	Protein Kinase B
PKC	Protein Kinase C
POMC	Proopiomelanocortin
REC	Research Ethics Committee
RNA	Ribonucleic Acid
RPM	Rotations Per Minute
SEM	Standard Error of the Mean
SGLT2	Sodium-glucose Transport Protein 2
SLC2A	Solute Carrier Family 2A

SLC2A2	Solute Carrier Family 2A Isoform 2
STAT3	Signal Transducer and Activator of Transcription 3
SUR1	Sulfonylurea Receptor-1
T1DM	Type 1 Diabetes Mellitus
T2DM	Type 2 Diabetes Mellitus
TAG	Triacylglycerol
TBC1D1	TBC1 Domain Family Member 1
TBC1D4	TBC1 Domain Family Member 4
TCA	Tricarboxylic Acid
UKPDS	UK Prospective Diabetes Study
VDCC	Voltage-dependent Calcium Channels

Chapter One

Introduction

1 Introduction

1.1 Glucose Homeostasis

Glucose, alongside protein and fat, represent the primary metabolic fuel sources in living organisms. Under normal physiologic conditions, glucose serves as the obligate energy source for the brain (1). In adults, the brain can account for 25% of basal energy expenditure and 50% of whole body glucose utilization (2). In periods of extended fasting when endogenous glucose sources are depleted, brain function can be supported through the metabolism of ketone bodies however, ketogenesis can be supressed during insulin-induced hypoglycaemia. Therefore, it is paramount that plasma glucose concentration is maintained within a strict range despite rapid changes in glucose flux between the fasted and fed state. This is achieved through the interplay of physiological processes that provide for “homeostasis” or balance between glucose release into the circulation with the energy needs of the body.

As a general background to the topic of glucose homeostasis, the following sections discuss the uptake, utilization, and storage of glucose in peripheral tissues. Glucose can enter the circulation via three routes: digestion and absorption of dietary carbohydrates, the breakdown of glycogen stores through glycogenolysis, and finally the synthesis of glucose from carbon precursors via gluconeogenesis. Following uptake from the circulation, the principal fates of glucose are storage as glycogen, notably in liver and skeletal muscle tissue, glycolytic metabolism, or metabolism to generate acetyl-CoA for oxidative phosphorylation or lipogenesis.

1.1.1 Uptake and utilization of glucose by peripheral tissue

The plasma membrane of a cell is impermeable to the hydrophilic glucose molecules in plasma. A family of proteins known as solute carriers 2A (SLC2A) with varying affinities for glucose are responsible for binding the monosaccharide and transporting it across the plasma membrane to be utilized by the cell. Fourteen types of these SLC2A proteins, also known as GLUT transporters, have been identified and their distribution in varying amounts across tissue types and the abundance of particular subtypes relate to the specific tissue’s role in metabolism (3) . The extent to which different GLUT transporter subtypes mediate peripheral glucose uptake depends on the metabolic state of the organism, i.e., the fasted or fed state. This section is focused

on the liver, adipose tissue, and skeletal muscle as the principal peripheral tissue types implicated in initial glucose uptake and clearance in in the periphery.

1.1.1.1 Liver

The liver is a significant player in glucose homeostasis, serving as an organ for the storage and synthesis of glucose. GLUT2 is the most abundant glucose transporter found in human hepatic tissue, and the main mediator of hepatic glucose storage. GLUT2 has a relatively high affinity and capacity for glucose (K_m ~17 mmol/L) compared to other SLC2A transporters and is bidirectional, meaning it well suited for rapid transport of glucose into the cell when plasma glucose levels are high, but also allows for easy movement of glucose out of the cell during gluconeogenesis and glycogenolysis, processes both outlined in subsequent sections (4–6). In the basal state, the liver is a net producer of glucose, but this rapidly changes once plasma glucose is elevated.

Whereas kinases such as hexokinase are responsible for phosphorylating glucose in other tissues such as skeletal muscle and adipose tissue , hepatic glucokinase has a higher catalytic capability and is better suited to deal with the higher throughput of glucose from the portal circulation (7,8). In the post-prandial state, when portal and systemic blood glucose is elevated, glucose freely flows into the hepatocyte via GLUT2, and is phosphorylated by glucokinase to yield glucose-6-phosphate (G6P). The abundance of G6P serves as a signal for the initiation of glycogen synthesis by allosterically activating glycogen synthase 2 (GS2) (7,9). This enzyme converts the phosphorylated glucose monosaccharide to a highly branched glycogen structure. GS2 is thus the enzyme responsible for hepatic glycogenesis, while in muscle this process is mediated by glycogen synthase 1 (7,10). Additionally, GS2 is covalently activated by dephosphorylation secondary to hepatic insulin receptor activation (11). As such, the combined effect of elevated plasma glucose and insulin during the post-prandial state contributes to rapid GS2 activation and glycogenesis.

Firstly G6P is converted to glucose-1-phosphate which is then used as a substrate by UDP-glucose pyrophosphorylase to catalyse the conversion of glucose-1-phosphase to the activated UDP-glucose (12). GS2 links UDP-glucose molecules together one at a time by glycosidic linkages to ultimately form glycogen structures which typically have a mass of 10^7 kDA, with the maximal amount of glycogen within the liver amounting to

110g/300 mM at capacity (13). In a healthy human, the mass of the liver is between 15-18 times less than the total mass of skeletal muscle but is responsible for over half of total body glycogen stores. Thus, the hepatic glycogen reserve can continue to be tapped for energy for between 24 and 48 hours of fasting and can be replenished within several hours after feeding.

Any phosphorylated glucose not committed to glycogenesis is metabolized by the liver through glycolysis, this amounts to approximately half of intestinally absorbed glucose from the diet. Pyruvate, a product of glycolysis may also be used as a substrate for indirect glycogen formation(7). The “reversibility” of the hepatic glycolytic pathway is discussed further is Section 1.1.6.

1.1.1.2 Adipose Tissue

Adipocytes constitute the majority of the whole-body energy store in humans, wherein energy is stored in the form of intracellular neutral triglycerides. While adipocytes also catabolize glucose to use as fuel, their primary use of glucose is as a metabolic substrate for the production of free fatty acids through *de novo* synthesis from the product of glycolysis acetyl-coenzyme A (acetyl-CoA)(14). Although GLUT1, an insulin-independent transporter, is responsible for basal glucose uptake in adipocytes it is the action of insulin induced translocation of GLUT4 to the adipocyte plasma membrane (the mechanism of which is described in Section 1.1.2.2) that initiates the cascade of events leading to *de novo* lipogenesis (DNL) (6).

Following GLUT4 mediated uptake, glucose is passed through the glycolytic pathway to yield the three carbon pyruvate, which is then converted to citrate and shuttled to the tricarboxylic acid (TCA) cycle to produce acetyl-CoA(14,15). During glycolysis, a portion of the glucose is converted to G3P which is the glycerol backbone onto which triglycerides are esterified. Acetyl-CoA is then carboxylated to malonyl-CoA by the enzyme acetyl-CoA carboxylase (ACACA) which is the rate limiting step of the fatty acid synthesis pathway. In addition to driving glucose into the cell to be used as a substrate, insulin also promotes the activation of ACACA (16,17). The 16 carbon fatty acid palmitate is the principal output of the fatty acid synthesis pathway in adipocytes, and may be utilized as a membrane components of the cell or esterified to a glycerol

backbone by the catalytic enzyme diacylglycerol acyltransferase and stored as lipid droplets (18).

1.1.1.3 Skeletal Muscle

In humans skeletal muscle is the largest organ by weight and responsible for approximately 80% of post-prandial glucose uptake and disposal(19–21). Skeletal muscle is the primary site of insulin mediated glucose disposal, with the fate of glucose in the fed state being nonoxidative metabolism through conversion to glycogen and subsequent storage (20). The glucose-binding SLC2A profile of human skeletal muscle is similar to that of adipocytes, with GLUT1 localized to the sarcolemma and the more abundant GLUT4 residing within intracellular vesicles in the basal state (22,23). Importantly, intracellular GLUT4 can be separated into two pools categorized by the stimuli that causes their translocation to the plasma membrane.

One pool of GLUT4 is translocated via an insulin mediated pathway and is described in detail in Section 1.1.2.2. Briefly, insulin binds to its receptor, catalysing the tyrosine phosphorylation of insulin receptor substrate isoforms, activating PI3K and Akt. Akt substrates in the unphosphorylated state act as an inhibitor to GLUT4 vesicle trafficking to the membrane. When Akt is activated and its substrates become phosphorylated, GLUT4 is free to localize to the plasma membrane thus facilitating glucose uptake.

An entirely separate pool of GLUT4 in skeletal muscle is available to translocate through the contraction (exercise) induced AMP-activated protein kinase (AMK) mediated pathway that does not rely on insulin-Akt signalling (24–26). During exercise, the α catalytic subunits of AMPK are phosphorylated by calmodulin-dependant protein kinase and liver kinase B1 (27–29). The activated AMPK can then directly phosphorylate its substrates TBC1D4 (also known as AS160) and TBC1D1 (22,27). In the phosphorylated state, these molecules facilitate GLUT4 vesicle translocation to the sarcolemma (3,30).

Once taken up by myofibers, the fate of glucose is to either be metabolized for ATP production or storage as glycogen. There are several metabolic pathways via which

glucose is handled, the first of which is glycogen synthesis. The capacity of skeletal muscle to convert glucose to glycogen is a primary determinant of an individual's sensitivity to insulin. Up to 90% of glucose infused during a hyperinsulinaemic-euglycaemic clamp, where the insulin response is maximal, is disposed of as glycogen in skeletal muscle in a healthy human(31). Whereas glycogen stored in the liver undergoes glycogenolysis to regulate whole body glucose homeostasis, skeletal muscle lacks the critical enzyme in this process (glucose-6-phosphatase) and thus uses glycogen as a short-term intracellular energy source. Muscle glycogen can anaerobically provide energy during low-oxygen conditions such as high-intensity exercise (32). As described in Section 1.1.1.1, GS2 is the glycogen synthase isoform responsible for glycogen synthesis in liver whereas in skeletal muscle it is glycogen synthase isoform 1 (GS1) (7,33). Skeletal muscle glycogen synthesis is initiated by insulin receptor activation which increases glycogen synthase activity and glucose uptake. Insulin mediated dephosphorylation (activation) of GS1 is augmented by allosteric activation by glucose-6-phosphate, an intracellular signal of glucose availability (33). With the glycogenic pathway primed by insulin and G6P glucose is stored as glycogen in a similar manner to previously described in hepatocytes. G6P is converted to glucose-1-phosphate (12). Muscle isoform GS1 links UDP-glucose molecules together in 1-4 glycosidic linkages to ultimately form glycogen structures in the cell. Although the glycogen concentration in the liver is greater, skeletal muscle actually accounts for the majority (80%) of whole body glycogen stores at a concentration of 80-150 mmol/kg/ww^{-1} (34).

As skeletal muscle myofibers are the product of cell fusion and differentiation and are hence post-mitotic, they do not have the biosynthetic needs of dividing cell types and hence their basal energy consumption is low and glycogen intracellular glucose flux is minimal (35). ATP is required to fuel skeletal muscle contraction. During exercise, the energy needs of the cell rapidly increase, and the readily available ATP stores liberated through the breakdown of phosphocreatine (PCr) and glycogen are only sufficient to support contraction in the short term (36,37). Therefore, other metabolic pathways must be employed to tap into available circulating glucose. As previously described, skeletal muscle contraction translocates an insulin-independent pool of GLUT4 to the plasma membrane promoting glucose uptake. Glucose may then be used as a substrate in two main catabolic pathways which vary in their contribution to ATP

synthesis, and partition glucose between them depending on the length and intensity of exercise.

During intense short-term exercise (<1 minute) once PCr stores are exhausted, rapid glycogenolysis occurs and the liberated glucose is metabolized to lactate through anaerobic glycolysis(38,39). In this pathway, glucose is first phosphorylated by hexokinase to glucose-6-phosphate to ensure the glucose molecule does not diffuse out of the cell. Glucose is then processed through five energy-consuming enzymatic steps to yield glyceraldehyde-3-phosphate, upon which the ATP generating phase of the pathway begins. Two three-carbon pyruvate molecules are products of these reactions resulting in a net yield of 2 ATP and 2 NADH molecules. In the anaerobic conditions of intense short-term exercise, pyruvate cannot be oxidated is then further metabolised to lactate. Lactate dehydrogenase converts pyruvate to lactate which can then be transported into the circulation by monocarboxylate transporters as part of the Cori cycling and resulting hepatic gluconeogenesis described in Section 1.1.4.2 (40,41). Although rapid, this method of ATP generation is not sufficient to meet the energy requirements of the muscle during prolonged exercise.

As the exercise stimulus in muscle increases in length, blood flow to the muscle increases resulting in an increase in oxygen availability which facilitates the mitochondrial oxidative phosphorylation of pyruvate. In these conditions, intramuscular glycogen still provide the majority of glucose substrate, but once exercise begins to extend into the long term (minutes to hours) the reliance on circulating blood glucose to serve as the substrate for oxidation increases.

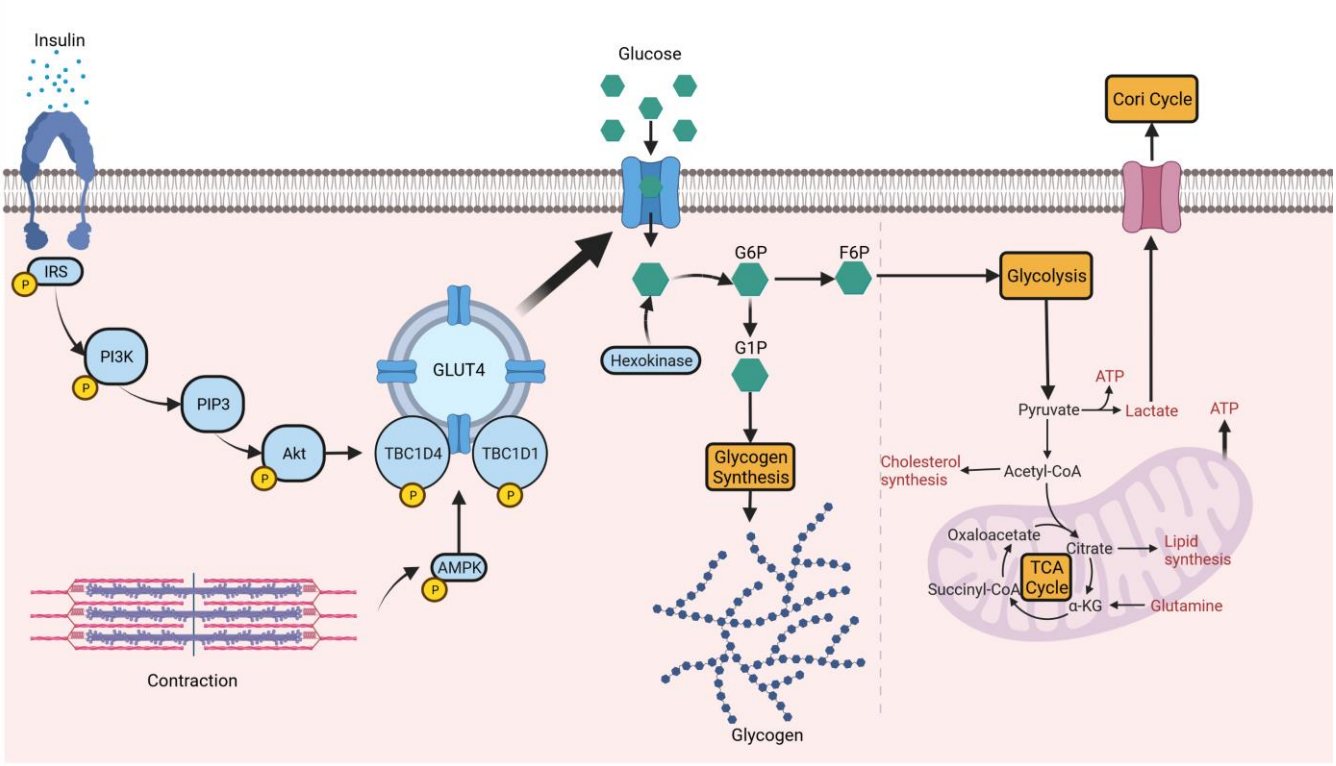

Figure 1.1 Overview of skeletal muscle glucose uptake and utilization

Insulin receptor agonism and contraction cause skeletal muscle GLUT4 translocation to the plasma membrane. Glucose diffuses into the cell and is phosphorylated by hexokinase and either processed to G1P for glycogen synthesis or F6P before undergoing glycolysis followed by either oxidative phosphorylation or anaerobic fermentation.

1.1.2 Normal Physiology of Insulin Release and Action

1.1.2.1 β-Cell Function and Insulin Secretion

The pancreas consists mainly of exocrine tissue interspersed with endocrine islets comprising approximately 3% of organ volume(42). These islets contain four principal cell types namely α, β, γ, and ε cells. The most abundant of these cells are the β cells representing approximately 60% of islet cell types by volume (42). Beta cells contain tightly packed granules of insulin sufficient for an approximately 2-week supply in healthy insulin-sensitive individuals (43). Although insulin also acts on essential pathways modulating lipid and protein metabolism, circulating levels of the hormone are most closely coupled to plasma glucose concentrations. The β-cell must rapidly and accurately respond to fluctuating plasma glucose concentrations, as well as

longer-term factors such as varying tissue sensitivity, to dynamically fine-tune the level of insulin release required to achieve euglycaemia.

Insulin hormone is a product of post-translational proteolytic cleavage of the preproinsulin polypeptide found within the cytoplasm of the β-cell(44). The cleavage of the N-terminal signal peptide from preproinsulin to yield proinsulin is primarily controlled by changing levels of plasma glucose (44,45), and is then further cleaved in the secretory granules of the cell to yield equimolar amounts of insulin hormone and C-peptide (45,46). After nutrient dependent depolarisation of the β-cell membrane, granules containing insulin and C-peptide are trafficked to the plasma membrane and released into circulation through calcium regulated exocytosis (45). This response is primarily associated with the facilitated transport of extracellular glucose into the cytoplasm through GLUT1, the most abundant glucose transporter found in the human β-cell (47), although it is suggested GLUT2 may also play a role in human insulin secretion (4). Once internalised, glucose is phosphorylated by glucokinase (hexokinase IV) before proceeding to the glycolysis pathway. As glucokinase is rate-determinant for the glycolytic pathway, it is thought of as the “glucose sensor” in the β-cell (47,48). The pyruvate yield from glycolysis enters the TCA pathway in the mitochondrion resulting in a net gain of ATP in the cell. The increase in cytosolic ATP resulting from glucose metabolism leads to the closure of K_{ATP} channels, depolarising the β-cell membrane. The depolarisation triggers an influx of Ca^{2+} from the extracellular space through voltage-dependant calcium channels (VDCCs). Calcium ions then bind to synaptotagmin 7, a binding protein co-localized with granules containing insulin, to induce exocytosis of the granules and release of insulin into the circulation(45,49,50). Calcium transient regulated exocytosis thus facilitates the rapid response of the β-cell to changing blood glucose(45).

Complementary to the downstream effects of glucose metabolism leading to insulin granule exocytosis, are pathways activated by pancreatic β-cell $G\alpha_s$-protein-coupled receptor agonism that augment insulin secretion by agonists known as incretins. These insulinotropic peptides, such as GLP-1 and GIP (51,52), bind to their respective $G\alpha_s$ receptors, activating adenylate cyclase and generating cyclic adenosine mono-phosphate (cAMP). An increase in cAMP mediates PKA-dependant mechanisms which increases signalling of proteins such as Epac2A and Piccolo that sensitize

calcium binding proteins and result in an increase in insulin granule exocytosis (53,54). As this mechanism relies on glucose metabolism to promote the flux of calcium ions into the cell, it is glucose-dependant and primarily having a physiologically relevant insulinotropic effect in the presence of elevated plasma glucose (52,55,56). The effect of incretins on insulin release is dose dependant, with a five-fold increase in an oral glucose load resulting in a two-fold increase of incretins such as GLP-1 and GIP (55–57). As the release of the GLP-1 and GIP (from enteroendocrine L-cells and K-cells respectively) are themselves dependant on nutrients passing through the digestive tract, this cascade of events is a powerful metabolic-amplifying pathway in β-cell physiology.

The kinetics of insulin release from β-cells in response to a glucose load is biphasic, with an initial 1st phase consisting of an acute burst of insulin release lasting several minutes from granules primed for exocytosis(58), followed by a sustained 2nd phase of insulin secretion that more closely tracks with changes in blood glucose (59). The magnitude of the 1st phase insulin secretory response is proportional to the elevations in plasma glucose, and typically represents 10% of the insulin required to be secreted to clear 75g of glucose during a standard oral glucose tolerance test (60). It is believed the purpose of this 1st phase is to suppress endogenous glucose production as well as prime peripheral tissue insulin receptors to take up glucose, thus blunting any prolonged hyperglycaemic excursions. The 2nd phase is a function of plasma glucose levels and the sensitivity of the β-cell to stimuli causing insulin release, and as such after the 1st phaser of release, insulin levels rise synchronous with glucose levels in a healthy insulin sensitive individual.

1.1.2.2 The Glucose Transporter Response to Insulin in Peripheral Tissue

Insulin secreted by the pancreas exhibits a wide range of anabolic effects in a multitude of peripheral tissues. The most relevant of which to this thesis is its role in maintaining blood glucose levels within a narrowly defined range by acting on the muscle and adipose tissue to promote glucose uptake and glycogen synthesis, and by inhibiting glycogenolysis and gluconeogenesis in the liver.

Insulin signal transduction begins with the ligand-receptor binding between the insulin peptide and the tyrosine kinase insulin receptor at the plasma membrane of the cell. Ligand binding initiates autophosphorylation of the intracellular β subunit region of the receptor, increasing the activity of the subunits and allowing for insulin receptor substrate docking (44,61,62). The next step following receptor autophosphorylation is rapid tyrosine phosphorylation of cytosolic proteins, the category of which is involved in the regulation of metabolism is the insulin receptor substrate (IRS) family of proteins. Insulin receptor isoforms IRS-1 and IRS-2 are most relevant to glucose homeostasis being expressed in muscle, fat, liver and pancreatic tissue (63), with IRS-3 not expressed in humans and IRS-4/5/6 having no demonstratable link to insulin action (64). This is the first of three critical steps in the insulin mediated pathway which ultimately leads to GLUT4 translocation to the plasma membrane and subsequent glucose uptake, the second of which is phosphatidylinositide-3 kinase (PI3K) activation.

Upon insulin-stimulated phosphorylation of IRS insulin receptor tyrosine kinase, IRS-1 and IRS-2 then proceed to bind the p85 subunit of PI3K, thus increasing the catalytic activity of the kinase. PI3K generates 3,4,5-triphosphate (PIP3) by phosphorylating glycolipids found on the intracellular plasma membrane, which then activate PIP3-dependant kinases. The PIP3-dependant kinases, PDPK1 and PDPK2, activate Akt isoforms which is the third critical node in insulin signal transduction. Activation of Akt, known also as protein kinase B (PKB) is caused by specific phosphorylation of its threonine (T308) and serine (S473) regions (65). In their unphosphorylated state, Akt substrates TBC1D4 and TBC1D1 (phosphorylation mediated by downstream AMPK activation) act as intracellular breaks on GLUT4 translocation to the plasma membrane by inhibiting actin filament exocytotic machinery (45,66). Once TBC1D4 is phosphorylated by the activated Akt, inhibition of GLUT vesicle trafficking is alleviated, allowing for exocytosis and fusion of GLUT transporters to the plasma membrane. GLUT 4, one of 14 species classified under solute carriers 2a (SLC2A), is the primary mediator of insulin induced glucose uptake in muscle and adipose tissue and is critical in post-prandial glucose homeostasis(3,22,66). Once docked at the plasma membrane, GLUT4 allows for rapid facilitated glucose transport from the blood to the intracellular space at a rate of up to 12 mmol min^{-1} at maximum hyperinsulinaemic and hyperglycaemic stimulation of muscle tissue (67). This rapid signal transduction from

insulin receptor tyrosine kinase to GLUT4 translocation facilitates an effective response to prevent excessive hyperglycaemic excursion in the post-prandial state.

1.1.2.3 Measurement of Insulin Release and Action

Quantitively measuring insulin release and action *in vivo* is an important goal in diabetes research. While an individual's sensitivity to insulin action can be inferred through surrogate indexes such HOMA-IR, and although useful in its simplicity, this may only be an accurate indicator of β-cell function and can be confounded by insulin resistance or signalling defects(68).

The oral glucose tolerance test (OGTT) is widely used clinically to diagnose glucose intolerance. A standard protocol consists of the patient ingesting 75g of liquid glucose following an overnight fast and serial blood samples taken over 2 hours. A diagnosis of diabetes can be made if blood glucose is elevated above 11 mmol/L after 120 minutes (69). Although the OGTT is a useful proxy for postprandial glucose and insulin dynamics other factors such as incretin effects and variability in gastric emptying hinder the techniques accuracy in assessing insulin sensitivity and β-cell response to glucose. (70,71).

Developed in the 1970's, the hyperglycaemic clamp involved a continuous intravenous infusion of glucose which exposes the β-cells to a square wave of hyperglycaemia by elevating and maintaining blood glucose (72). The main benefit of this technique is its ability to tease apart the biphasic response of insulin secretion by the pancreas. In the first 5-8 minutes, there is a sharp burst of insulin release followed by a progressive slow increase that lasts as long as hyperglycaemia is maintained. The value of this measurement lies predominantly in the measurement of the 1st phase response, as defects in this response are an accurate predictor of β-cell dysfunction and onset of diabetes (60,73,74).

As discussed throughout this thesis, the hyperinsulinaemic-euglycaemic clamp developed by Ralph A. DeFronzo is the most valuable quantitative tool in assessing whole body insulin sensitivity(72,75). Detailed further alongside it's use Chapter 4, the purpose of this method is to obtain an accurate and reproducible measurement of whole body insulin sensitivity (71,72). Briefly, hyperinsulinaemia is induced in subjects via a continuous and fixed intravenous insulin infusion. In this condition, endogenous

glucose production is supressed and euglycaemia is maintained by a variable intravenous glucose infusion. A quantitative measurement of whole body glucose uptake can then be imputed through the weight adjusted rate of glucose infusion needed to maintain euglycaemia. This allows the relationship between insulin secretion and sensitivity to be teased apart and is valuable in the pharmacodynamic assessment of interventions impacting glucose homeostasis. However, this method does have its limitations. Safely and successfully conducting this experiment is time consuming and requires highly trained personnel as blood samples need to be taken every 5 minutes and the variable glucose infusion rate adjusted manually in real time. Although computational algorithms have been developed to automatically adjust glucose infusion rates, they have not found widespread use (76,77). Nonetheless, the hyperinsulinaemic-euglycaemic clamp remains the method of choice in assessing changes in whole body insulin sensitivity where resources allow.

1.1.3 Glycogenolysis

At its resting glucose consumption rate of on average 8g per hour, the body would metabolise all circulating blood glucose within 30 minutes without the constant supply of endogenous glucose. Following an overnight fast, the breakdown of hepatic glycogen stores, termed glycogenolysis, is responsible for approximately 40% of endogenous glucose production (78). During glycogenolysis, glucose molecules are liberated one at a time from the branched glycogen structures and released into circulation to maintain glucose homeostasis. This metabolic pathway is regulated by the activity of glycogen phosphorylase which cleaves the α 1-4 glycosidic links of the glycogen molecules to yield glucose-1-phosphate. The enzyme phosphoglucomutase converts glucose-1-phosphate to glucose-6-phosphate by transferring the phosphate group from carbon 1 to carbon 6. Once G6P is hydrolysed it is free to pass through the bidirectional GLUT2 transporter due to the high glucose gradient and be released into circulation.

1.1.3.1 Regulation of Glycogenolysis

The shifting dominance between glycogen synthesis and catabolism is gradual, with the hepatic glucose flux a function of glycogen synthase and glycogen phosphorylase activity. Activation of glycogen phosphorylase is a result of glucagon binding to its receptor on the hepatocyte and initiating a cascade of metabolic signals. Glucagon

receptor is a $G\alpha_s$ protein coupled receptor type, and its agonism rapidly increases intracellular cAMP through adenylyl cyclase activation (79). cAMP initiates the signalling cascade wherein cAMP-dependant protein kinase A is activated, leading to phosphorylation and subsequent activation of phosphorylase kinase. Lastly, this phosphorylase kinase converts the inactive glycogen phosphorylase to its active form (11).

Initiation of glycogenolysis is principally controlled by a key enzyme that react to the metabolic state of the hepatocyte. As described in Section 1.1.1.1 glycogen synthase is activated by dephosphorylation, whereas its reciprocal enzyme glycogen phosphorylase is activated by phosphorylation. Protein phosphatase 1 (PP-1) dephosphorylates both enzymes, thus inhibiting glycogenolysis. Glucose-6-phosphate mediates PP-1 activity by binding to glycogen synthase, catalysing the phosphorylation of the enzyme by PP-1, but also binds glycogen phosphorylase to reduce its activity through enhanced PP-1 dephosphorylation (11,80). Therefore, the influx of glucose into the hepatocyte and subsequent rise in G6P concentration is a key regulator of glycogenolysis.

1.1.4 Gluconeogenesis

Gluconeogenesis is a metabolic process defined as the biosynthesis of glucose from 3-carbon precursors, e.g., glycerol, pyruvate, and lactate and amino acids such as alanine and glutamine. In the fasting state, gluconeogenesis accounts for 50-60% of endogenous glucose production (78). Gluconeogenesis occurs in the two tissue types, the liver and kidney renal cortex, that express the essential enzyme in the process glucose-6-phosphatase. The liver accounts for approximately 90% of gluconeogenic activity and the kidney the remaining 10% (78).

1.1.4.1 Glucagon Release from Pancreatic α-cells

Glucagon is the main endocrine product of pancreatic α-cells, with its release mediated by hypoglycaemia, mixed nutrient ingestion, and autonomic nervous system (ANS) activity. The main physiological function of the peptide hormone is to raise blood glucose levels by stimulating glycogenolysis and gluconeogenesis whilst inhibiting glycogenesis and glycolysis.

The 29 amino acid sequence of glucagon is highly conserved between mammalian species. The glucagon gene produces the 180 amino acid preprohormone termed proglucagon (81). Proglucagon can be tissue specifically post-translationally modified to yield a multitude of peptides in the glucagon superfamily, such as glucagon like peptides 1 and 2 (GLP-1/2) and glucagon-related polypeptide (GRPP). In the pancreatic α-cells, glucagon is the main peptide produced by proglucagon processing(81).

The secretory mechanism of the α-cells in the release of glucagon in response to blood glucose levels shares much of the same exocytotic machinery and K_{ATP} ion channels as that of β-cell insulin release. In summary, whereas in β-cells the increase in intracellular ATP levels as a result of glucose metabolism causes exocytosis in response to potassium channel closure, in α-cells membrane depolarization inhibits rather than stimulates the exocytotic machinery (82,83).

The ANS is an important counter regulator of hypoglycaemia through its actions on the α-cell to stimulate glucagon release via parasympathetic and sympathetic limb activation. The threshold for activation of the ANS by central hypoglycaemia is typically above the levels at which signs of hypoglycaemia begin to manifest themselves, between 75-85 mg/dl (84,85). Once stimulated, postganglionic terminals found within the pancreatic islets release norepinephrine and acetylcholine which bind to their receptors on the α-cell plasma membrane. Additionally, a third component of sympathetic branch driven glucagon release occurs via the effects of epinephrine, (86). Thus this trifecta of autonomic stimuli increase intracellular cAMP, liberates intracellular Ca^{2+} stores and accelerates glucagon exocytosis (87).

After release by the pancreatic α-cells and transport through the bloodstream to the liver, glucagon binds to the hepatic glucagon receptor inducing the transcription of the key gluconeogenic enzyme PEPCK whose action is described in detail in Section 1.1.4.3 (88).

1.1.4.2 Substrates of Gluconeogenesis

Three carbon molecules, amino acids, and glycerol can all be used as substrates for gluconeogenesis, entering the pathway at different points depending on the origin of the carbon precursor. The adaptability of the pathway to use a wide range of metabolites ensures glucose homeostasis can be maintained even in states where there is low nutrient availability.

The Cori cycle provides lactate as a by-product of glycolysis in peripheral tissues, in particular the skeletal muscle, and transports them to the liver where they are converted to pyruvate and used to create glucose (89,90). During periods of low oxygen supply, such as bouts of physical activity, lactate is produced through anaerobic fermentation of glucose in the muscle cells. When the muscle is at rest, lactic acid diffuses out of the myocyte and into the bloodstream, where it may be further oxidized by the heart or taken up by the liver where it is taken up by plasma membrane monocarboxylate transporters to be used as substrate for gluconeogenesis (41,91).

Alanine and glutamine are the two most relevant amino acid substrates for gluconeogenic pathway(91). In the liver alanine is the main contributor, while in the kidney it is glutamine. In what is known as the Cahill cycle, alanine is released into circulation after skeletal proteolysis, where it is taken up by the liver and deaminated(40,92). Once in the hepatocyte, the alanine is transaminated to glutamate by glutamic-pyruvic transaminase, then once again deaminated to yield the gluconeogenic substrate pyruvate(93). Similar to the Cori cycle, the Cahill cycle serves to repurpose skeletal muscle metabolic by-products to maintain glucose homeostasis. The entry of glutamine into the gluconeogenic pathway is unique in that unlike alanine or direct three carbon precursors, there is a net yield of energy in the form of ATP as a result of its processing (94). Glutamate is first converted to glutamine by mitochondrial glutamate-alanine-transaminase in a similar fashion to the metabolism of alanine described previously. Three carbon segments of glutamine are then liberated in the mitochondria by the Krebs Cycle at which point glutamine enters the gluconeogenic pathway as oxaloacetate as described in the following section.

Although not as significant a contributor as the aforementioned amino acids and lactate, glycerol provided by the lipolysis of triglycerides in adipocytes is responsible

for 3-7% of substrate contribution for gluconeogenesis (91,95). Once released by the adipocyte, glycerol is phosphorylated to glycerol-3-phosphate (G3P) by the liver specific glycerol kinase. G3P is then converted to dihydroxyacetone phosphate (DHAP) which is the entry point of glycerol into the gluconeogenic pathway. From here DHAP can proceed up through the reversible steps in glycolysis to yield a glucose molecule.

1.1.4.3 The Gluconeogenic Pathway

Eleven key enzymes may be employed in the gluconeogenic conversion of pyruvate to glucose. Four of these enzymes are exclusive to the gluconeogenic pathway, while seven are involved in reversible steps in the glycolytic breakdown of glucose-6-phosphate. Pyruvate is first transported into the hepatic mitochondrion by a mitochondrial pyruvate carrier where gluconeogenesis begins, and it is converted to the 4-carbon oxaloacetate (OAA) by pyruvate carboxylase. The next major step is the decarboxylation of OAA by the cytosolic isoform of phosphophenolpyruvate carboxykinase (PEPCK-C). However, the mitochondrial membrane is impermeable to OAA, and so it must first be converted to malate by the enzyme malate dehydrogenase via NADH oxidation before passing through the malate-aspartate shuttle into the cytosol. The malate molecule is now localized in the cytosol of the hepatocyte where it is then converted back into OAA by the action of cytosolic malate dehydrogenase. It is now readily available as a substrate for PEPCK-C to yield phosphoenolpyruvate (PEP). PEP is an intermediate product of the glycolytic pathway, and the enzymatic steps in the mitochondrion just described present an intuitive way to bypass the irreversible step in glycolysis that is the breakdown of PEP to pyruvate. Now in the cytosol, PEP then proceeds back through the six reversible enzymatic steps in glycolysis (described in Section 1.1.1.3) resulting in fructose, 1-6-bisphosphate. Conversion of fructose, 1-6-bisphosphate to fructose-6-phosphate involves the removal of a phosphate group by fructose 1-6-bisphosphatase, and then proceeds to another reversible step of glycolysis which is the hexose isomerase reaction of fructose-6-phosphase to glucose-6-phosphate. The final step of gluconeogenesis that is the dephosphorylation of glucose-6-phosphate to yield glucose which can then enter the bloodstream involves a key enzyme complex, glucose-6-phosphatase (G6Pase), only found within the endoplasmic reticulum of the hepatic and renal cortex tissue. G6P is brought into the endoplasmic reticulum through the translocase known as T1. Once

delivered to the G6Pase complex, the final phosphate group is removed, glucose is returned to the cytoplasm via the T2 translocase where it is free to diffuse through GLUT2 and into the bloodstream thereby raising circulating glucose levels.

1.1.4.4 Regulation of Gluconeogenesis

As with the balance between glycogenosis and glycogenolysis previously described, the regulation of gluconeogenesis is a gradual change between the fed and fasted states involving transcriptional regulation through specific gene promoters as well as acute regulation by hormones and metabolites through allosteric and covalent modification of key gluconeogenic enzymes.

Acute regulation of gluconeogenesis takes place in the short term (seconds to minutes) to rapidly change hepatic glucose flux in response to plasma glucose levels. The acute regulation of gluconeogenesis primarily takes place at the reversible steps shared with the glycolysis and serve to promote/inhibit these opposing pathways.

Pyruvate dehydrogenase (PDH) decarboxylates pyruvate in the mitochondrion to yield OAA in an early step of gluconeogenesis. In the fed state, PDH is phosphorylated which serves to allosterically inhibit the enzyme. This is due to hepatic insulin receptor activation increasing expression of pyruvate dehydrogenase kinases which repress gluconeogenesis by keeping PDH phosphorylated thus inhibiting its action (96). Pyruvate carboxylase (PC) is one of the more potent gluconeogenic enzymes, converting pyruvate to OAA by carboxylation in the mitochondrion. Acetyl-CoA is a strong allosteric activator of pyruvate carboxylase (97). The absence of hepatic Acetyl-CoA induces a conformational change in the structure of the PC enzyme, preventing its binding and carboxylation of pyruvate. In the fasted state, when fatty acid oxidation is increased and thus acetyl-CoA as a result, gluconeogenesis is stimulated (97). Pyruvate kinase (PK) is responsible for converting PEP to pyruvate in the liver, and has long been known to serve as a negative regulator of gluconeogenesis by antagonising the actions of both PDH and PC(96,98,99). PK is inactivated by downstream glucagon receptor activation mediated by cAMP-PKA signalling. The phosphorylation of PK by PKA decreases the enzymatic activity on its substrate PEP, thus allowing PEP to be further processed in the gluconeogenic pathway instead of being directed towards glycolysis. The final critical step in which gluconeogenesis is

acutely regulated are the irreversible steps involving the enzymes fructose,1-6-bisphosphatase (F1-6B) and phosphofructokinase (PFK) in gluconeogenesis and glycolysis respectively. These two enzymes reside at a junction of pathways that represent complementary but irreversible steps in which they catalyse the conversion of fructose, 1-6-bisphosphate to fructose-6-phosphate by F1-6B and vice-versa by PFK. Hepatic PFK is allosterically inhibited by the presence of PEP and citrate, both of which indicate high abundance of gluconeogenic substrates and available energy. Additionally, PFK is also inhibited by the product of F-1-6B, fructose,1-6-phosphate.

Following shifts between the fed and fasted state that acutely regulate gluconeogenesis just described, come longer term regulation of the pathway through influence over the transcription of gluconeogenic gene expression. The two opposing forces in this transcriptional regulation are the hormones insulin and glucagon, with glucagon increasing intracellular cAMP which increases the activity of transcription factors, and insulin repressing these effects by disabling the key gluconeogenic transcriptional regulator FOXO1 as detailed below.

These transcriptomic shifts are primarily manifested through their influence on the expression of PEPCK, F1-6B, and G6Pase. Glucagon is a principal activator of PEPCK and G6Pase gene expression. Upon binding to the hepatic glucagon receptor, PKA activated downstream phosphorylates c-AMP response element binding (CREB) in the nucleus. CREB binds to its response element in the genes encoding for PEPCK and G6Pase, initiating transcription of these enzymes (100,101). Although the mechanisms by which have not been fully elucidated, the release of insulin initiates the primary transcriptomic counterregulatory response to gluconeogenesis (102,103) . Agonism of hepatic insulin receptor phosphorylates IRS and PI3K and the phosphorylation cascade that activates Akt previously described in Section 1.1.2.2. Akt then phosphorylates forkhead transcription factor 1 (FOXO1). FOXO1 is a promoter of PEPCK and G6Pase transcription in its active (unphosphorylated) state. Through insulin mediated FOXO1 phosphorylation, gluconeogenic gene expression is inhibited as this key transcription factor is deactivated (80,102). PGC-1α is another gene expression promoter with influence over the gluconeogenic pathway that exerts its effecting during the basal state (102,104). PGC-1α is essential to the expression of main gluconeogenic enzymes (PEPCK, F1-6B, and G6Pase) and is activated in

response to glucagon receptor cAMP generation and CREB(104). Once activated by phosphorylation, PGC-1α binds to gene promoters of the gluconeogenic enzymes and enhances their expression.

1.2 Skeletal Muscle Glucose Metabolism in Diabetes Mellitus

Having described the broad picture of glucoregulatory physiology in the preceding sections, the following pages address the failure of glucoregulation in diabetes, with a focus on changes in skeletal muscle biology as they pertain to pathogenesis and the mechanism of action of anti-diabetic drugs.

1.2.1 Classification of Diabetes Mellitus

The majority of cases of diabetes mellitus (DM) are classified either Type 1 DM (T1DM), resulting from autoimmune β-cell destruction and insulin deficiency or Type 2 DM (T2DM) due to the gradual loss of normal β-cell function in the context of insulin resistance. The American Diabetes Association defines an additional two broad categories in their 2022 update to *Standards of Medical Care* (69), gestational diabetes and diabetes from other causes (encompassing monogenic syndromes, disease of the exocrine pancreas, chemical-induced diabetes, and post-organ transplantation). However, today it is clear that T1DM and T2DM are heterogenous diseases in which there are a wide range of symptoms and rates of disease progression.

The disease progression of T1DM is more clearly defined and can be separated into 3 distinct stages, with the age of onset, autoantibody levels, and autoantibody specificity being the main predictors rate of progression (105). Stage 1 of T1DM is typically pre-symptomatic, with the individual being normoglycaemic but presenting with autoimmunity via islet autoantibodies. In Stage 2, the individual is still free from microvascular and macrovascular complications but presents some dysglycemia. Stage 2 can be diagnosed by an increase in autoantibody levels, fasting glucose of 5.6-6.9 mmol/L, a 2-hour glucose level following an OGTT of 7.8-11 mmol/L, or HbA1C 39-47 mmol/mol. By Stage 3, profound hyperglycaemia and ketoacidosis is presented in untreated cases, and β-cell function is effectively lost. Although the specific mechanisms in which β-cell death occurs remains controversial there is substantial evidence that destruction of the cell is due to an autoimmune response. For example,

in Caucasian children diagnosed with TD1DM at a young age, 90% were positive for at least one of the four autoantibodies associated with TD1DM (106).

T2DM accounts for 80-90% of diabetes and in the past has been referred to as “adult-onset diabetes” or “noninsulin-dependent diabetes”, however those terms have been deemed redundant by the rapidly growing body of research describing the heterogeneity of the disease. Typically, autoimmune destruction of the pancreatic β-cell does not occur, and most patients have a body mass index (BMI) in the obese range (>30kg/m^2) and insulin resistance. Disease progression can be significantly slower than in T1DM, with individuals going undiagnosed for several years as carbohydrate metabolism is gradually dysregulated during prediabetes. In terms of glucose homeostasis, prediabetes is defined by HbA1C levels of 5.6-6.4%, but high circulating triglycerides or low HDL cholesterol may also be present (69). As prediabetes progresses into T2DM, endogenous insulin secretion becomes insufficient to overcome insulin resistance and impaired glucose tolerance becomes prominent.

Recognizing the heterogeneity of the disease, Ahlqvist et al. have proposed a refined classification system that may be used as a tool with the aim of improving patient outcomes by personalizing treatment (107). Using data-driven cluster analysis in 8980 patients with newly diagnoses diabetes, five clusters of patients each with distinct characteristics and diabetic complications were observed. Cluster 1, representing 6.4% of patients studied, fits the classical description of T1DM in which the patient has low BMI, insulin deficiency and evidence of an autoimmune response. Cluster 2, 17.5% of patients, were also insulin-deficient, low BMI, and early age of onset but demonstrated no evidence of an autoimmune response. Cluster 3, fitting the traditional definition of T2DM, was characterized by high BMI with severe insulin resistance and hyperinsulinaemia. This cluster classified 15.3% of subjects studied. Patients in cluster 4, 21.6% of those examined, had no evidence of insulin resistance but high BMI indicative of obesity. The largest cluster comprising 39.1% of patients studied was Cluster 5 in which patients were characterized by old age with moderate metabolic dysregulation. The authors also found that these clusters displayed discrete rates of disease progression and incidence of complications. Cluster 1 and 2 displayed significantly elevated HbA1c and frequent ketoacidosis. Cluster 3 had a high rate of Non-alcoholic fatty liver disease (NAFLD) and chronic kidney disease (CKD), with

lower incidence rates found in Clusters 4 and 5. In terms of disease management through pharmacotherapy, insulin was prescribed in 42% of patients in Cluster 1 and 29% of patients in Cluster 2, but <4% in Clusters 3-5. Interestingly, Cluster 3 had a lower rate of metformin in comparison to Clusters 4 and 5. This cluster, defined by obesity and insulin resistance, would be thought to benefit the most from metformin use. In conclusion, an increasingly stratified approach to the classification of DM, such as that proposed by Ahlqvist et, al. may be useful in a personalized medicine approach to the treatment of diabetes. This approach may be particularly useful in identifying responders to novel pharmaceutical treatments that may only be effective in certain disease states.

1.2.2 Mechanisms of Skeletal Muscle Insulin Resistance

While insulin resistance (IR) can arise in multiple tissues and organs, skeletal muscle IR is of particular relevance to dysglycaemia.

Skeletal muscle accounts for 80% of insulin mediated post-prandial glucose disposal and metabolic defects in this tissue result in profound dysregulation of glucose homeostasis. These metabolic defects are underpinned by impairment of insulin signal transduction, and attendant impairment of glucose uptake, glycogen synthesis and glucose oxidation (75,108). It has been demonstrated that skeletal muscle insulin resistance may predate hepatic insulin resistance in T2DM disease progression, with the fate of postprandial carbohydrates being directed to hepatic *de novo* lipogenesis in individuals with skeletal muscle insulin resistance which lead to further metabolic complications (75,109). Once clinical manifestations of T2DM begin to appear, patients often have a multitude of metabolic abnormalities such as hyperglycaemia, hyperinsulinaemia, and elevated FFA levels(75,110).

Although the relative contributions of these factors to the pathogenesis of insulin resistance is a challenge to quantify, elevations in circulating FFA leading to ectopic lipid accumulation is widely acknowledged to act as a mediator of skeletal muscle insulin resistance. Adipocytes provide a buffer to lipid accumulation in other peripheral tissues, and the inability of adipocytes to store excess fatty acids leads to ectopic lipid accumulation in skeletal muscle that is commonly observed in patients with skeletal

muscle insulin resistance (111–114). Circulating FFA's increase when the capacity of white adipose tissue to take up and utilize the fatty acids is reached and as a result these are taken up by skeletal muscle. In lipoatrophic mice lacking adipocytes, a marked increase in fat accumulation is observed in skeletal muscle and liver tissue (115). When fat is transplanted from wild-type littermates subcutaneously into these same mice, ectopic lipid content is normalized and insulin signalling restored. Additionally, in mice overexpressing lipoprotein lipase intracellular fat is accumulated specifically in skeletal muscle and hepatic tissue (116,117). As lipid accumulation in the muscle is a product of the difference between fatty acid uptake and oxidation, disruptions in mitochondrial metabolism are a principal predisposing factor for insulin resistance. Reduced mitochondrial density and activity in offspring of patients with T2DM suggests this can be an inherited genetic defect (118,119). Furthermore, as intracellular lipid accumulates, gene expression linked to mitochondrial oxidation is decreased, leading to the increased production of reactive oxygen species which further impair the function of the mitochondrion and exacerbate accumulation of fatty acid metabolites such as diacylglycerol and ceramides(108,114).

Skeletal muscle glucose uptake in response to insulin relies on efficient coupling of intracellular signalling events between starting with receptor activation and terminating with GLUT4 translocation. The intracellular environment in the context of ectopic fat accumulation can lead to multiple points of failure in this signalling cascade. Over the last two decades the laboratory of Gerald Shulman (Yale University) has generated substantial evidence implicating diacylglycerol (DAG) accumulation in inhibiting GLUT4 translocation at specific locations in the skeletal muscle insulin signalling pathway (114,120). Humans and mice with transiently increased FFA levels caused by lipid infusions demonstrated a significant reduction in G6P concentration in skeletal muscle, demonstrating the fault lies in GLUT4 translocation and increased glycolytic flux t (121,122). It was then established in both human and animals that elevated free fatty acids increased intracellular DAG, which activates a novel protein kinase (nPKC) that directly inhibits IRS-1 phosphorylation through a serine-threonine kinase cascade, ultimately stopping GLUT4 translocation (123–125). These data was substantiated in genetic studies in mice where this serine-threonine phosphorylation cascade was inhibited through IRS-1 mutation which resulted in subsequent protection from lipid induced insulin resistance (126). These findings are particularly important they suggest

a dissociation between neutral lipids such as triacylglycerol (TAG) and insulin resistance, instead implicating DAG in signalling defects. However, DAG accumulation does track with an increase in intracellular TAG deposition, thus the presence of TAG in muscle is still a reliable indicator of insulin resistance.

Numerous other points of failure in insulin mediated glucose uptake in resistant skeletal muscle have also been observed. Evidence for signalling defects can be found at various upstream locations such as the site of receptor activation in addition to post-receptor reaction steps. Activation of the insulin receptor leads to insulin receptor tyrosine kinase activity as described in Section 1.1.2.2. In insulin resistant diabetics (both obese and non-obese subjects), insulin receptor tyrosine kinase activity is decreased (125,127–129). However, the effect being reversed in patients with improved glycaemic control after weight loss suggests defects at this signalling step may be secondary to hyperglycaemia (130). Studies examining the skeletal muscle of individuals with T2DM during hyperinsulinaemic-euglycaemic clamps have also observed reduced IRS phosphorylation, and downstream Akt/PKA activity in addition to failure of the receptor to autophosphorylate (125,129,131,132).

Further to the aforementioned defects in insulin signalling, discrete impairment of glycogen synthesis in skeletal muscle is associated with T2DM. Insulin resistant patients display a marked reduction in skeletal muscle glycogen synthesis and glucose uptake during hyperinsulinaemic-euglycaemic clamps (72,133,134). Although insulin has been shown to have no influence on glycogen synthase expression (135,136), glycogen synthase mRNA levels are significantly decreased in patients with T2DM (136,137). This metabolic pathway may be another point at which genetic defects may predispose an individual to developing insulin resistance. Healthy offspring of parents with skeletal muscle insulin resistance and T2DM have been shown to display impaired glycogen synthesis (138). To date, studies investigating this phenomenon have found no specific genetic defects linking the impairment of glycogen synthase to T2DM (139,140). While there is not yet a molecular explanation for the impairment of glycogen synthesis in this context, studies to date have clearly shown this can be another point of failure in the transduction of insulin signalling in resistant skeletal muscle.

In summary, there are a multitude of post-receptor signalling defects that may contribute to metabolic dysregulation in insulin resistant skeletal muscle, although the precise mechanisms of which are not yet fully elucidated. Despite this, targeting of the insulin mediated glucose uptake remains an attractive and highly effective pharmacological method of managing glucose homeostasis in individuals with diabetes mellitus.

1.2.3 Insulin-Centric Pharmacological Management of Diabetes

Due to advances in modern medicine, both T1DM and T2DM are highly treatable diseases. In addition to diet and exercise, the pharmacological management of glucose homeostasis in diabetes mellitus represents a critical part of the overall therapeutic strategy. An improvement in glycaemic control is strongly associated with a reduction in diabetic complications and an improvement in overall disease outcomes. In T1DM, the Diabetes Control and Complications Trial (DCCT) demonstrated that intensive insulin therapy reduced early stage microvascular complications by up to 76% (141), and it's follow up study the Epidemiology of Diabetes and its Complications (EDIC) demonstrated reduction in macrovascular diseases with long term insulin therapy (142). The UK Prospective Diabetes Study (UKPDS) showed that for every 1% reduction in HbA1C in patients with T2DM,there was a 35% reduction in microvascular complications and 25% reduction in diabetes related mortality (143). Therefore, pharmacological strategies modulating the release and action of insulin present an attractive and effective target in managing the disease. Classes of drugs currently used as part of this strategy are summarized below.

1.2.3.1 Pharmacological Agents Targeting of Insulin Action and Secretion

Insulin secretagogues, such as the sulfonylurea Glipizide, are oral agents that are agonists at the sulfonylurea-1 receptor (SUR1). These SUR1 agonists act by regulating the action of the K_{ATP} channel on the pancreatic β-cell and stimulating insulin secretion (144,145). Secretagogues are typically only used in T2DM where β-cell function is still largely intact, and have proved effective when initiated as a combination therapy, often co-formulated with metformin, in newly diagnosed T2DM (146,147). These orally administered drugs have a long duration of action leading to them often only having to be administered once daily with the effect of lowering fasting glucose by potentiating basal insulin secretion. As an alternative dosing regimen to once a day administration,

the dose of secretagogues may be reduced but administered twice a day thereby reducing the risk of acute hypoglycaemic episodes. Second-generation sulfonylureas such as the aforementioned Glipizide, are designed to slow their absorption, thus reducing the peak of action of the drug and lowering the risk of hypoglycaemic episodes (148,149). Differences in pharmacokinetic profiles between drugs in this class lead to varying side effects. For example, chlorpropamide, which is no longer in use, can only be cleared by the kidneys and results in hypoglycaemia when renal clearance is compromised. Additionally, sulfonylureas have been associated with increased risk of myocardial infarctions (149), although long term safety has been demonstrated when using long acting agents such as gliclazide, glyburide and glipizide (150,151). More recently, insulin secretagogues distinct from sulfonylureas have been developed. Known as meglitinides, these agents have a shorter half-life and a different SUR1 binding site (145). The limited half-life of these drugs necessitates a different dosing regimen. They are typically taken orally immediately following a meal, acutely managing post-prandial glucose excursions. There is also less risk of overnight or fasting hypoglycaemia, as they do not last long enough to increase basal insulin secretion as in the case of sulfonylureas. However, disadvantages include a high cost and need for multiple daily doses in comparison to traditional sulfonylureas.

GLP-1 receptor agonists are either short or long-acting analogues of the human GLP-1 peptide hormone. Agonism of GLP-1 receptor increases pancreatic insulin secretion in a glucose dependant manner, slows gastric emptying, reduces glucagon secretion and improves satiety (52,152). Exanatide is a short-acting agonist and the first GLP-1 analogue to gain marketing authorization. Exanatide has a total duration of approximately six hours, with twice daily pre-prandial injections resulting in a 1% reduction in HbA1c and modest weight loss in the long term (>16 weeks) (153,154). Recently, long acting GLP-1 agonists such as liraglutide and semaglutide have entered clinical use. These agents have the same mode of action as their shorter half-life counterparts but impart greater benefits to the patient through larger reductions in HbA1c due to their prolonged overnight effects (152,155). Additionally, liraglutide and semaglutide, in the LEADER and SUSTAIN-6 respectively, have demonstrated reduction in cardiovascular death, all-cause mortality and albuminuria progression in patients with T2DMat risk of cardiovascular complications (156,157). As the

potentiation of insulin secretion by GLP-1 agonists is glucose depending, there is reduced risk of hypoglycaemic complications.
The endogenous GLP-1 hormone has a short half-life of approximately 2 minutes as a result of its rapid inactivation in plasma by dipeptidyl peptidase-4 (DPP4) (158). Oral DPP4 inhibitors have been developed that when administered can raise endogenous postprandial GLP-1 twofold (159). Although not affecting satiety, gastric emptying or bodyweight, DPP4 inhibitors can reduce HbA1c levels by 0.5-1% as demonstrated in meta-analysis of 80 clinical studies administering these agents (159). As is the case with sulfonylureas, GLP-1 receptor agonists and DPP4 inhibitors rely on functioning pancreatic β-cells to cause improvements in glycaemic control.

Insulin treatment is critical in patients with T1DM and decompensated T2DM. It is the longest used and most studied therapeutic agent in managing DM, with a multitude of formulations currently available. The majority of analogues today are recombinant human insulin that are either short or long-acting agents. Long-acting insulins are typically modified to ensure a slow release from the tissue following subcutaneous injections. For example, detemir has myristic acid, a 14-carbon fatty acid, bound to the insulin molecule which causes the agent to be more slowly absorbed (160). Insulin glargine is another long-acting insulin analogue that is modified to have an isoelectric point of 6.7. Soluble in its injection formulation, it rapidly comes out of solution at physiological pH resulting in a slower subcutaneous absorption (161). Neutral protamine Hagedorn (NPH) is the most common form of long-acting insulin currently in use, with a duration of 12-16 hours it is typically taken twice a day. Unlike insulin glargine, and similar to detemir, NPH has a pronounced peak of action which carries an elevated risk of hypoglycaemia. Long-acting insulins are preferred in T1DM and T2DM requiring insulin as they improve both fasting and post-prandial glycaemia control in patients who are still insulin sensitive. Short-acting and rapid-acting insulin analogues are typically only administered in settings where there is severe insulin resistance and acute post-prandial glycaemic control is needed. Regular short-acting insulin typically has a time of onset of about 30 minutes and a duration of up to 8 hours, while rapidly acting insulin can begin acting within 15 minutes and having an effect over 4 hours(161,162).

1.2.3.2 Complications of Insulin-based Therapy

Hypoglycaemia is the most common acute complication in patients undergoing intensive therapy with insulin secretagogues and analogues outlined previously. The critical risk factor for hypoglycemia in diabetes is the absolute or relative level of therapeutic insulin as a result from insulin analogues and/or secretagogues. The ratio of insulin to glucose may be increased when there is an ill-timed administration of pharmacotherapy, or there is an impairment of renal clearance of insulin or secretagogues.

In T1DM the hierarchy of counterregulatory responses to low glucose levels are impaired, thus these patients are at high risk of hypoglycaemia. Amplifying this risk is the fact that the source of insulin in these patients is exogenous, and as such circulating levels of insulin won't decrease in response to falling blood glucose. Analysis of large cohort studies indicate that between 7-10% of deaths in patients with T1DM are due to hypoglycaemia (163,164). In the DCCT, severe symptomatic hypoglycaemia was observed in 61.2% of patients on intensive insulin therapy (165). Although occurring less frequently, patients with progressed T2DM are also at risk for hypoglycaemia as a combination of pharmacotherapies are often employed in their therapeutic strategy(166). The U.K Hypoglycaemia Study group found that the frequency of hypoglycaemic episodes increase with time in patients on insulin therapy with T2DM, increasing from 7% for <2 years on treatment to 25% for >5 years (166).

Glucose is an essential fuel source for the brain, and while other fuel sources such as ketones can be utilized, they cannot be delivered in sufficient amounts to maintain normal function during acute bouts of hypoglycaemia. Cognitive function begins to be impaired at blood glucose levels <3 mmol/L which is when symptoms of severe hypoglycaemia begin to manifest (1). While glucose levels <3.9 mmol/L are defined as an "alert level" by the ADA (167), hypoglycaemia does not have a universally accepted definition as clinical manifestations can be nonspecific(1,168). These manifestations of symptoms can be categorized by their cause either being neuroglycopenic, a direct result of central glucose deprivation, or neurogenic which are results of systemic responses triggered by the sympathetic neural system in response to hypoglycaemia (168,169). Neuroglycopenic symptoms are often not directly measurable, and manifest in cognitive impairments such as a lack of awareness,

deterioration of motor skills and if allowed to progress seizure and coma. Neurogenic are more easily measured as vital functions are affects. Heart rate and systolic blood pressure are raised alongside cutaneous vasoconstriction, and excessive sweating can be observed after cholinergic sweat gland activation (170). Recurring hypoglycaemic episodes can result in hypoglycaemic-associated autonomic failure (HAAF) in which the sympathoadrenal response to low blood glucose is reversibly impaired (171). Repeated bouts of hypoglycaemia attenuate epinephrine secretion and sympathetic neural activation, thereby reducing a patients awareness to symptoms of hypoglycaemia, their ability to mount a counterregulatory response, and overall cognitive function (168,172,173). Although HAAF is more common in T1DM, it is also a significant risk in patients with severe T2DM (171).

The anabolic effects of intensive insulin therapy can lead to weight gain that leads to the obvious physiological consequences, but also detrimental psychological impact. This weight gain can further impede glycemic control, particularly in patients who are overweight prior to beginning treatment. For example, in the UKPDS T2DM patients on intensive insulin therapy gained 2.9kg more weight on average than the conventionally treated group, and 4kg more than those treated with secretagogues (151). This weight gain can further compound cardiovascular risk factors, even in T1DM. In the DCCT, weight gain as a result from intensive insulin therapy was associated with atherosclerosis, increased blood pressure, and dyslipidemia (174,175). Another significant issue is the retention of an estimated 500 kcal previously lost through glycosuria once insulin therapy is initiated however, this weight gain due to this cause has been demonstrated to be offset by metformin use as an adjunct therapy (176).

Improvement in glycaemic control is paramount in managing complications in DM. Although insulin-independent adjunct therapies are available such as biguanides, α-glucosidase inhibitors, and SGLT2, in T1DM and severe cases of T2DM reliance on the insulin signalling pathway to manage the disease is unavoidable. Potentiating insulin signalling and secretion is highly effective but not without risk of acute hypoglycaemic events and weight gain with intensive therapy. Novel treatment approaches that could facilitate improvements in glycaemic control in both T1DM and T2DM with minimal risk to the patient are highly anticipated. As described in the

following section, pre-clinical data suggests a novel pituitary-skeletal muscle endocrine axis unexplored in human biology has potential to fill this niche.

1.3 The Melanocortin System and Energy Homeostasis

1.3.1 Melanocortin Receptors and Ligands

The melanocortin system is a collective term for the melanocortin neuropeptides and adrenocorticotropic hormone (ACTH), the endogenous antagonist's agouti signalling protein (ASP) and agouti-related protein (AgRP), and G protein-coupled melanocortin receptors (MCRs). The melanocortin system is involved in a wide array of physiological functions both centrally and peripherally such as appetite control, pigmentation, sexual function, energy homeostasis and inflammation. Cross-species variability in the tissue specific distribution of MCRs melanocortin receptors, particularly in the periphery, show significant variability in published literature. Additionally, MCRs have been detected in most tissue types in varying amounts, leading to many proposed functions that have not yet been fully elucidated and are in the very early stages of research. As such, the data presented in this section will focus on highlighting the physiological effects pertaining to humans that are sufficiently supported in published literature, with attention still given to animal data that is relevant to the topic of this thesis.

1.3.1.1 Processing of Pro-opiomelanocortin

Pro-opiomelanocortin is the 241 amino acid precursor to ACTH and the melanocyte-stimulating hormones (MSH) α-MSH, β-MSH, and γ-MSH. In humans, the POMC gene is expressed in cells within the anterior pituitary, the hypothalamus and the skin where the polypeptide precursor is tissue specifically post-translationally processed by the enzymes carboxypeptidase E (CPE) prohormone convertases (PC) 1, 2, and 3. The degree of processing is dependent on the extent these enzymes are present in the tissue(177–180). The arcuate nucleus of the hypothalamus is the site at which POMC is most extensively processed, with α-MSH, β-MSH, and γ-MSH resulting as the end products of the proteolytic pathway. PC1/3 initially cleaves POMC to generate the precursor peptide fragments ACTH, β-lipotropic hormone (β-LPH), and pro-γ-MSH which are then used to generate the active forms of the melanocortin peptides. The generation of α-MSH is as follows; PC1 sequentially cleaves POMC to yield pro-ACTH

then ACTH. ACTH is cleaved by PC2 to yield the peptide fragment ACTH1-17, which has its C-terminal end cleaved by CPE to yield the deacetylated version of α-MSH. Deacetylated α-MSH is finally acetylated by n-acetyltransferase to generate the active form of the hormone(178). To produce β-MSH, Beta-LPH is cleaved at its Lys-Lys bond by PC2 to generate γ-LPH, which is cleaved again by PC2 to generate the active peptide. Finally, to yield γ-MSH, pro-ACTH is sequentially cleaved first by PC1/3 to yield Pro-γ-MSH, then once more by PC2 to yield the active γ-MSH.

POMC processing in the human anterior pituitary is less extensive, with only ACTH and α-MSH being generated in physiologically relevant amounts (179,181). However, the anterior pituitary is the primary source of circulating melanocortin peptides as will be outlined in Section 1.3.1.2. Although it is unclear how critical PC1/3 is in the generation of α-MSH as an end product due to their variable abundances in the tissues the hormone is present is, ablation of PC2 inhibits the biosynthesis of POMC fragments beyond ACTH cleavage suggesting α-MSH generation is at least dependant on PC2 in the tissues it has been detected in (182). POMC processing in the skin follows a similar path to the hypothalamus due to the presence of the same proteases, but the function of the peptides produced here is to stimulate melanogenesis through α-MSH mediated MCR1 activation.

Co-localized in the arcuate nucleus are neurons expressing AgRP which acts as both an inhibitor of POMC processing and a competitive antagonist of central MCR3/4 (183,184). Similarly to the aforementioned peptides, AgRP precursor undergoes proteolytic cleavage to generate the active form of the peptide that is stored in secretory granules to be released in response to metabolic signals (184,185).The primary role of interaction of POMC/AgRYP neurons in the hypothalamus is in the central regulation of satiety and energy balance, as summarised in Section 1.3.2.

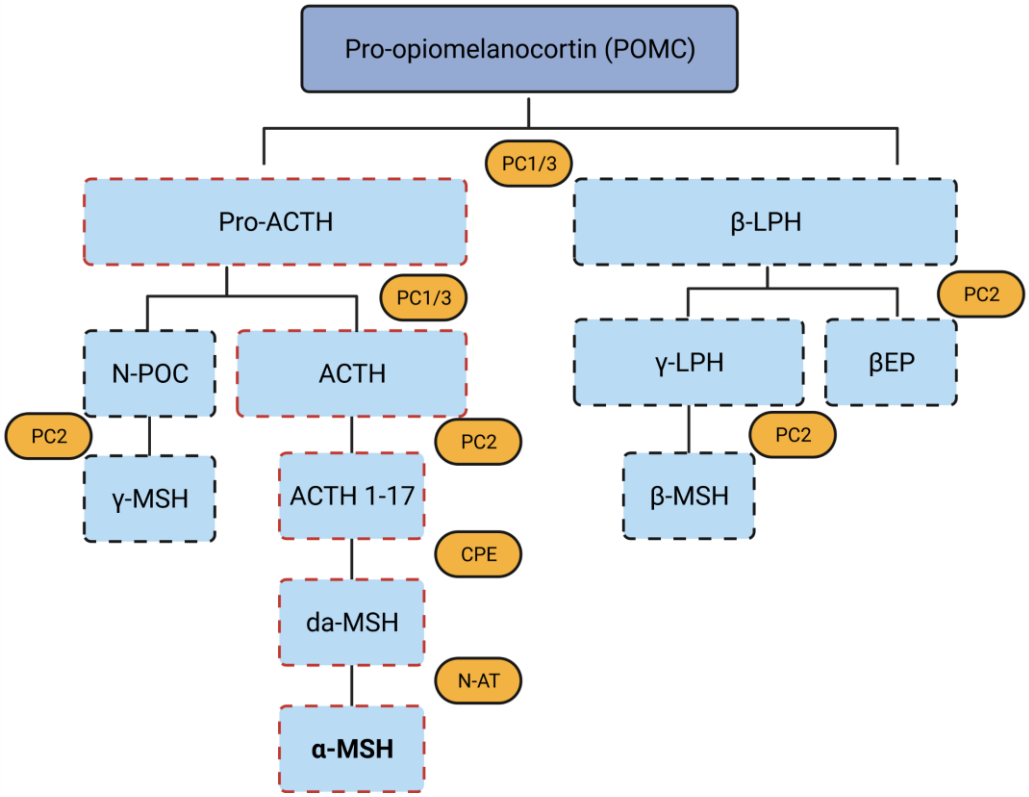

Figure 1.2 Processing of pro-opiomelanocortin to active melanocortin peptides.

1.3.1.2 Melanocortin Receptor Binding and Activation

The five melanocortin receptors are a family of seven-transmembrane G-protein coupled receptors with varying sequence homology, binding affinities, and tissue distribution. Melanocortin receptors are classified as $G\alpha_s$ receptor subtypes, and their signalling relies on cAMP generation by activated adenylyl cyclase. These receptors have both orthosteric, the site identified at which endogenous ligands bind, and allosteric binding sites, the latter of which has recently begun to be exploited as a pharmaceutical target with the highly selective and potent MCR4 allosteric agonist Setmelanotide gaining marketing authorisation in 2021 for the treatment genetic

obesity caused by MCR4 mutation (186). Human MCRs have high levels of sequence homology, being as high as 60% between MCR4/5 and 45% between MCR1/3(187,188). This leads to a range of binding affinities for the endogenous melanocortin ligands, with the exception of MCR2 which exclusively binds ACTH(189). The broad functions of the MCRs, their binding capacities, and human tissue distribution are outlined below, with their physiological effects further expanded upon in subsequent sections.

MCR1 is the most extensively characterised receptor, best known for its role in melanogenesis in cutaneous melanocytes mediated by α-MSH (190,191), it has also been found in human pituitary and testes (192). MCR1 preferentially binds α-MSH=ACTH> β-MSH>γ-MSH however, whereas ACTH produces a similar effect to α-MSH in melanocytes the physiological role of the latter two peptides at this receptor has not been fully elucidated in humans (193,194). MCR2 is the classical melanocortin receptor of the adrenal gland, binding exclusively to ACTH with no affinity to other endogenous melanocortin ligands (189,192). The agonism of MCR2 by ACTH is a crucial part of the hypothalamic-pituitary-adrenal axis, increasing the concentration of circulating glucocorticoids as a stress response. MCR3 is primarily found centrally in the hypothalamus, thalamus but also in low levels in the heart and intestines (192,195). MCR3 is unique in that α-MSH is the only endogenous agonist with binding affinity for this receptor. MCR3 is antagonised by AgRP and ASP as part of the central melanocortin control of food intake and energy homeostasis (184,194,195). MCR4 is widely expressed in the central nervous system, often alongside MCR3 such as in the hypothalamus and thalamus (192). In the periphery, there has been conflicting evidence of its expression in the human GI tract, and its peripheral functions are still not clear (196,197). MCR4 is an important central regulator of food intake, with disruptions of this gene causing hyperphagia and is the most common monogenic cause of obesity in humans (198,199). Briefly, leptin receptor activation causes central α -MSH release and MCR3/4 agonism, supressing food intake. This axis is described in further detail in Section 1.3.2. MCR4 has a similar binding affinity profile to MCR1, preferentially binding α-MSH=ACTH>β-MSH>γ-MSH (194). MCR5 is the most recent melanocortin receptor to be sequenced, and shares approximately 60% sequence homology with MCR4 (187,200). It is diffusely expressed in peripheral tissues including such as skeletal and cardiac muscle, skin, and exocrine glands (192,200,201). Very

little data exists, particularly in humans, establishing a physiological role for MCR5. The research that has been translated to human models has shown a potential role of MCR5 in sebocyte differentiation and sebum secretion in the skin (202–204). Our collaborator Professor Michael Cowley (Monash University, Melbourne) has pioneered investigation of MCR5 mediated glucose uptake in skeletal muscle and this work forms the backdrop to the human translation based studies in this thesis.3 (205,206).

1.3.2 Central Melanocortin Regulation of Food Intake in Humans

Central melanocortin system control of food intake is regulated by the balance of agonism of MCR3/4 by α-MSH and antagonism by NPY and AgRP occurring in POMC cells in the arcuate nucleus. MCR4 insufficiency in humans results in increased adipose and lean mass, hyperphagia, hyperinsulinaemia and obesity, accounting for approximately 5% of monogenic causes of obesity (198,207). Anatomically, neurovascular supply to the arcuate nucleus is permits direct input from the periphery, from hormones and nutrients outside the blood-brain-barrier(208).

Leptin, and to a lesser extent insulin, are the primary hormonal mediators of the anorexigenic effect of the central melanocortin system (180,209,210). Leptin is an adipokine secreted by adipose tissue at levels proportional to the amount of body fat, and insulin secreted by pancreatic β-cells in response to nutrients but also by the presence of fat mass in the long term. Leptin and insulin receptors are found in high concentrations in the arcuate nucleus, the primary site of central POMC expression (209,210). Activation of hypothalamic insulin receptor has been shown to play an important role in the control of food intake, with central administration of insulin enhancing satiety and ablation of brain-specific insulin receptor inducing hyperphagia and weight gain (210,211). The evidence for the anorectic function of insulin lies in its inhibition of endogenous melanocortin antagonist expression. In animals, central administration of insulin decreases AgRP mRNA expression therefor reducing the competition of α-MSH MCR3/4 binding (209,210).

The action of leptin on the central regulation of food intake is more established. Binding of leptin to its hypothalamic receptor hyperpolarizes POMC neurons, activating Janus kinase which phosphorylates LEPR-b, in turn activating STAT3. STAT3 binds to POMC gene promoters increasing the expression of the POMC precursor polypeptide and its

subsequent proteolytic product α-MSH (180,209,212). POMC neurons project from the arcuate nucleus to the paraventricular nucleus (PVN) which contains a high concentration of MCR3 and MCR4 that bind α-MSH. Melanocortin receptor activation in the PVN has been shown to modify vagal afferent fibre signalling from the gut which promotes satiety, (213,214). As demonstrated by genetic ablation, MCR3 does not appear to have as impactful a role as MCR4 in control of food intake. Knockout of MCR3 results in increased adiposity and reduced energy expenditure but does not affect food intake (215), whereas disruptions in MCR4 signalling result in profound obesity induced by hyperphagia, hyperinsulinaemia, and increased fat and lean mass (199,207). Setmelanotide (brand name Imcivree) is a first-in-class selective allosteric MCR4 agonist approved in 2021 for the treatment of obesity resulting from POMC, proprotein subtilisin/kexin type 1, or leptin receptor deficiency (186,216). Setmelanotide restores MCR4 signalling in disease states where the pathway is still intact but is lacking endogenous stimulation, in the Phase III trial weight loss of 10% over 1 year was observed in 80% of patients with POMC deficiency and 45% lacking leptin receptor (217).

The blockade of central MCR4 signalling by endogenous antagonists provided the first evidence of the role of the central nervous system in the control of energy balance. The agouti yellow mouse is one of the oldest models of genetic obesity (218,219). The cause for the phenotype of this model defined by a yellow coat, hyperphagia, increased fat and lean mass and obesity (218,219), became clear after the cloning of the melanocortin receptors in the 1990s when MCR4 was shown to be expressed in the hypothalamus (187,188). It was found that these mice overexpress agouti, a MCR1 and MCR4 antagonist which blocks MCR4 centrally to increase food intake and MCR1 peripherally to halt eumelanin production thus resulting in a distinct yellow coat (184,218,219). Whilst the innervation of POMC neurons to supress food intake is chronic in nature, the inhibitory actions of AgRP neurons can be acutely regulated by fasting (220,221). Ghrelin is secreted primarily by the stomach and circulating levels rapidly increase in the fasted state (222,223). Ghrelin is a ligand for the growth hormone secretagogue receptor (GHSR), which is expressed on neurons in the arcuate nucleus (212,224). Agonism of this receptor stimulates NPY and AgRP gene expression which antagonize the downstream anorectic effect of leptin and increase

food intake and obesity (225). Thus, ghrelin provides a potent acute inhibitory signal which contributes to its appetite stimulatory effects.

1.3.3 Peripheral α-MSH and Improvements in Glucose Tolerance

1.3.3.1 The Anterior Pituitary as the Source of Circulating α-MSH

In fasted humans plasma α-MSH levels fluctuate between 15-25 pM, rising ~3-fold postprandially (205,226,227). Whereas α-MSH derived from POMC cells in the skin and brain act on other tissues in a paracrine fashion, the endocrine pituitary releases α-MSH directly into circulation to act on peripheral tissue. It has been demonstrated that the anterior pituitary releases α-MSH independently of hypothalamic control in response to elevated blood glucose (205,228). Zelent et al. hypothesized that based on their discovery showing glucokinase, an enzyme traditionally serving as a glucose sensor in endocrine tissue, being highly expressed in anterior pituitary cells that it may serve to detect elevations in blood glucose and send paracrine signals to other pituitary cells (228). The mechanism is which this signal could be transduced, to what cell type, and the physiological relevance of this discovery was unknown at the time.

Recently, Enriori et al. established a link between this previously described glucose sensing ability of the pituitary and the postprandial increase in circulating α-MSH levels (205). Immunofluorescence imaging revealed high concentrations of α-MSH co-localized with ACTH in the pituitary of rhesus macaques. Additionally, in humans with panhypopituitarism and craniopharyngioma after surgery, α-MSH was undetectable in the circulation. These findings establish the pituitary as the source of peripheral α-MSH. To investigate whether elevated glucose levels were the cause of α-MSH release, glucose tolerance tests were performed in lean mice, monkeys, and humans. Following the glucose load, α-MSH levels increased while ACTH levels were unchanged despite the two peptides shown to be co-localized in the pituitary. In POMC-null mice, a glucose tolerance test produced no elevations in plasma α-MSH levels. These results support the hypothesis that glucose sensing cells in the pituitary are responsible for release of α-MSH into the periphery.

1.3.3.2 α-MSH Improves Post-Prandial Glucose Tolerance in Animals

Our collaborators have published extensive pre-clinical data describing a novel endocrine circuit in animals that improves post-prandial glucose tolerance through skeletal muscle glucose uptake mediated by MCR5 agonism(205,206). This body of work served as the basis for the first steps in translating these findings to humans that comprise the contents of this thesis. These pre-clinical data are summarised below.

1.3.3.2.1 Direct Action on Skeletal Muscle Improves Glucose Tolerance and Increase Glucose Uptake via MCR5

Incubation with α-MSH (100nM) significantly increased glucose uptake in rat and mice muscle explants and rat L6 myotubes. When co-incubated with insulin the effect size was further increased, suggesting the effects of the hormones on glucose uptake is additive. Systemic infusion of α-MSH in lean mice improves glucose tolerance during a GTT, and during a hyperinsulinaemic-euglycaemic clamp results in an increase in the glucose infusion rate required to maintain remain euglycaemia. These studies also demonstrated a direct increase in glucose disposal in gastrocnemius and soleus muscles. Additionally, systemic infusions in sheep raised post-prandial muscle temperature supporting the hypothesis that muscle takes up and utilizes glucose in response to α-MSH. Seahorse analysis suggested that the fate of glucose in response to α-MSH in rodent skeletal muscle is disposal via glycolysis.

A non-specific melanocortin agonist, α-MSH has binding affinity at MCR1, MCR3, MCR3, MCR4 and MCR5. Blockade of central MCR3/4 in mice by the endogenous antagonist AgRP did not abolish the glucose tolerising effects of α-MSH, eliminating the possibility the effect is mediated centrally by these receptors. Knocking out MCR5 abolished any effect α-MSH had on glucose uptake and clearance and administering the MCR5 specific agonist PG-901 in lean mice replicated the effect of α-MSH. These data strongly suggest that the effects of α-MSH on skeletal muscle are mediated by MCR5(205).

MCR5 is a $G_{\alpha s}$ protein coupled receptor, with its activation stimulating adenylyl cyclase to generate cAMP. After stimulation with α-MSH, cAMP levels in skeletal muscle were significantly elevated and treatment with a cAMP inhibitor blocked the effects of α-

MSH. In mice with diet-induced obesity (DIO) that underwent glucose tolerance tests and insulin clamps, the glucose lowering effects of α-MSH were ablated. Pre-treatment of DIO mice with a phosphodiesterase inhibitor, thus inhibiting the breakdown of cAMP, allowed α-MSH to produce similar effects to that found in lean mice. This establishes that α-MSH initially produces a signal through the classical cAMP mediated GPCR signalling pathway which is disrupted in mice with diet induced obesity.

1.3.3.2.2 Evidence for an Insulin-Independent Pathway

Møller et al. presents compelling proteomic evidence that the signalling mechanism behind α-MSH induced glucose uptake in rodent skeletal muscle is insulin independent (206).

Activation of MCRs lead to the generation of the signalling molecule cAMP as previously described. This in turn activates PKA which in turn phosphorylates AMPK, a kinase that plays a crucial role in the regulation of glucose transport in muscle. In muscle obtained from lean mice, α-MSH caused an increase in PKA and a dose-dependent increase in AMPK. When treated with a PKA inhibitor, α-MSH was still capable of inducing phosphorylation of AMPK suggesting this is independent of upstream PKA. AMPK phosphorylation in response to α-MSH was previously reported by An et al. in which data indicates that the peptide increases fatty acid oxidation in rat skeletal muscle (229). To investigate whether AMPK was also crucial in the signalling pathway that causes glucose uptake, muscle explants from AMPK-knockdown (AMPK-KD) mice were incubated with α-MSH and glucose uptake measured. AMPK-KD explants still displayed an increase in glucose uptake in response to α-MSH, suggesting that although the peptide does cause phosphorylation of AMPK this is not involved in glucose uptake.

TBC1D1 and TBC1D4 are phosphorylated to induce GLUT4 translocation as part of the exercise and insulin mediated glucose uptake pathways respectively. In AMPK-KD mice, TBC1D1 was phosphorylated independently of AMPK. In both wild type and AMPK-KD mice, TBC1D4 phosphorylation did not increase in response to α-MSH and instead displayed reduced phosphorylation of sites T642 and S704. To establish whether phosphorylation of TBC1D1 was mediated by PKA, phosphorylation of the protein was measured after treatment with a PKA inhibitor. No reduction in TBC1D1

phosphorylation was observed in mice treated with a PKA inhibitor compared to control. Finally, due to the aforementioned data showing TBC1D1 phosphorylation, GLUT4 translocation to the plasma membrane was measured after α-MSH stimulation. No increase in GLUT4 translocation was observed during α-MSH induced glucose uptake.

In summary, these data suggest α-MSH activates MCR5 to stimulate a cAMP dependant increase in glucose uptake in skeletal muscle that appears to be independent of traditional insulin and exercise mediated signalling mechanisms and translocated an unknown GLUT receptor to the plasma membrane of the myotube.

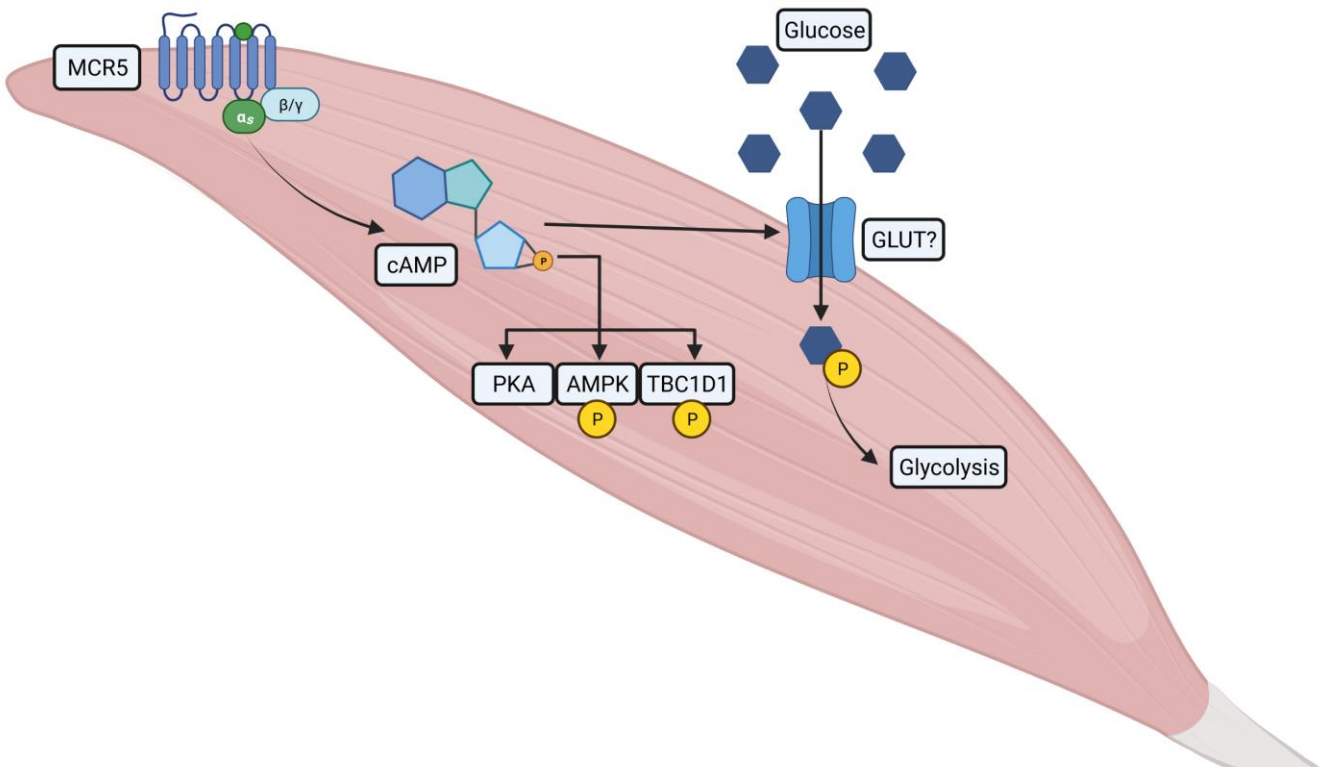

Figure 1.3 Molecular overview of MCR5 mediated glucose uptake in rodent skeletal muscle.

In rodent skeletal muscle, MCR5 agonism leads to cAMP generation by GPCRα_s mediated adenylyl cyclase activation which causes an unknown GLUT transporter to translocate to the plasma membrane and induce glucose uptake and glycolysis. PKA is activated, with AMPK and TBC1D1 being phosphorylated but these steps are not essential for glucose uptake.

1.4 Summary and Research Aims

Pre-clinical data demonstrates a role for α-MSH in skeletal muscle glucose uptake and utilization in animals. As a sequel to these findings, the aim of this research project was to take the first steps in translating these pre-clinical findings to human studies interrogating the glucoregulatory effect of α-MSH *in vitro* and *in vivo*. This was investigated using relevant *in vitro* primary culture models in addition to a clinical study in healthy volunteers, constituting the first time α-MSH will be continuously infused in humans.

Well-characterised human myotube cultures were first established using muscle biopsies obtained from healthy volunteers. In comparison to immortalized animal myotube cell lines, this primary human myotube model was used to increase translational relevance to human biology. The melanocortin receptor profile of the cell lines was then assessed and the impact of α-MSH on glucose uptake measured. This was the first study examining the effect of direct stimulation of melanocortin receptors in human skeletal muscle *in vitro* in any context. An MCR5 specific agonist was used to elucidate whether any effect may be mediated by MCR5. To further translate the findings from rodent myotubes, insulin was co-incubated with α-MSH to investigate whether any effects on glucose uptake are complimentary. Obese mice were previously reported to be resistant to the glucose tolerising effects of α-MSH. Using lipid loaded insulin resistant primary human myotubes treated with α-MSH, whether this phenomenon translated to human myotubes was investigated. Melanocortin receptor expression and response to α-MSH stimulation was assessed. This may assist in elucidating whether any effects on glucose uptake are muscle specific.

Finally, a first of its kind clinical investigation was carried out in which healthy volunteers were recruited to undergo OGTT and hyperinsulinaemic-euglycaemic clamps whilst being infused with various doses of α-MSH. In addition to glucose tolerance during OGTTs and glucose disposal during clamps, biochemical analysis was carried out to assess whether α-MSH has a concomitant impact on insulin and GLP-1 levels.

Aims:

1. To establish primary human myotube cell lines from biopsies obtained from healthy volunteers and validate using functional and transcriptomic approaches.
2. To interrogate whether α-MSH induces glucose uptake in the context of *in vitro* human skeletal muscle and adipocyte culture
3. To assess in healthy human volunteers, the effect of α-MSH on glucose tolerance during an oral glucose tolerance test and glucose disposal during hyperinsulinaemic-euglycaemic clamp.

Chapter Two

Establishment and Characterisation of Primary Human Myotube Models

2 Chapter 2: Establishment and Characterisation of Primary Human Myotube Models

2.1 Introduction

Muscle precursor cells, or myoblasts, are quiescent satellite cells found within the basal lamina of adult muscle that are released to repair damaged muscle or differentiate to form new multinucleated fibres(230–232). When isolated *in vitro*, myoblasts can be proliferated and terminally differentiated to mature, multinucleated myotubes. Myotubes cultures reflect the metabolic characteristics of their parent tissue(233–236) in addition to preserving the donor's genetic background thus allowing the establishment of cell lines from a known phenotypic background(21,119,237,238). This facilitates relevant *in vitro* models to be used in the study of peripheral glucose metabolism, particularly in diabetes research.

A large proportion of seminal *in vitro* studies on muscle glucose metabolism have used either the immortalized C2C12 cell line derived from mice(239), or the L6 cell line derived from rats(30,240). These rodent cell lines are readily available, do not require complex or expensive culture conditions, and are often used in commercial assay optimization thus ensuring compatibility. However, these models possess several key metabolic differences to human myotube cultures. In an extensive study by Abdelmoez et al., transcriptomic profiles and metabolic characteristics of L6, C2C12, and human myotube cell lines were compared (241). They found that in comparison to human myotubes, L6 cells have a lower rate of basal glucose uptake (decreased GLUT1 expression), a greater insulin-induced glucose uptake response (increased GLUT4 expression), and higher oxidative capacity. Similarly, C2C12 cells were shown to have a similar GLUT profile to L6 cells, and exhibited reduced glycolytic activity compared to human myotubes. This leads to a higher "fold-difference" of glucose uptake in insulin stimulated versus basal C2C12 and L6 cells when compared to human, and has been corroborated in numerous other studies (234,235,242,243). As such, when conducting experiments investigating potentially novel pathways in glucose metabolism, such as those found in Chapter 4, it is prudent to employ a model that will most accurately reflect the translational relevance of any novel findings to human biology.

Isolated human muscle samples are impractical to use as model to extensively study glucose uptake and related pathways due to the short timespan they are viable *ex vivo* and the heterogenous cell types found within samples. Human myoblasts can be isolated from the heterogenous cell population of skeletal muscle by enzymatic digestion or migration of cells out of a seeded muscle fragment (244–246). Once further purified, these myoblast cultures can then be expanded and differentiated to multinucleated myotubes which better represent the metabolic profile of adult skeletal muscle (242,247). With the derived cells retaining the metabolic characteristics of the donor, a volunteer cohort of a pre-defined phenotype, such as healthy volunteers, can be recruited to donate skeletal muscle biopsies which can then be used to establish a relevant *in vitro* model.

The aim of this chapter was to establish multiple characterized primary human myoblast cell lines from healthy volunteers to be used as a platform in which to conduct first-in-human *in vitro* experiments examining the novel role of α-MSH on skeletal muscle glucose uptake can then be conducted.

2.2 Methods

2.2.1 Muscle Biopsies from Healthy Volunteers

2.2.1.1 Ethical Approval

This study was approved by the UCD Human Research Ethics Committee (study reference LS-18-101-Docherty) to be conducted from February 2019 to August 2020.

2.2.1.2 Study Design

Healthy male and female adults were recruited to attend a screening visit in which eligibility was assessed against inclusion and exclusion criteria then if passing screened, attending a follow up visit in which a muscle biopsy of the *vastus lateralis* was taken. This muscle biopsy was then transported to the Conway Institute on ice and processed for downstream myogenic satellite cell isolation.

2.2.1.2.1 Inclusion and Exclusion Criteria

Participants were entered into the study based on the inclusion criteria of being between 18-50 years of age and capable of giving informed consent. Potential participants were excluded on the diagnosis of diabetes mellitus, a clotting disorder or active treatment with an anti-coagulant, and evidence of muscle wasting (sarcopenia).

2.2.1.2.2 Screening Visit

Potential participants first attended a screening visit at UCD. A doctor or nurse took medical history and conducted a physical examination which included anthropometric measurements and blood pressure and heart rate. Fasting blood glucose was measured via fingerprick blood sampling. If deemed eligible for the study, participants were given a copy of the patient information leaflet to review and the consent form to sign and bring to the follow-up muscle biopsy visit.

2.2.1.2.3 Muscle Biopsy Visit

Participants that passed the screening visit were invited to attend a follow-up visit in which microbiopsies of the *vastus lateralis* were obtained by a qualified medical doctor. Participants were allowed to rest and administered subcutaneous 2% lidocaine as a local anaesthetic. A 14G cannula was inserted at an angle directly into the skeletal muscle. A co-axial springle loaded needed was then repeatedly inserted into the cannula to obtain up to two 20mg muscle biopsies. These biopsy samples were placed

in a solution of DPBS with 1% penicillin streptomycin on ice and transported to the lab for processing.

2.2.2 Biopsy Digestion and Satellite Cell Isolation

2.2.2.1 Preparation of Enzymatic Digestion Solution

An enzymatic digestion solution was prepared **(Table 2.1)** and sterile filtered through a 0.2 µM membrane before being warmed to 37 °C.

	Specific activity/molar mass	**Final Concentration**	**Mass/Volume for 10mL solution**
Collagenase D	0.15 U/mg	10mg/mL	100mg
Dispase II	0.5 U/mg	4.8 mg/mL	48mg
250mM $CaCl_2$	110.98 g/mol	2.5 mM	100 uL

Table 2.1 Composition of enzymatic digestion solution for muscle biopsies

2.2.2.2 Mechanical and Enzymatic Digestion of Muscle Biopsies

In a sterile biosafety cabinet, biopsies were removed from DPBS and briefly submerged in 70% ethanol to eliminate microbial contamination. Biopsies were then washed in DPBS before being immerse in 1mL of warmed enzymatic solution in a petri dish to be minced with a scalpel and forceps. Any observable fat and fibrotic tissue were discarded. The enzymatic solution, sample and an additional 1mL of enzymatic solution was transferred to a 50mL falcon tube and incubated at 37°C for 40 minutes with gentle agitation every 5 minutes.

Two volumes (4mL) of warmed Skeletal Muscle Growth Medium (Cell Applications Inc. 151-500) was added to the enzymatic solution containing the sample to stop digestion and repeat pipetted 10 times to break up the biopsy. If any visible muscle fragments were present, they were incubated again with fresh enzymatic solution. Digested muscle was filtered through a 70 µM cell strainer and the suspension centrifuged at 443 x g for 5 minutes at room temperature. The supernatant was discarded, and the pellet resuspended in 2mL of warmed Skeletal Muscle Growth Medium.

2.2.2.3 Initial Seeding of Cell Suspension

Filter capped culture flasks were incubated with collagen coating solution (Cell Signalling Technologies 125-50) for 30 minutes at 37°C. The collagen solution was then discarded, yielding a culture surface coated with an extracellular collagen matrix. This coating technique was used for all further myoblast and myotube cultures.

Filtered cell suspensions were initially seeded in coated T25 culture flasks and left undisturbed for 24 hours. After 24 hours, the growth medium was changed to remove any debris and unattached cells, yielding a population of viable myoblasts and fibroblasts. Medium was replaced every 48-hours until cultures approached 80% confluency.

2.2.2.4 Pre-plating Technique

A technique known as pre-plating was employed to eliminate fibroblast contamination from the cell lines. When 80% confluency was reached in the culture vessel biopsy suspensions were initially seeded in, media was removed and incubated with TrypLE Express (ThermoFisher 12604013) until cells were visually observed to have detached. The cell suspension was aspirated and added to a falcon tube containing 2 volumes of warm DMEM, then centrifuged at 350 x g for 10 minutes at room temperature. The supernatant was discarded, and the pellet resuspended in warmed growth medium. The cell suspension was incubated undisturbed in an uncoated T75 culture flask for 40 minutes. The growth medium, containing the myoblasts unable to attach to the uncoated surface, was aspirated and seeded in a fresh collagen coated T75 flask with the fibroblasts eliminated by their attachment to the uncoated T75.

2.2.3 Culture of Primary Human Myoblasts and Myotubes

2.2.3.1 Expansion of Myoblast Cultures

Once myoblasts reached 80% confluency, they were passaged to avoid spontaneous differentiation to myotubes. Cells were detached using TrypLE Express as previously described and seeded at a density of 1:4 in new flasks.

2.2.3.2 Cryopreservation

Cells were detached as previously described and counted using the Countess™ Cell Counting System, then centrifuged at 350 x g for 10 minutes at room temperature and the pellet resuspended in growth medium supplemented with 8% dimethylsulphoxide

(DMSO) at a concentration of $1x10^6$ cells per millilitre. Suspended cells in 8% DMSO medium were transferred to cryovials and placed in a -80°C freezer within a Mr. Frosty™ freezing container for 24-hours before being transferred to liquid nitrogen. Aliquots of cells were cryopreserved at each passage.

2.2.3.3 Differentiation of Myoblasts to Myotubes

Once terminally differentiated to myotubes, the cells cannot be moved or further passaged. Myoblasts were seeded in flasks or plates to be used in experiments, and growth medium changed every 48 hours until the myoblasts reached maximum confluency. The medium used was then changed to Skeletal Muscle Differentiation Medium (Promocell C-23061) and replaced every 48 hours for 5-7 days. Once observed to have differentiated to elongated multinucleated myotubes, cells were used within 24 hours for further experiments.

2.2.3.4 Culture of Primary Human Adipocytes

Primary human preadipocytes were purchased from Merck (S802S-05A) and grown to confluency in Human Preadipocyte Growth Medium (Merck 811-500). Growth medium was changed every 48 hours. Once a fully confluent monolayer of preadipocytes was observed medium was changed to Human Adipocyte Differentiation Medium (811D-250) and changed every 48 hours. After 10-15 days differentiation of lipid filled adipocytes was complete.

2.2.4 Immunofluorescent Microscopy

The presence of desmin and myosin heavy chain isoform 3 (MHC3) was visualized by immunofluorescent microscopy in myotubes.

2.2.4.1 Cell Fixation and Staining

To prepare cells for immunofluorescence, cells in 6-well plates were first rinsed with DPBS before being fixed by 10-minute incubation in 4% formaldehyde at room temperature. Cells were rinsed again with DPBS and 1.5 mL blocking solution (DPBS containing 2% horse serum and 0.5% Triton X-100) was added and incubated for 30 minutes at room temperature. Blocking solution was aspirated and 1.5 mL primary antibody solution diluted 1:1000 in blocking solution (anti-desmin ab15200,MHC3 ab124205) was added to the fixed cells then incubated overnight at 4°C on a plate shaker. The next morning, primary antibody solution was removed, and cells washed twice with blocking solution, then incubated with 0.8 mL of secondary antibody solution

consisting of goat anti-rabbit AlexFluor® 488 diluted 1:1000 in blocking solution (Thermofisher A-11008) in the dark at room temperature for 1 hour. Cells were then washed twice with DPBS and incubated with 1 µg/ml DAPI solution in the dark at room temperature for 15 minutes. Cells were washed a final time with DPBS then 1 mL DPBS added to each well and visualized under an inverted fluorescent microscope.

2.2.4.2 Image Acquisition

Fixed and stained cells were visualized in the dark at 405nm (DAPI) and 488nm (AlexFluor® 488) under an inverted fluorescent microscope (Leica SP8) and images acquired at 10x and 40x magnification (AxioVision Viewer 4.8).

2.2.5 RNA Isolation

RNA isolation of both cell and tissue samples were carried out using the RNEasy mini kit (Qiagen 74104). On dry ice, 20mg of mice gastrocnemius muscle was transferred to a chilled round-bottomed eppendorf containing a metal tissue lysis bead. After chilling the sample on ice, 350 µL of RLT buffer was added and the eppendorf placed in the Tissue Lyser LT (Qiagen) then sonicated at 50 Hz for 5 minutes. Sample homogenate was then transferred to a new tube and 1 volume of 70% ethanol added. For the lysis of cell samples, RLT buffer was directly added to pelleted cells and pipetted repeatedly to lyse the sample.

The lysed sample was then transferred to RNEasy spin columns inserted into 2mL collection tubes. The spin columns were centrifuged at 13,500 RPM for 15 seconds at 4°C. The flow-through was discarded and DNase (Qiagen 79254) was added directly to the spin column membrane and allowed to sit at room temperature for 15 minutes. The spin column was then washed with 350 µL buffer RW1 and buffer discarded. 500 µL of buffer RPE was then added followed by centrifugation for 2 minutes at 13,500 RPM and 4°C. The spin column was removed from the waste collection tube and placed in a fresh 2mL eppendorf. 40 µL of sterile RNase free water was added to the column followed by a centrifugation step of 10,000 RPM for 1 minute at 4°C. The eluted water containing the extracted RNA was measured and qualified using the NanoDrop 2000 (ThermoFischer) and stored at -80°C.

2.2.6 RNA Quality Determination

The quality of the extracted RNA was determined using the Agilent 2100 bioanalyzer.

The bioanalyzer assays are based on a traditional gel electrophoresis technique in a chip format. Each chip contains a set of micro-channels that are filled with a polymer matrix and fluorescent dye. Once filled with gel, the chip represents a complete electric circuit. Charged molecules such as RNA are driven by a voltage gradient and separated by size. The dye binds with the RNA and this is detected by fluorescent measurements. Images and electropherograms are then generated. A ladder is run alongside samples so that migration time versus fragment size can be plotted, indicating the integrity of the RNA sample.

The procedure was carried out as per the manufacturers protocol. The gel dye matrix was prepared by mixing 65 µL of filtered matrix gel with 1 µL of dye. This solution was then vortexed briefly and centrifuged for 10 minutes at 10,000 x g. The chip was primed by pipetting 9 µL of dye into a designated well and placing it in the chip loading station. Five microliters of marker were loaded in every well. Samples and ladders were denatured by heating to 70°C for 2 minutes and then 1 µL of each denatured sample added to each well. The chip was then run by the machine within 5 minutes of preparation.

2.2.7 cDNA Synthesis

First strand cDNA synthesis was performed with 1 µg of RNA using Superscript II reverse transcriptase according to manufactures protocol. Two controls were set up: a no template control containing no RNA, and a reverse transcriptase control containing no superscript. Reactions were carried out in RNAse free PCR reaction tubes and a tube was prepared for each sample as per **Table 2.2.**

Component	Amount per sample
RNA	1 µg in 2 µL
DEPC water	6 µL
10x DNase buffer	1 µL
Total	8 µL

Table 2.2 cDNA Synthesis Master Mix 1

Samples were DNAse treated with 1 μl of DNase for 10 minutes at room temperature. DNase was then neutralized by adding 1 μl of EDTA followed by incubation at 65°C for 10 minutes using a thermo cycler (T3000 Biometra). A master mix was set up as per **Table 2.3.**

Component	**Amount per reaction**
50 ng/ μl Random Primer	1 μl
5 X First Strand Buffer	4 μl
0.1M DTT	2 μl
10mM dNTP	1 μl
TOTAL	**8 μl**

Table 2.3 cDNA Synthesis Master Mix 2

cDNA master mix 2 (8 μl) was added to each sample and mixed. The samples were incubated at 65°C for 5 minutes followed by 25°C for 2 minutes. Superscript II reverse transcriptase (1 μl) was added to each sample and mixed gently. The reaction tubes were returned to the thermo cycler for the remaining steps: 25°C for 10 minutes, 42°C for 50 minutes and 70°C for 10 minutes. cDNA was stored at -20°C.

2.2.8 Real Time Polymerase Chain Reaction

In real-time PCR, the quantity of DNA is determined after each cycle via fluorescent dyes whereby the increasing fluorescent signal is directly proportional to the number of PCR amplicons generated. Amplification plots are then generated by plotting fluorescent signal from each sample against cycle number which represents the accumulation of product over the duration of the experiment.

For endogenous controls, 18S was used for mice gastrocnemius samples and human GAPDH for myoblast, myotube and adipocyte samples. A list of TaqMan assays used for gene expression studies can be seen in **Table 2.4.**

Taqman Assay	Gene	TaqMan Assay ID
Mouse melanocortin receptor 5	Mc5r	Mm00442970_m1
Human melanocortin receptor 1	Mc1r	Hs00267167_s1
Human melanocortin receptor 3	Mc3r	Hs01562847_s1
Human melanocortin receptor 4	Mc4r	Hs00271877_s1
Human melanocortin receptor 5	Mc5r	Hs00271882_s1
Human insulin receptor	INSR	Hs00961557_m1
Human myosin heavy chain 3	MYH3	Hs01074230_m1
18S	18S	Hs03003631_g1
Human GAPDH	GAPDH	Hs02786624_g1

Table 2.4 Taqman assays used

Reactions were carried out in duplicate for each sample within each assay run. A PCR master mix was prepared for each gene target as outlined in **Table 2.5**. Sufficient master mix was prepared for all samples, reverse transcriptase control, no template control and to account for pipetting error. The master mix was vortexed and centrifuged briefly.

Reagent	Volume per sample
Target probe	1 µL
PCR master mix	10 µL
DEPC water	8 µL
Total	**19 µL**

Table 2.5 PCR Master Mix

Eppendorfs were labelled for each sample and 19 µl of master mix was pipetted into each. cDNA (1 µl) was added into its corresponding eppendorf. Samples were vortexed and centrifuged briefly and 9 µl was carefully pipetted in duplicate into a 384 well plate. The plate was sealed and vortexed briefly. Quantitative RT PCR was performed using QuantStudioTM 7 Flex System. Comparative quantification was used for analysis using the $\Delta\Delta C_t$ method which compares results from experimental samples with both a calibrator (untreated) and a normalizer (18S housekeeping gene). Using this method, the C_t value for the gene of interest is normalized by the C_t value for the housekeeping gene.

The ΔCt for the sample is calculated by subtracting the $Ct_{\text{endogenous control}}$ from the $Ct_{\text{target gene}}$. As the purpose of these PCR experiments was to confirm the expression or absence of target gene expression, the ΔCt were used as the endpoint of this experiment for data analysis.

2.2.9 Palmitic Acid Conjugation

In vivo free fatty acids are bound to carrier proteins to facilitate their uptake by cells. Bovine serum albumin (BSA) was used as a carrier protein for *in vitro* experiments involving palmitic acid.

Lyophilized palmitic acid was first dissolved in 100% ethanol at a concentration of 500mM and incubated at 70°C to fully dissolve. This 500mM stock solution was then added to 10% BSA (Merck A1595-50ML) to yield a palmitic acid concentration of 1.5 mM and a palmitic acid to BSA ratio of 3.3:1. To conjugate the BSA and palmitic acid, the mixture was incubated with agitation at 40°C for 30 minutes. The conjugated solution was then sterile filtered in a biosafety cabinet and added to Skeletal Muscle

Differentiation Medium to yield a final concentration in medium of 0.75 mM. Myotubes were then incubated with this fatty acid supplemented medium in the final 24-hours of differentiation in experiments requiring ectopic lipid accumulation.

2.2.10 Oil Red O Stain

Oil Red O was used to stain for ectopic lipid accumulation after incubation with palmitic acid supplemented culture medium. Cells were first rinsed twice with sterile DPBS then incubated with 10% formalin for 1 hour at room temperature to fix. The formalin was then aspirated, and cells gently washed twice more with DPBS. Cells were incubated with 60% isopropanol at room temperature for 5 minutes. The isopropanol was aspirated, and Oil Red O solution (Merck O1391) was gently pipetted onto the cells and allowed to sit for 5 minutes. The oil red o solution was removed, and the cells repeatedly rinsed with water until no visible stain remained. Intracellular lipid was observed in red by visualization under an inverted light microscope.

To perform semi-quantitative analysis, Oil Red O was solubilized from fixed cells by incubation with 100% isopropanol for 10 minutes. The solubilized Oil Red O in solution was then measured for absorbance at 492 nM in a plate reader (BMG Labtech Clariostar).

2.2.11 Cell Treatments Preparation

2.2.11.1 Insulin

Recombinant human insulin in solution at a concentration of 1.8 mM was purchased from Merck (I19278). Insulin solution was diluted in serum and glucose free DMEM to yield a concentration of 1.8 µM stock solution and frozen. This was further diluted to 10nM in serum and glucose free DMEM for use as a working solution in cell treatments.

2.2.11.2 Radiolabelled 2-deoxy-D-glucose

A working solution consisting of both labelled and unlabelled 2-deoxy-D-glucose was prepared for use in glucose uptake assays.

2-deoxy-D-glucose (Merck D8375-10MG) was dissolved in DPBS supplemented with 0.2% BSA for a concentration of 304.5 mM, then sterile filtered and stored in the fridge. On the day of experiment 137 µL of this unlabelled 2-deoxy-D-glucose was

supplemented with 13 µL of tritiated [^{3}H] 2-deoxy-D-glucose (PerkinElmer NET549250UC) to yield a concentration of 278 mM and 83 µCi/mL. This was sufficient for 25 wells of a 24-well plate.

2.2.12 Measurement of Glucose Uptake

The principle of using measuring the radioactivity of cell lysates by liquid scintillation counting after incubation with glucose labelled with a radioisotope as a proxy for glucose uptake was employed in myotubes and adipocytes.

2.2.12.1 Glucose Uptake Assay

Cells in 24-well plates were first serum starved for 6-hours by incubating with low glucose serum-free DMEM (Lonza BE12-707F). In the final hour of this serum starvation, media was changed to serum and glucose free DMEM (Lonza BE12-604F) to glucose starve the cells. Three hundred microliters of experimental treatments (preparation detailed in Section 2.12) were added to duplicate or triplicate wells depending on the experiment and placed in an incubator for 1 hour. The basal control for each experiment was cells incubated with serum and glucose free DMEM during this 1-hour treatment incubation time. After 1 hour, 6 µL (0.5 µCi) of the radiolabelled 2-deoxy-D-glucose (preparation detailed in Section 2.12.4) was swiftly added directly to the treatment media and gently agitated then placed in the incubator for 10 minutes. After 10 minutes, 24-well plates were placed immediately on ice and media containing the treatment and labelled glucose swiftly aspirated. Cells were then rinsed 3 times with ice-cold DPBS. To lyse the cells, 600 µL of Cell Lytic™ MT (Merck C3228-50ML) was added to each well and incubated with gentle agitation in the cold room for 30 minutes. Once lysis was visually confirmed under a microscope, radioactive lysates were transferred to eppendorfs. To 4 mL of Ultima Gold™ liquid scintillation fluid (Merck L8286-5L) in liquid scintillation counting vials, 400 µL of cell lysate was added and vortexed. These vials were then placed in a liquid scintillation counter (Perkin Elmer Tri-Carb 5100TR) and counts per minute measure for 1 minute per sample.

2.2.12.2 Protein Normalization

An aliquot of lysates from the glucose uptake assay was retained for protein quantification and normalization. The Pierce™ BCA Protein assay (ThermoScientific 23225) was carried out according to manufacturer's protocol. In duplicate, 25 µL of cell lysate was added to wells of a 96-well plate. BCA working reagent was prepared by adding 50 parts Reagent A to 1 part Reagent B, and 200 µL of working reagent was added to each standard and sample well. The plate was gently agitated then incubated for 30 minutes at 37°C before absorbance at 562 measured in a spectrophotometer. The concentration of protein in µg/mL was used to normalize the CPM gained from measuring the radioactivity of 400 µL cell lysate by liquid scintillation counting, and glucose uptake was expressed as cpm/µg protein.

2.3 Results

2.3.1 Seeding of Myoblasts from Biopsies

Six discrete cultures of proliferating primary myoblasts from six different participants were successfully established. Initial yield from biopsy digestion was low **(Fig 2.1 A)** however, after the first passage and pre-plating step a stable culture was established **(Fig 2.1 B)**. Of the six participants who yielded stable cultures, there were 2 females and 4 males with a mean age of 29 ± 5.5 and BMI of 22.5 ± 2.6 . Aliquots of cells were taken during the first four passages for cryopreservation.

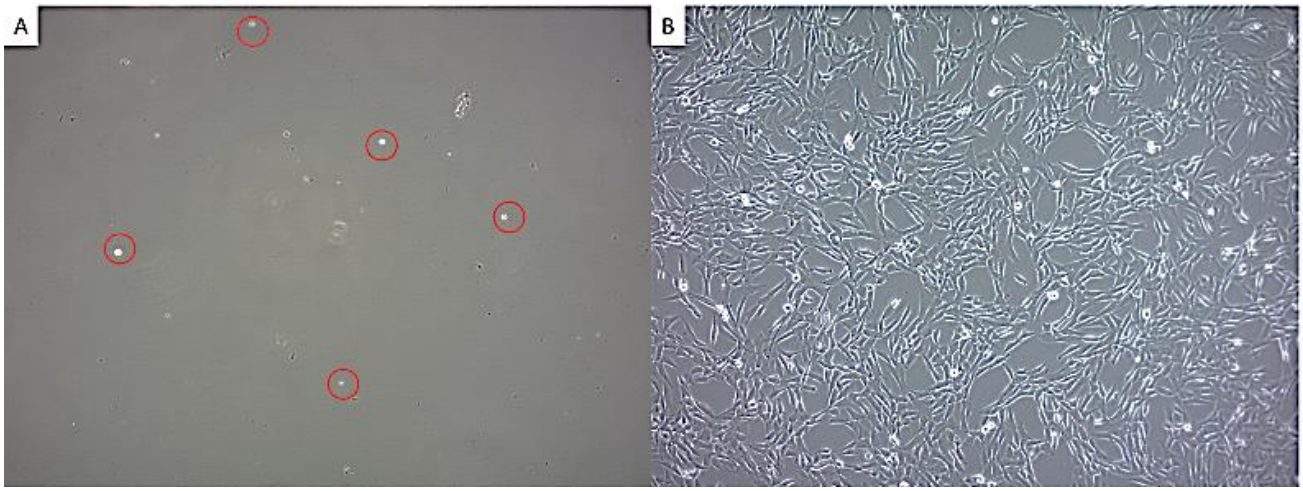

Figure 2.1 Initial cell yield and establishment of stable primary myoblast culture.

A) 10x light microscope image taken 6 hours after seeding the cell suspension gained from the biopsy digestion. Myoblasts that have attached to the collagen coated surface highlighted in red. B) 10x light microscope image taken at Passage 2 of stable myoblast culture after fibroblast contamination has been eliminated in pre-plating.

2.3.2 Assessment of Cell Line Purity

To confirm a pure myoblast culture had been obtained from biopsies, and fibroblasts eliminated, each of the six myoblast cell lines were stained for desmin and visualised under a fluorescent microscope after passage 2. Cultures of undifferentiated, mononucleated myoblasts were confirmed by staining positive for desmin **(Fig 2.2 overleaf)**.

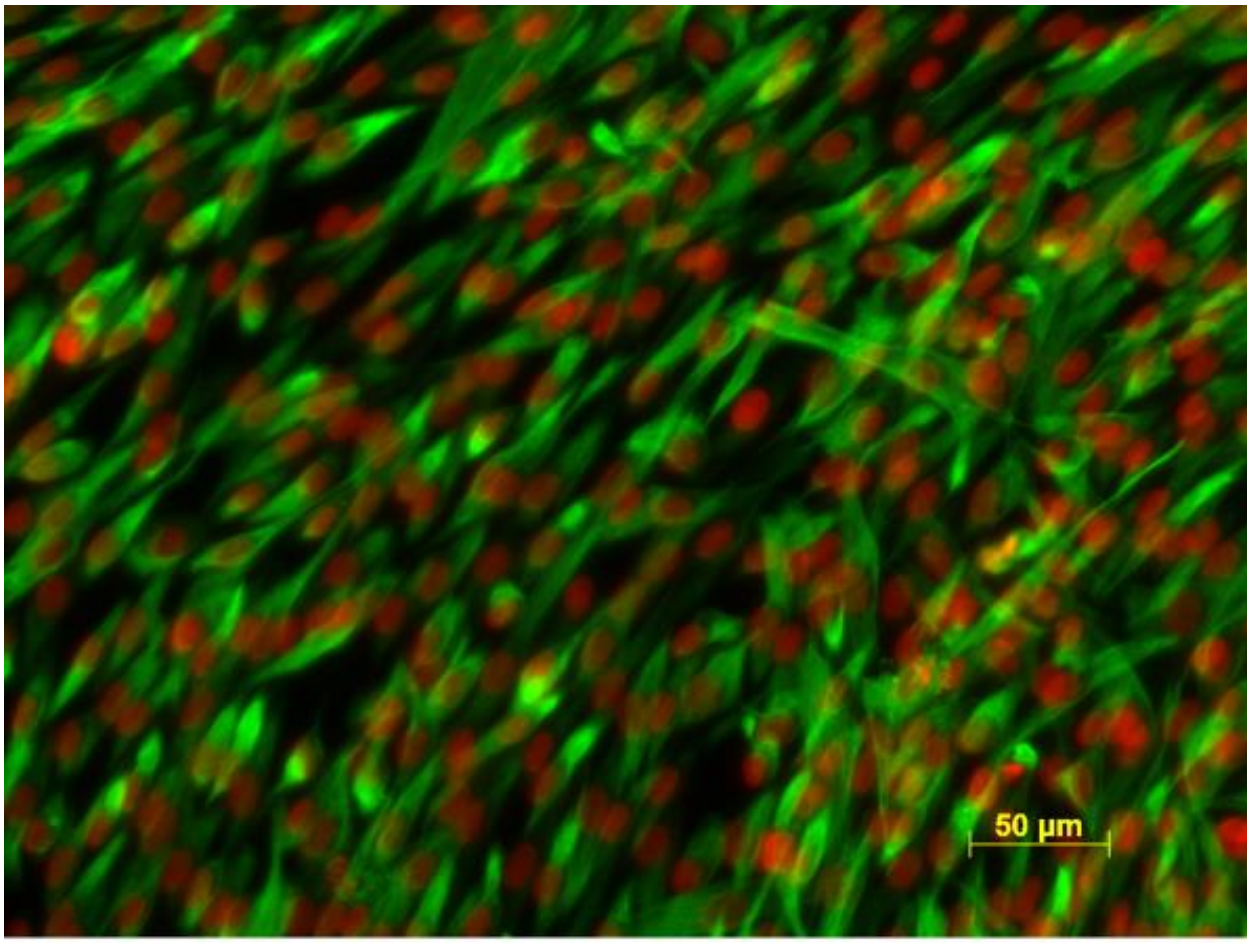

Figure 2.2 Immunofluorescent desmin expression in primary myoblasts.

Representative immunofluorescent image of a pure myoblast culture expressing desmin (green). Nuclei shown in red.

2.3.3 Assessment of Capacity to Differentiate

Mononucleated myoblast cultures were assessed for their capacity to differentiate to form mature multinucleated myotubes. After reaching confluency, culture media was switched from growth to a differentiation formulation and observed over 7 days under a light microscope. During incubation with differentiation medium, myoblasts were observed to align, elongate then fuse to form mature striated myotubes after 5-7 days **(Fig. 2.3 overleaf)**.

To confirm the myoblasts had successfully differentiated, the presence of the structural contractile protein myosin heavy chain 3 (MHC3) was observed via immunofluorescence and substantiated by qRT-PCR. Immunofluorescent images from post-mitotic cultures of each cell line indicated the myoblasts had fused to form multinucleated myotubes and express MHC3. A population of myoblasts in each culture, approximately 30%, do not terminally differentiate and can be seen by the nuclei not expressing MHC3 **(Fig 2.4 A overleaf)**. Increased expression of MHC3 mRNA demonstrated by RT-qPCR was used to validate differentiation, with uniform expression observed across all six cell lines. MHC3 mRNA was present at varying levels in myoblasts as spontaneous differentiation occurs when the cultures approach the confluency required for RNA isolation **(Fig 2.4 B overleaf).**

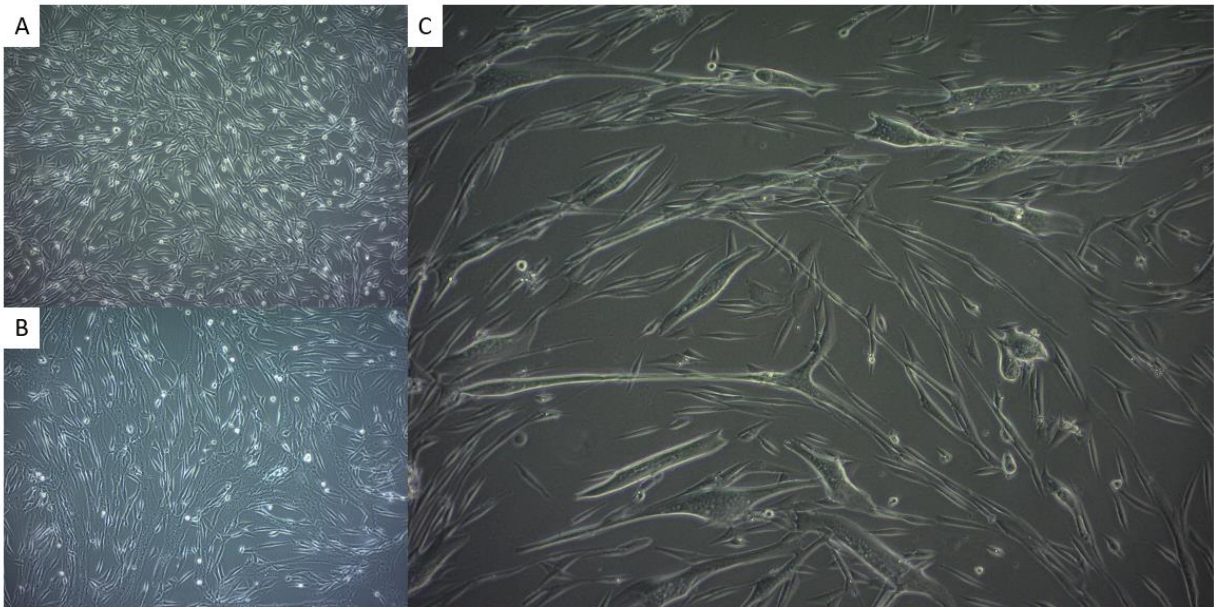

Figure 2.3 Differentiation timeline of myoblasts to myotubes.

Representative images taken under light microscope at 10x magnification. A) 2 days after commencing incubation with differentiation medium cells begin to align and elongate. B) 4 days after beginning differentiation, cells begin to fuse and begin forming multinucleated cells. C) Between 5 and 7 days of differentiating, the myoblasts are terminally differentiated into striated, multinucleated myotubes.

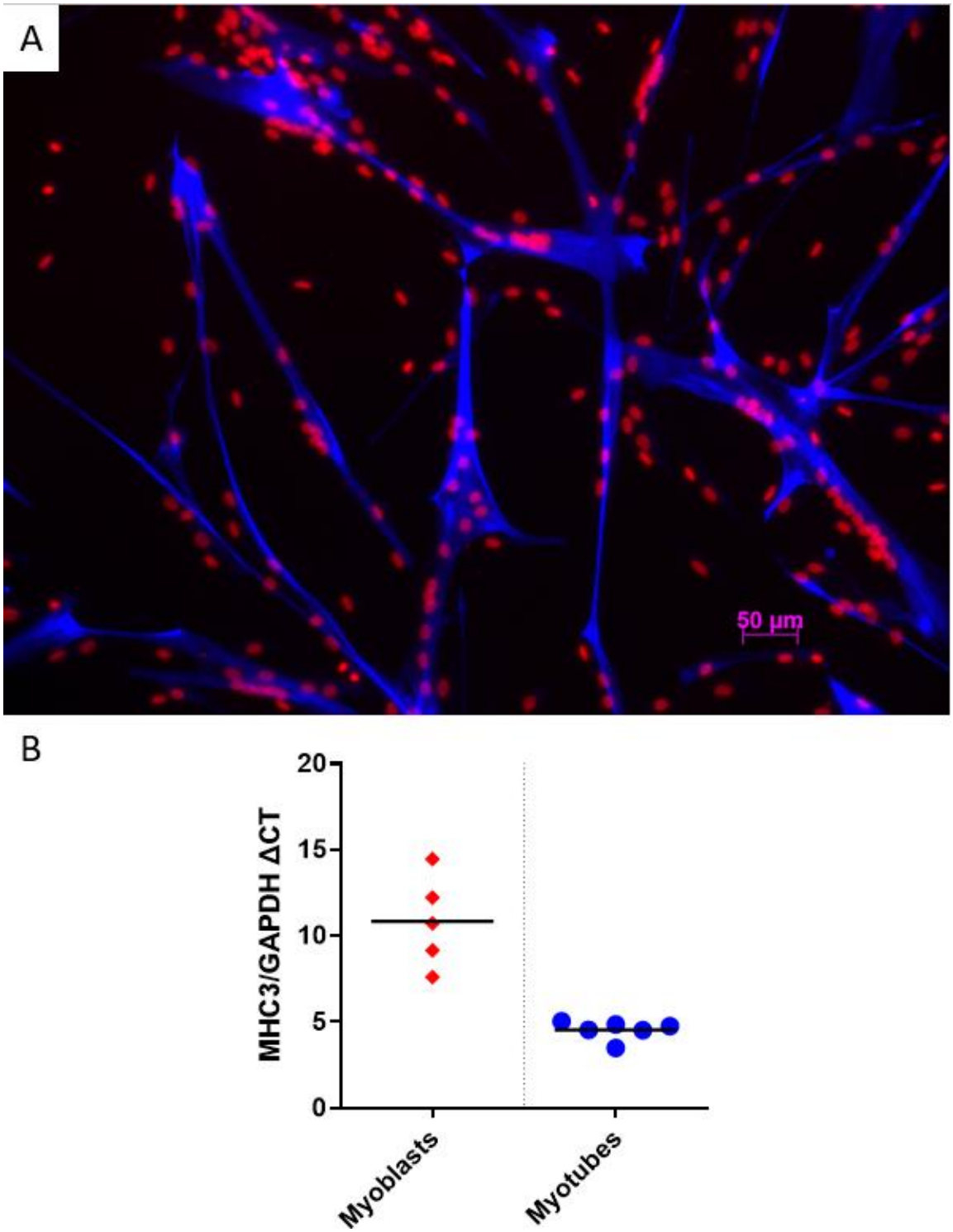

Figure 2.4 Contractile protein expression in mature differentiated myotubes.

Myotubes express the structural protein MHC3 when differentiated. A) Representative immunofluorescent image of myotube cultures expressing MHC3 (blue) after 5-7 days of differentiation. Nuclei shown in red. B) Myoblast and myotube MHC3 mRNA levels as assessed by qRT-PCR. Each data point represents a discrete cell line n=6.

2.3.4 Insulin Receptor Profile and Response

2.3.4.1 Presence of Insulin Receptor

qRT-PCR was used to confirm the presence of insulin receptor in established myotube lines. Insulin receptor was consistently found to be present in high abundance across all cell lines **(Fig 2.5)**.

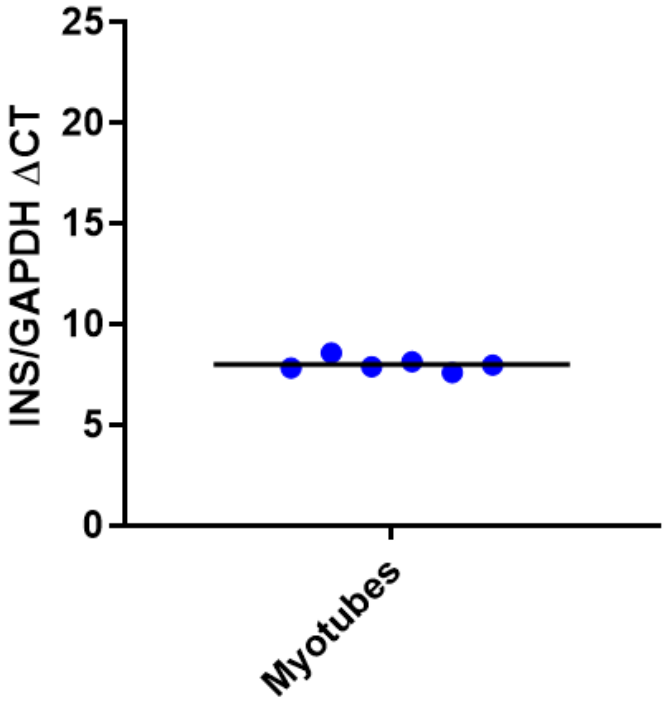

Figure 2.5 Presence of insulin receptor in myotubes.

Insulin receptor mRNA levels in established cell lines with GAPDH used as a reference gene. Insulin receptor was found in high abundance across all lines (mean ΔCT=7.99).

2.3.4.2 Insulin Stimulated Glucose Uptake

One-hour incubation of myotubes with 10nM insulin significantly increased glucose uptake over untreated control as measured by uptake of tritiated 2-deoxy-D-glucose via liquid scintillation counting (7.88 CPM/µg ± 2.5 vs. 16.66 CPM/µg ± 1.6, unpaired t-test $p<0.0001$) **(Fig. 2.6 overleaf)**. In a dose-response experiment, 10nM insulin was found to produce the maximal glucose uptake response, with no further increment at 100nM (Appendix 6.2)

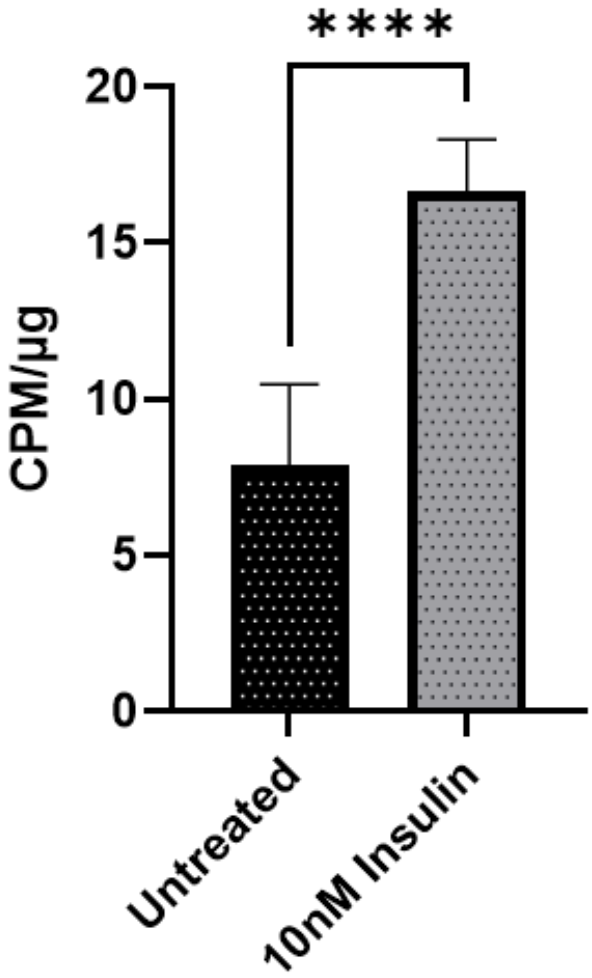

Figure 2.6 Glucose uptake in response to insulin in myotubes.

*Glucose uptake represented as counts per minute (CPM) of cell lysates as measured by liquid scintillation counting normalized by protein content (n=6). ****p<0.0005 vs Untreated. Data are presented as mean ± standard deviation. Statistical analysis was performed with unpaired t-test.*

2.3.5 Establishment of Insulin Resistant Lipid-Loaded Myotube Model

Differentiated myotubes were incubated with 0.75mM palmitic acid conjugated to bovine serum albumin to induce ectopic lipid accumulation and downstream impairment of insulin induced glucose uptake.

2.3.5.1 Ectopic Lipid Accumulation in Myotubes

Myotubes incubated with differentiation medium supplemented with 0.75 mM BSA-conjugated palmitic acid for 24 hours exhibit intracellular lipid accumulation **(Fig. 2.7 overleaf)**. Incubation with conjugated palmitic acid at concentrations of 0.25 mM and 0.50 mM did not ablate the insulin induced glucose uptake response (Appendix 6.3).

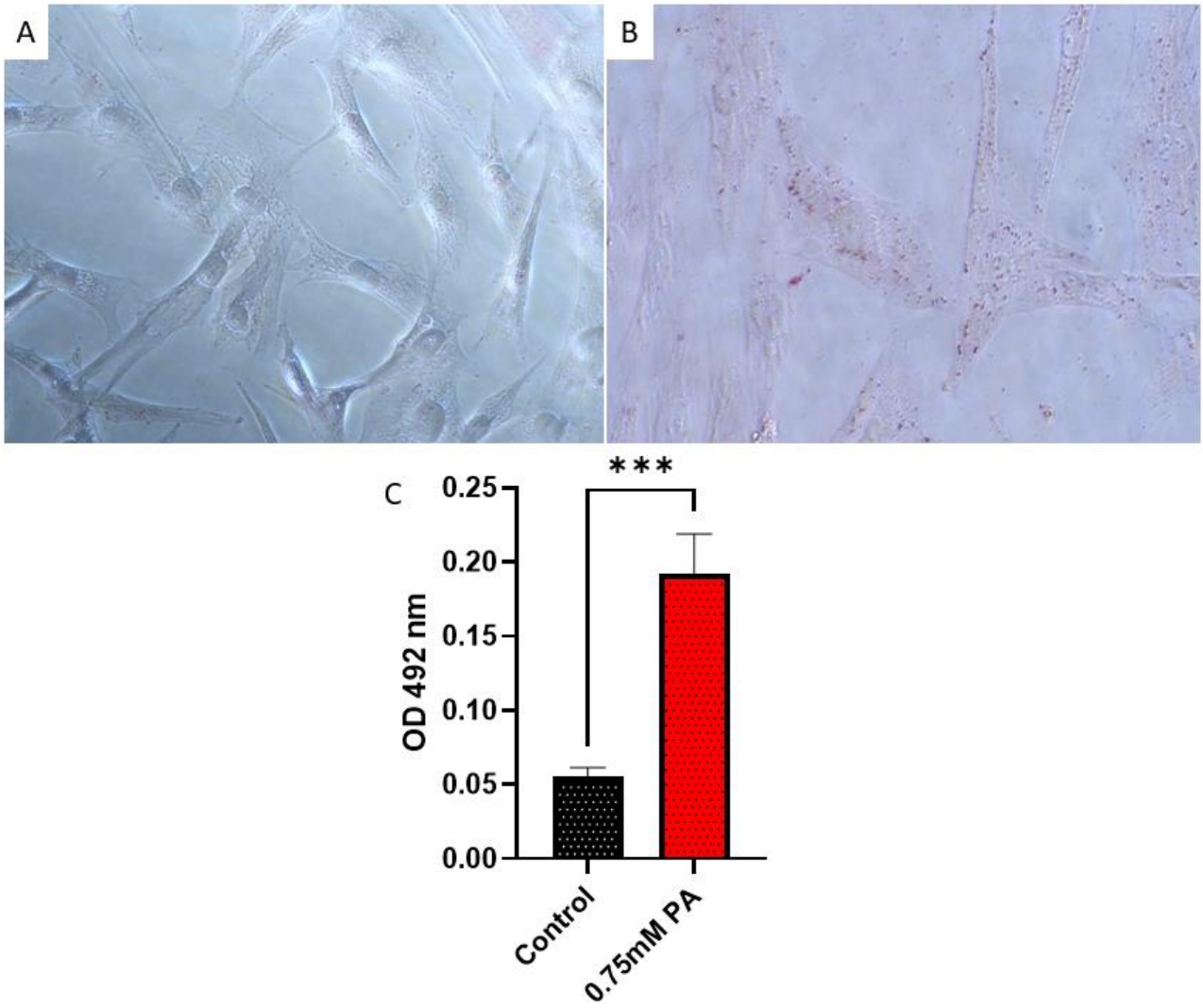

Figure 2.7 Ectopic lipid accumulation after incubation with palmitic acid.

Myotubes incubated with palmitic acid accumulate ectopic lipid droplets. Cells stained with Oil Red O demonstrate intracellular lipid accumulation after incubation with palmitic acid (A-Control, B- 0.75mM palmitic acid, 40x magnification). C) Semi-quantitative measurement of oil red o extracted from fixed cells shows significant increased absorption at 492 nm after 0.75mM palmitic acid treatment (n=3, unpaired t-test p<0.0005).

2.3.5.2 Glucose Uptake in Lipid-Loaded Myotubes

Insulin induced glucose uptake was measured in myotubes after 24-hour incubation with 0.75 mM palmitic acid. Glucose uptake in lipid-loaded myotubes treated with insulin was reduced compared to myotubes treated with insulin and without palmitic acid **(Fig. 2.8)**.

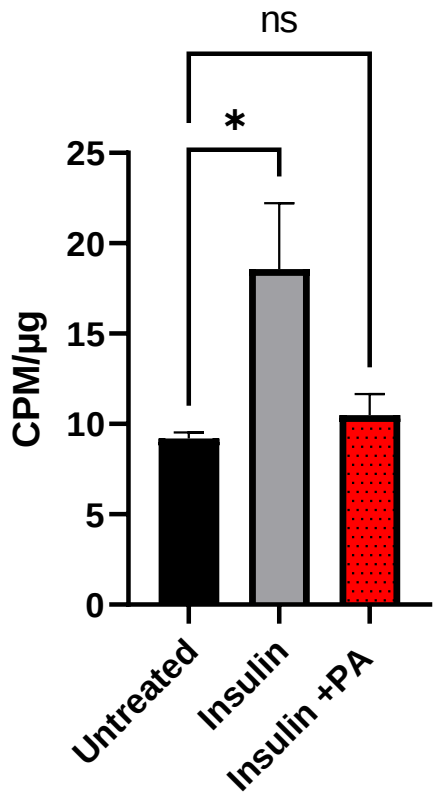

Figure 2.8 Insulin resistance induced by ectopic lipid accumulation.

*Glucose uptake represented as counts per minute (CPM) of cell lysates as measured by liquid scintillation counting normalized by protein content (n=4). *p<0.05 vs Insulin. Data are presented as mean ± standard deviation. Statistical analysis was performed with one-way ANOVA and post-hoc Dunnett's multiple comparisons test.*

2.4 Discussion

The aim of this chapter was to establish multiple characterized primary human myoblast cell lines from healthy volunteers to be used as a platform in which the first human *in vitro* experiments examining the novel role of α-MSH on skeletal muscle glucose uptake can then be conducted. Strict criteria were laid out that the established myotubes must meet in order to be used for further experiments in that they must be free from fibroblast contamination, display normal morphology and mitotic behaviour, capacity to differentiate into mature myotubes, and exhibit basal and insulin-stimulated glucose uptake and lipid induced insulin resistance at levels in line with published data.

In a study approved by the UCD Human Research Ethics Committee, fifteen healthy volunteers between the ages of 18-50 with no history of metabolic complications were recruited to donate *vastus lateralis* skeletal muscle biopsies under local anaesthesia. From each participant, a maximum of two ~20mg biopsies were obtained and pooled together for downstream enzymatic digestion following published protocol (245,248). As muscle biopsies were obtained by repeated insertions of a co-axial biopsy needle into an *in-situ* cannula, tissue obtained beyond the second needle insertion resulted in significantly increased intramuscular haemorrhaging and thus were not used in downstream isolation due to the risk of non-myogenic cell type contamination. From the fifteen pooled biopsy samples obtained from participants, six of these were successfully established as stable myoblast cell lines.

Cell suspensions derived from enzymatically digested human skeletal muscle contain an abundance of fibroblasts which if co-cultured with myoblasts, will quickly overrun the culture (249,250). A technique known as pre-plating was employed during the first passage to eliminate fibroblast contamination. Once the cell suspension that was initially seeded follow biopsy digestion forms a confluent monolayer on the collagen-coated culture flask, the cells are detached and incubated in an uncoated culture flask for 45 minutes. Unlike myoblasts, fibroblasts do not need a protein matrix such as collagen to attach to in vitro, and as such will readily adhere to the flask during this incubation step. The cell suspension that is harvested after 45 minutes from this uncoated flask contains a pure myogenic cell population that can be further expanded. The larger, star-like fibroblasts were observed to have attached in the uncoated flask

during this step. To confirm a pure population of myoblasts all cell lines were screened for positive desmin expression, a marker of myogenic cells not found in fibroblasts, via immunofluorescent microscopy prior to further expansion.

Myotubes are mature muscle cells containing highly organized contractile protein structures and comprised of up to thousands of post-mitotic myonuclei. These myotubes are formed during a process known as myogenesis, which is characterized by the fusing of the mononucleated myoblasts into elongated, multinucleated myotubes and the formation of protein structures that comprise the sarcomere, the basic contractile unit in mature skeletal muscle(237,251). The established cell lines were confirmed to have myogenic potential after being cultured in conditions promoting differentiation for 5-7 days. Elongated, multinucleated cells were visually confirmed under phase-contrast microscopy. Relative levels of myosin heavy chain 3 (MHC3) expression, a marker of mature myotube formation (248), between myoblasts and myotubes was assessed by qRT-PCR and found to be consistently increased in post-mitotic cells. At the confluency that these myoblasts were required to be cultured at for sufficient RNA isolation, spontaneous differentiation began to occur, thus leading to increased MHC3 levels in myoblasts and a lower relative increase in expression in myotubes in comparison. Although the difference in MHC3 expression between the two cell sub-types shown may be lower than expected due to spontaneous differentiation in myoblasts, the consistent increase in this protein expression in mature myotubes can be interpreted as sign of successfully differentiation. GAPDH was used as a reference gene for this analysis and all subsequent transcriptomic analysis as it's expression is stable in differentiated myotubes, as well as remaining relatively unchanged before and after the differentiation process (252). MHC3 was also visualized by immunofluorescent microscopy, with the striated contractile structures clearly visible within multinucleated cells.

A significant population of myoblasts, approximately 30%, were not observed to differentiate even after extended periods in differentiation medium. This phenomenon is frequently observed in human myoblast cultures (245,247,248), and it has been suggested that myoblasts are not a homogenous cell type that are all capable of terminal differentiation and instead adopt divergent fates, with some myoblasts

remaining in a quiescent state in vitro mimicking the pool of myogenic satellite cells found within intact muscle tissue in vivo (253,254).

In the early stages of experimental protocol optimisations, it was found that in 96-well culture plates myoblasts fail to differentiate into elongated multinucleated myotubes. During the differentiation process, instead of elongating and fusing, myoblasts would aggregate then detach from the culture surface. Several variations of culture plastics and extracellular matrix coatings were used in an attempt to induce differentiation in 96-well plates but were unsuccessful, this phenomenon was not found to be reported in published protocols. We hypothesise this is due to the decreased culture surface area of 96-well plates not providing enough space for the several millimetre-long myotubes to develop, as myotube formation was successful in culture surface areas equivalent to 48-well plates and above. This proved to be an obstacle in conducting several experiments that were designed to function in a 96-well plate setting. For example, significant attempts were made to convert the Agilent pH-Xtra Glycolysis assay from the intended 96-well plate setup to a 48-well and despite technical support, a reliable signal could not be obtained from the assay using myotubes in this setting. Similarly, myotube formation could not be induced in Seahorse compatible culture cartridges as they have half the surface area of 96-well plates. Therefore, it was not feasible to obtain data on the glycolytic capabilities of α-MSH, as demonstrated in animal models *in vitro* (205), during the course of this project.

Human primary myotubes retain the insulin-mediated glucose uptake signalling pathway found in their parent tissue (21,238,241–243), allowing cultured myotubes to act as a suitable model for skeletal muscle glucose uptake *in vitro*. To ensure the myogenic cell lines established were capable of normal insulin induced glucose uptake, the presence of insulin receptor and capability for downstream glucose uptake was assessed. Using qRT-PCR, insulin receptor was found to be abundant and consistent across the six cell lines. Measurement of tritiated 2-deoxy-D-glucose taken up by the cell after 1-hour treatment with 10nM insulin resulted in a 2-fold increase in glucose uptake over the basal state. This proportional increase in insulin stimulated glucose uptake is consistent with those levels widely published (238,242,243). An effort was made to increase the effect size by prolonged serum starvation prior to the

glucose uptake assay, however the 6-hour serum starvation used was the maximum time in these conditions before detachment of the myotubes were observed

The main disadvantage of using primary human myotubes in this context is the effect size of an insulin treatment on glucose uptake compared to the basal state is not equivalent to that observed *in vivo,* which is closer to an 8-10-fold difference. This is due to the significantly elevated GLUT1 transporters found in cultured myotubes (241). Although it is possible to reduce GLUT1 levels through RNA interference (255), this may detract from the benefits of having a primary, unaltered cell line derived from humans with a known phenotype. However, this increase in basal glucose uptake should not be significant enough to mask any increases in glucose uptake in response to a treatment.

Elevated levels of circulating free fatty acids are linked to metabolic disorders such as obesity and Type 2 diabetes, and lead to defects in skeletal muscle insulin signalling mediated by intramuscular lipid accumulation (124,125,256). An *in vitro* model commonly employed to study these lipotoxic effects on glucose uptake is one in which intracellular lipid accumulation is induced by extended incubation in media supplemented with high levels of free fatty acids(257–259). This leads to accumulation of neutral lipids in particular ceramides and diacylglycerols (258,260) which then leads to downstream defects in Akt/PKB activation and inhibited GLUT4 trafficking to the plasma membrane (260). The primary human myoblast cell lines established in this chapter were incubated with differentiation medium supplemented with 0.75 mM palmitic acid conjugated to bovine serum albumin in the final 24-hours of differentiation. Ectopic lipid accumulation was confirmed both visually by staining with Oil Red O, and semi-quantitively by measuring the absorbance of solubilized and extracted Oil Red O stain. With this lipid-loaded model established, insulin induced glucose uptake was measured after palmitate incubation. Glucose uptake after 10 nM insulin treatment was significantly blunted in myotubes incubated with palmitate compared to those without, with glucose uptake levels in lipid-loaded myotubes resembling those of the untreated control. This lipid-loaded, insulin resistant myotube model will be used in the subsequent chapter to investigate the effects of α-MSH on glucose uptake in an insulin resistant environment *in vitro*.

In this chapter, *vastus lateralis* skeletal muscle biopsies obtained from healthy volunteers were used to establish six discrete cell lines of primary human myoblasts. The purity of the cell type obtained was established, and their capability to successfully differentiate into multinucleated myotubes confirmed. The effect size of insulin-stimulated glucose uptake in these myotubes was comparable to published data, indicating a functioning pathway downstream of the insulin receptor. An insulin-resistant, lipid-loaded myotube model was then developed by incubation with palmitic acid. Thus established and characterized, these myotube cultures were subsequently deployed in the investigation of the effect of α-MSH on human skeletal muscle glucose uptake.

Chapter Three

Effect of α-MSH on Glucose Uptake in Human Myotube and Adipocyte Culture

3 Chapter 3: Effect of α-MSH on Glucose Uptake in Human Myotube and Adipocyte Culture

3.1 Introduction

α-MSH is a 13 amino-acid acetylated peptide hormone belonging to the melanocortin family of peptides. It is produced through tissue specific proteolytic processing and post-translational modification of the of the proopiomelanocortin (POMC) polypeptide (177,179). Although produced in small amounts within melanocytes and keratinocytes in response to ultraviolet light exposure(193,261,262), the primary source of peripheral α-MSH in humans is the anterior lobe of the pituitary (205,263), from where it has been demonstrated to be released into the circulation in response to transient elevations in blood glucose (205,228,264). A-MSH is an agonist at melanocortin receptors MCR1, MCR3, MCR4 and MCR5 but not MCR2 (187,193).

While central MCR expression is primarily limited to MC3R/4R, MCR1, MCR2 (limited to the adrenal gland), MCR3 and MCR5 can be expressed to varying degrees across a range of peripheral tissues(193–195). The central role of the melanocortin system in energy balance is well characterized as part of the leptin signalling pathway. Briefly, leptin binds to the leptin receptor found in the hypothalamus which then activates posttranslational processing of POMC in POMC neurons to release centrally binding α-MSH(209). This leads to an agonistic effect on MC3/4R which in turn leads to reduced food intake (265–267). To date, published data on the role of the peripheral melanocortin system in the context of energy homeostasis is sparse, particularly in human models. A-MSH has been shown to increase fatty acid oxidation in murine myotubes (both primary and C2C12) and lipolysis in adipocytes derived from mice (229,268). Interestingly, administration of an insulin bolus proves fatal to POMC-knockout mice in which both glucose tolerance and fasting insulin/glucose levels are normal However, administration of α-MSH to these mice restores insulin tolerance in association with elevations in circulating glucagon, which increases by 130% (269). Additionally, agonism of MC5R has been demonstrated to have a protective effect against glucose-induced hypertrophy in rat cardiomyocytes and high-glucose damage in retinal cells(201,270).

Prior pre-clinical work carried out by our collaborators on this project (Prof. Michael Cowley, Monash University) points to a MC5R-mediated stimulatory effect of α-MSH on glucose uptake in rodent and primate skeletal muscle (205,206). To summarize the *in vitro* and *ex vivo* data to date; a novel endocrine circuit has been discovered in which α-MSH acts directly on rodent and primate skeletal muscle to cause glucose uptake downstream of MC5R. This appears to proceed in an insulin-independent manner, wherein GLUT4 is not translocated to the plasma membrane nor is the effect reliant on upstream PKA or AMPK involvement. This discovery provides the basis for this research project which aims to take the first steps in translating these findings to human biology.

This chapter aims to establish whether the enhancement of glucose uptake in response to α-MSH and MC5R selective agonism previously observed *in vivo* and in rodent myotube cultures translates to the context of primary cultures of human myotubes and adipocytes. To achieve this, the MCR expression profile of primary human myoblast cell lines was assessed, then glucose uptake after incubation with varying concentrations of α-MSH measured and compared to the myotubes response to insulin. PG-901, a peptidomimetic MC5R-specific agonist was used to establish whether any changes in glucose uptake were directly mediated by MC5R, as has been demonstrated in rodents. In obese mice, α-MSH induced improvements in glucose tolerance were blunted (205). The lipid-loaded myotube model of insulin resistance was used to assess whether lipid loading impacted on α-MSH responses. Additionally, with the intention of investigating whether α-MSH stimulated glucose uptake occurred in other insulin sensitive cells relevant to metabolic control, primary human adipocytes were treated with α-MSH, and glucose uptake assessed.

3.2 Methods

3.2.1 Measurement of Glucose Uptake

The principle of using measuring the radioactivity of cell lysates by liquid scintillation counting after incubation with glucose labelled with a radioisotope as a proxy for glucose uptake was employed in myotubes and adipocytes as detailed in Section 3.2.12.1. Treatments were prepared as detailed below.

3.2.1.1 Glucose Uptake Assay Treatment Preparation

3.2.1.1.1 Alpha-Melanocyte Stimulatory Hormone

Pharmaceutical grade α-melanocyte stimulatory hormone was custom synthesized by Auspep Clinical Peptides Australia to GMP standards for both *in vitro* and human infusion studies in this project.

For *in vitro* studies, 33mg aliquots of the peptide were first reconstituted in 50mL deionised H_2O to yield a concentration of 394.4 µM stock solution and 1mL aliquots of this stock solution immediately frozen. For further use, this stock solution was diluted in serum and glucose free DMEM to yield a 1000nM solution, which was then serially diluted to 100, 10 and 1 nM working solutions for cell treatments.

3.2.1.1.2 PG-901

Professor Michael Cowley (Monash University) kindly provided the MC5R peptidomimetic agonist PG-901 for use in this project. Having the same molecular weight as α-MSH, PG-901 followed an identical dilution protocol as detailed in Section 2.12.1.

3.2.1.1.3 Insulin

Recombinant human insulin in solution at a concentration of 1.8 mM was purchased from Merck (I19278). Insulin solution was diluted in serum and glucose free DMEM to yield a concentration of 1.8 µM stock solution and frozen. This was further diluted to 10nM in serum and glucose free DMEM for use as a working solution in cell treatments.

3.2.2 Real Time Polymerase Chain Reaction

Ribonucleic acid was isolated, analysed and used to synthesize cDNA as detailed in Section 3.2.5-7. Real time polymerase chain reaction was carried out as detailed in Section 3.2.8 with the probes used in **Table 3.1** overleaf.

Taqman Assay	Gene	TaqMan Assay ID
Human melanocortin receptor 1	Mc1r	Hs00267167_s1
Human melanocortin receptor 3	Mc3r	Hs01562847_s1
Human melanocortin receptor 4	Mc4r	Hs00271877_s1
Human melanocortin receptor 5	Mc5r	Hs00271882_s1
Human GAPDH	GAPDH	Hs02786624_g1

Table 3.1 Taqman assays used.

3.3 Results

3.3.1 MCR Expression in Primary Human Myotube Cultures

To compare the relative abundance of expression across cell lines and targets, the target cycle threshold (CT) was normalized to the GAPDH endogenous control CT and displayed as ΔCT (Target CT- GAPDH CT). The presence of MCR1, MCR3, and MCR4 was confirmed with mRNA levels of MCR1 being the most abundant (mean ΔCT 7.99 ±0.33) followed by MCR3/4 (means ΔCT 17.8 ± 1.5 and ΔCT 16.33 ± 1.1 respectively) at similar levels.

MC5R was faintly detected, only being amplified in PCR cycles 35-40 with a ΔCT of 21.65 ± 1.09. Additionally, amplification was not observed consistently in duplicate samples **(Fig 3.1 overleaf).**

3.3.2 MCR Expression in Commercially Obtained Human Skeletal Muscle RNA

In order to substantiate the above findings, human skeletal muscle tissue RNA was commercially obtained and analysed for MCR expression. Relative expression levels between the receptors were similar to those found in isolated primary human myotubes, with MCR1 most abundant (mean ΔCT 16.7) followed by MCR3/4 (means ΔCT 20.4 and ΔCT 20.1 respectively). MCR5 was not detected (**Fig 3.2 overleaf**).

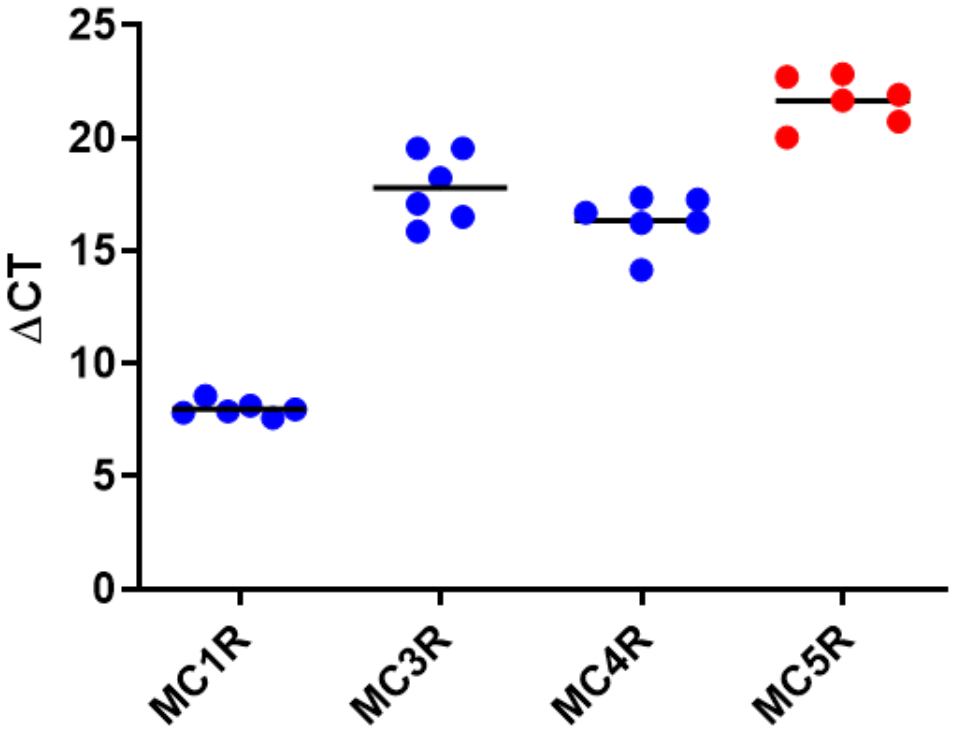

Figure 3.1 Melanocortin receptor profile of primary myotube lines.

Melanocortin receptor mRNA expression in established cell lines with GAPDH used as a reference gene, expressed as the difference in cycle thresholds of the target and reference gene (ΔCT) as measured by qRT-PCR. Each data point represents a discrete cell line assayed in duplicate.

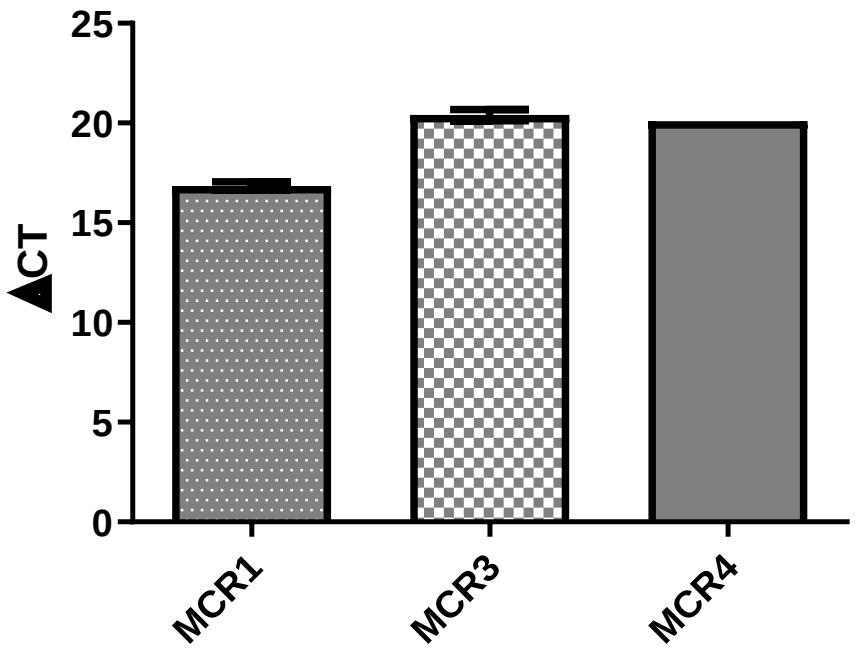

Figure 3.2 Melanocortin receptor profile of commercially obtained human skeletal muscle RNA.

Melanocortin receptor mRNA expression in established cell lines with GAPDH used as a reference gene, expressed as the difference in cycle thresholds of the target and reference gene (ΔCT) as measured by qRT-PCR. RNA was used to prepare cDNA template in duplicate. Each duplicate template was assayed in triplicate and means of each triplicate shown above (n=2).

3.3.3 α-MSH Induced Glucose Uptake in Human Primary Myotubes

Glucose uptake was measured under various treatment conditions by liquid scintillation counting of tritiated 2-deoxy-D-glucose uptake by differentiated myotubes.

3.3.3.1 α-MSH-induced Glucose Uptake in the Absence of Insulin

A 60-minute incubation of myotubes with 10nM and 100nM α-MSH elevated glucose uptake approximately 2-fold above untreated basal glucose uptake (7.8±2.5 CPM/µg vs. 15.24±4.19 CPM/µg and 15.71±4.52 CPM/µg respectively, one-way ANOVA p=0.0014). The summary effect was thus comparable in magnitude, to the increase in glucose uptake in response to 10nM insulin (16.66±1.66), though less consistent, **(Fig. 3.3 overleaf).**

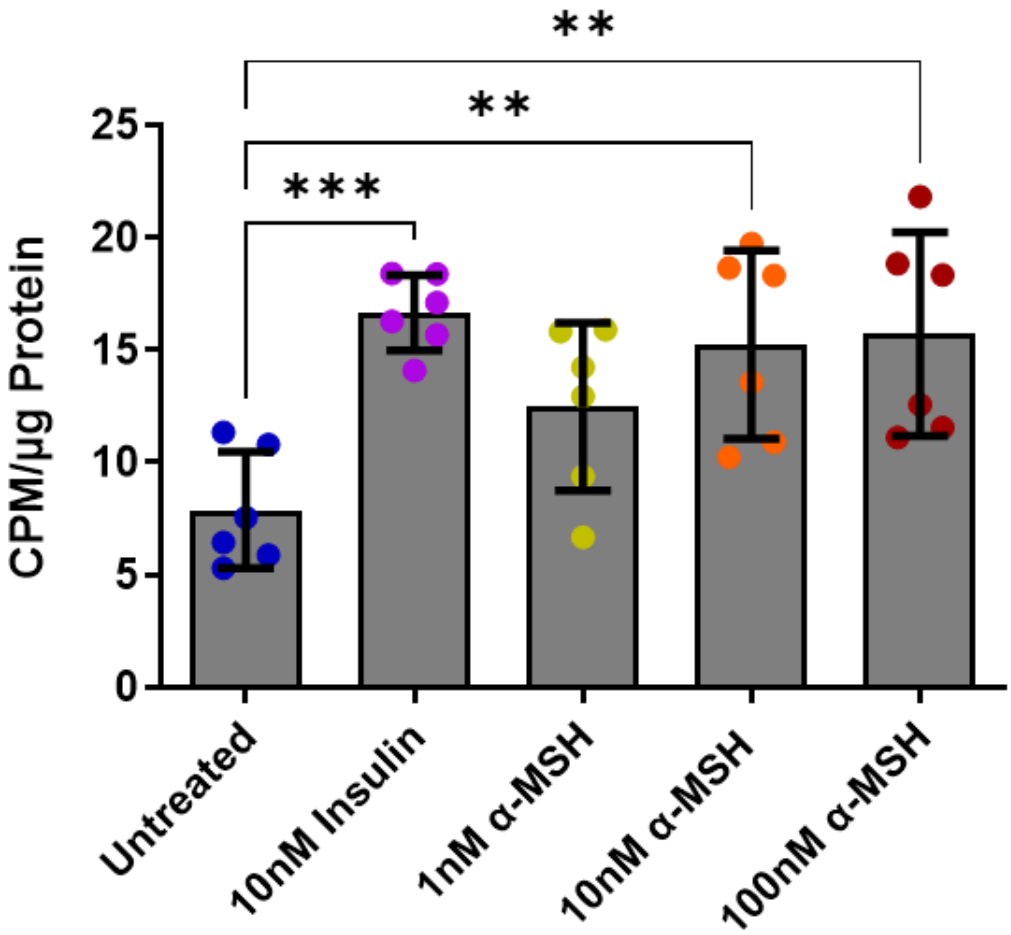

Figure 3.3 α-MSH induced glucose uptake in primary human myotubes.

*Glucose uptake represented as counts per minute (CPM) of cell lysates as measured by liquid scintillation counting normalized by protein content (n=6). **p<0.005 vs. Untreated, ***p<0.0005 vs. Untreated. Data are presented as mean ± standard deviation with each data point shown as the mean of duplicates. Statistical analysis was performed with one-way ANOVA with post-hoc Dunnett's multiple comparison test.*

3.3.3.2 Glucose Uptake in Response to α-MSH and Insulin Co-Incubation

Co-incubation of 10nM α-MSH with 10nM insulin resulted in a significant increase in glucose uptake over insulin alone (16.66±1.66 CPM/µg vs. 28.58±11.31 CPM/µg, one-way ANOVA p=0.0003) **(Fig 3.4)**.

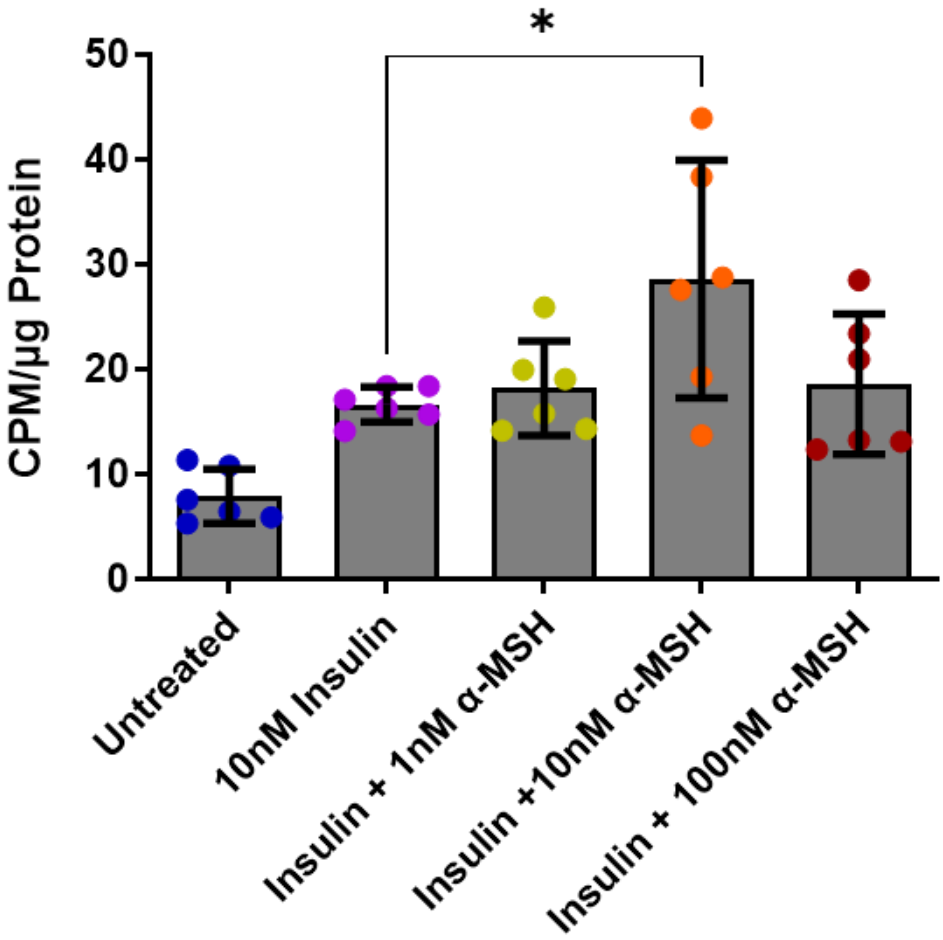

Figure 3.4 The effect of insulin and α-MSH co-incubation on glucose uptake in myotubes.

*Glucose uptake represented as counts per minute (CPM) of cell lysates as measured by liquid scintillation counting normalized by protein content (n=6). *p<0.05 vs Untreated. Data are presented as mean ± standard deviation with each data point shown as the mean of duplicates. Statistical analysis was performed with one-way ANOVA with post-hoc Dunnett's multiple comparison test.*

3.3.4 MC5R Agonism

PG-901, a MC5R specific agonist was used to identify the MCR responsible for α-MSH induced glucose uptake.

Incubation with the peptidomimetic agonist PG-901 significantly increased glucose uptake over untreated control at a concentration of 100nM (9.61±1.05 CPM/µg vs. 14.74±2.87 CPM/µg, one-way ANOVA p=0.002) **(Fig. 3.5).**

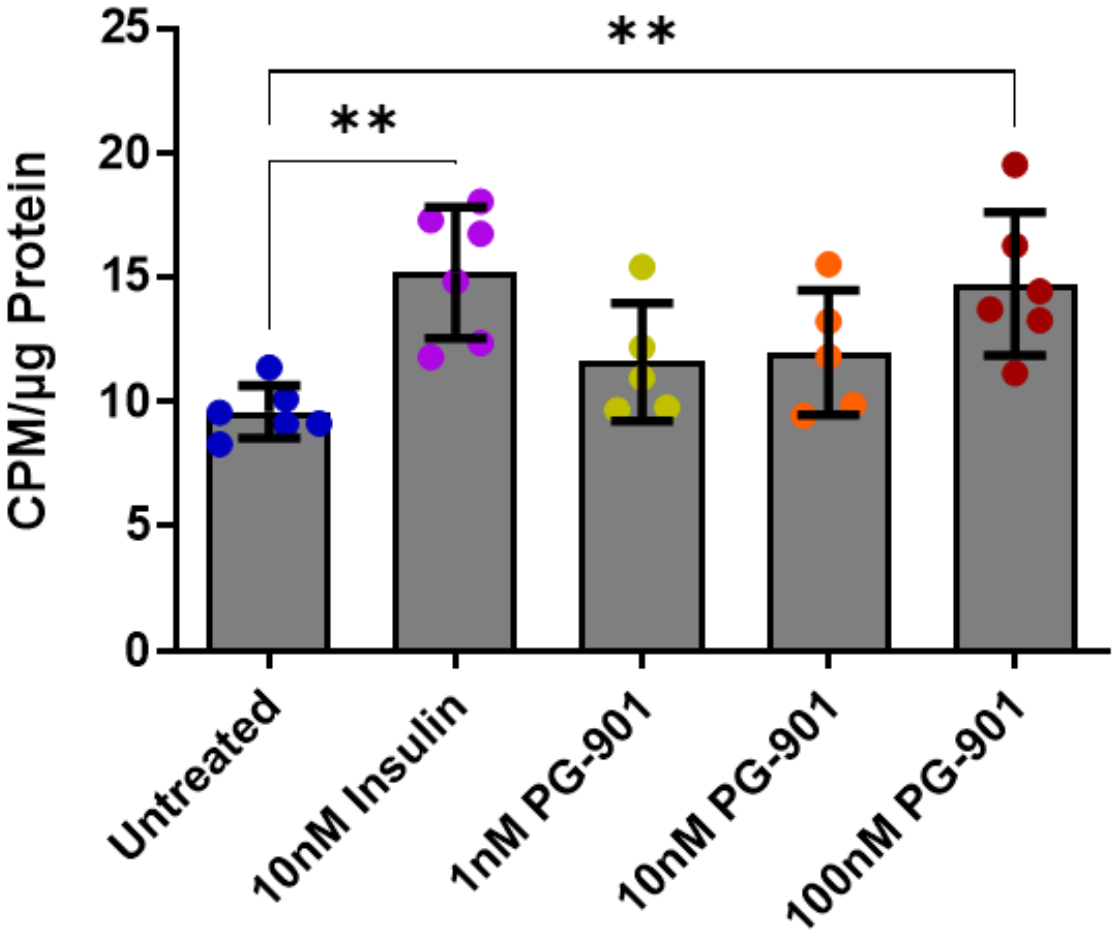

Figure 3.5 Glucose uptake in response to MCR5 agonism by PG-901.

*Glucose uptake represented as counts per minute (CPM) of cell lysates as measured by liquid scintillation counting normalized by protein content (n=6). **p<0.005 vs Untreated. Data are presented as mean ± standard deviation with each data point shown as a mean of triplicates. Statistical analysis was performed with one-way ANOVA with post-hoc Dunnett's multiple comparison test.*

3.3.5 α-MSH Induced Glucose Uptake in Lipid-Loaded Myotubes

Ectopic lipid accumulation was induced in myotubes as previously described, and glucose uptake in response to α-MSH was measured.

In myotubes incubated with 0.75 mM palmitic acid for 24-hours, α-MSH failed to induce a significant increase in glucose uptake that was comparable to insulin as shown in Figure 4.2 **(Fig. 3.6).**

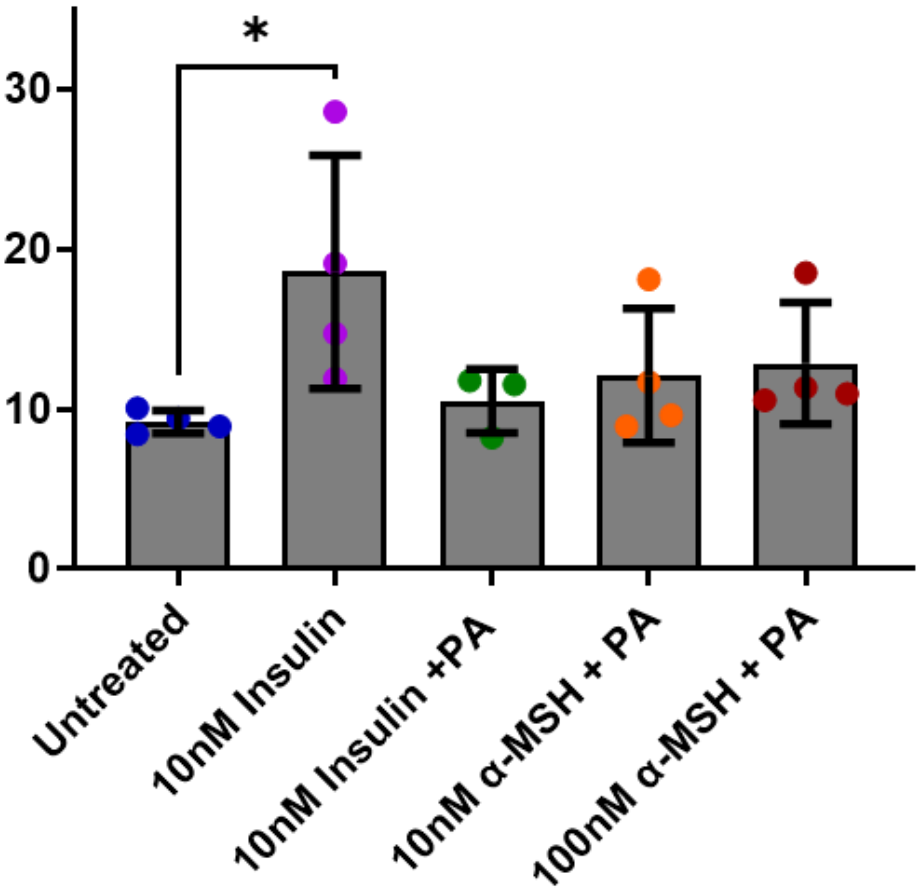

Figure 3.6 The effect of palmitic acid on α-MSH induced glucose uptake.

*Glucose uptake represented as counts per minute (CPM) of cell lysates as measured by liquid scintillation counting normalized by protein content (n=4). *p<0.05 vs Untreated. Data are presented as mean ± standard deviation with each data point shown as a mean of triplicates. Statistical analysis was performed with one-way ANOVA with post-hoc Dunnett's multiple comparison test*

3.3.6 Melanocortin Receptor Profile and Glucose Uptake in Primary Human Adipocytes

A commercially obtained primary human preadipocyte cell line was cultured and differentiated into adipocytes. The melanocortin profile of this cell line was assessed by qRT-PCR and glucose uptake measured by liquid scintillation counting of tritiated glucose.

3.3.6.1 Primary Human Adipocyte Melanocortin Receptor Profile

qRT-PCR was used to profile the abundance of MCR1, MCR3, MCR4, and MCR5 mRNA in differentiated adipocytes.

The presence of melanocortin receptors 1 and 3 were confirmed with mRNA levels of MC1R being the most abundant (mean 10.83 ± 0.13 ΔCT) followed by MC3R (mean 16.18 ± 2.5 ΔCT) **(Fig. 3.7)**. Melanocortin receptors 4 and 5 were not detected.

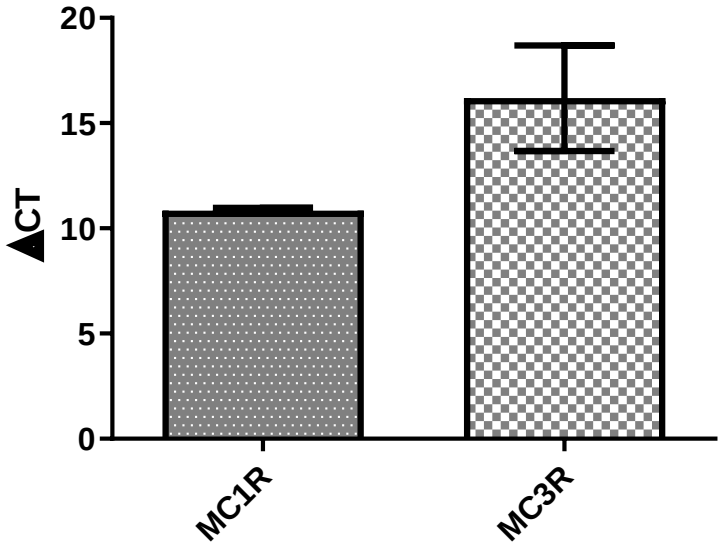

Figure 3.7 Melanocortin receptor profile of commercially obtained primary human adipocytes.

Melanocortin receptor mRNA expression in commercial primary adipocytes with GAPDH used as a reference gene, expressed as the difference in cycle thresholds of the target and reference gene (ΔCT) as measured by qRT-PCR (n=3).

3.3.6.2 α-MSH Induced Glucose Uptake in Primary Human Adipocytes

Glucose uptake was measured under various treatment conditions by liquid scintillation counting of tritiated 2-deoxy-D-glucose taken up by differentiated adipocytes. Whereas 10nM insulin induced a significant increase in glucose uptake over untreated control (p=0.04), α-MSH did not increase uptake at any dose used **(Fig. 3.8)**.

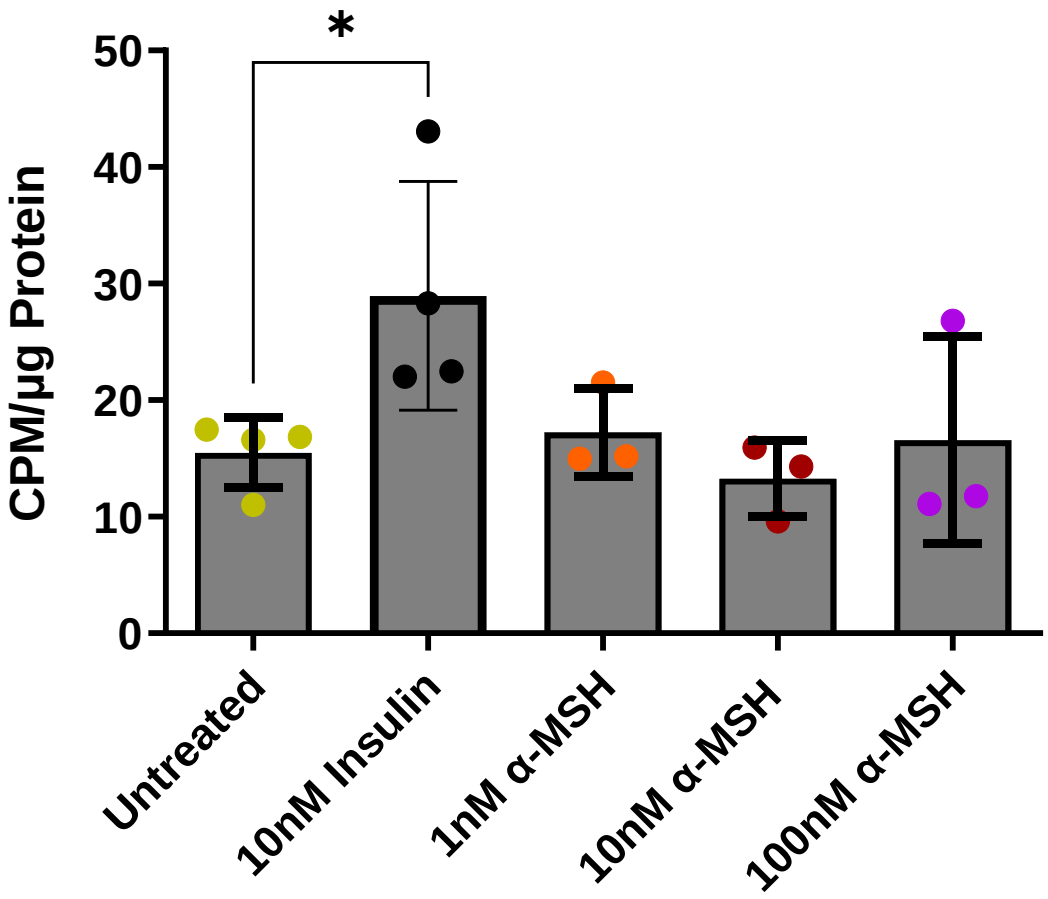

Figure 3.8 α-MSH induced glucose uptake in primary human adipocytes.

*Glucose uptake represented as counts per minute (CPM) of cell lysates as measured by liquid scintillation counting normalized by protein content (Untreated and 10nM insulin n=4) (1, 10 and 100nM α-MSH n=3). *p<0.05 vs Untreated. Data are presented as mean ± standard deviation with each data point shown as a mean of triplicates. Statistical analysis was performed with one-way ANOVA with post-hoc Dunnett's multiple comparison test.*

3.4 Discussion

This chapter aimed to establish whether the enhancement of glucose uptake in response to α-MSH and MC5R selective agonism previously observed *in vivo* and in rodent myotube cultures translates to the context of primary cultures of human myotubes and adipocytes. This was achieved by characterising the expression levels of melanocortin receptors in previously established primary human myotubes, commercially obtained primary human adipocytes, and RNA extracted from human skeletal muscle tissue. Glucose uptake in response to α-MSH with and without insulin was measured in both myotubes and adipocytes. To investigate whether the glucose uptake effect was MCR5 mediated, the selective agonist PG-901 was used. Using the lipid-loaded myotube model established in Chapter 2, the impact of ectopic lipid accumulation on α-MSH induced glucose uptake was measured. This marked the first time direct MCR agonism in human skeletal muscle has been investigated.

The melanocortin receptor profile of skeletal muscle in mice and rats is well characterized, with MC5R shown to be highly abundant and MC4R detectable at low levels (205,206). Scant data exists on the melanocortin receptor profile in human skeletal muscle and at the time of writing, this is the first study examining the direct action of α-MSH on human skeletal muscle in any context. In contrast to rodents where it is shown to be the MCR primarily expressed in skeletal muscle, MC5R has been shown to have very low levels of expression in human skeletal muscle(192,200,271,272). No evidence of melanocortin receptors 1,3 and 4 expressions in human skeletal muscle could be found in published literature, although tissue expression databases such as the Human Protein Atlas show MCR1 and MCR4 are present.

All six primary human myoblast cell lines were assayed for melanocortin receptors 1, 3, 4 and 5. MC2R was not investigated as α-MSH has no binding properties at this receptor. MC1R was found in high abundance and in consistent levels across all cell lines. MC3/4R were expressed at lower levels but routinely detectable. MC5R was faintly detected, not being consistently amplified between technical replicates across multiple PCR experiments. When amplified, MCR5 expression would only cross the

detection cycle threshold in the last 5 (of 40) amplification cycles. RNA used in cDNA template preparation for these experiments was found to be free from contamination and largely intact (see **Appendix 6.3** for RNA quality assessment). Extracting RNA from myotubes cultured in a high glucose environment, which has been shown to upregulate MC5R expression in cardiomyocytes (201), did not result in increased MC5R expression in human myotubes (**Appendix 6.4**). Additionally, no difference in MC5R amplification was observed when using three-fold higher cDNA template in the PCR assay. Total RNA extracted from human skeletal muscle tissue was commercially obtained and MCR expression analysed. MCR1/3/4 were found to be expressed at similar levels relative to each other in comparison to myotubes, and MCR5 not being detectable. These data suggest that, in contrast to rodents, MC5R is expressed at extremely low levels in human myotube culture.

Serum and glucose starved myotubes were incubated with insulin or a range of doses of α-MSH for 1-hour, and uptake of tritiated 2-deoxy-D glucose measured. In an effort to control for the impact of any genotypic or phenotypic differences between biopsy donors on the α-MSH response, the experiment was repeated twice within a cell line from three separate biopsy donors for a total of 6 experimental replicates. Within each experiment, treatments were assayed in duplicate. Incubation of myotubes with α-MSH at concentrations of 10 and 100 nM increased glucose uptake over untreated control. The effect size was comparable to that the of measured insulin-induced glucose uptake. As cultured primary myotubes retain some metabolic characteristics of their donor organisms (21,119,237,238), biopsy donors were screened for any history of diabetes or metabolic disease. As expected, this resulted in a highly consistent insulin mediated glucose uptake response across all cell lines assayed. However, there was more variability in glucose uptake in cells treated with α-MSH. Experimental duplicates in each cell line had consistent α-MSH responses, suggesting the variability may be derived from differences in donor characteristics manifesting in the inter-cell line variability observed in these data. This represents the first time this novel mechanism of glucose uptake in response to direct α-MSH stimulation has been measured in human cells.

Next, the impact of co-incubation of insulin and α-MSH on glucose uptake was measured to assess whether combined downstream signalling of insulin receptor and

MCR's result in a response greater than either alone. Data in rodent models has shown that glucose uptake mediated by MC5R activation is independent of insulin signalling, and that the glucose uptake effect size of combined incubation is additive (205,206). In the human myotubes assayed, co-incubation of 10nM insulin and 10nM α-MSH resulted in a statistically significant increase in glucose uptake over insulin alone. A similar effect can be seen in insulin co-incubated with 1 and 100nM α-MSH however, the results are variable, and the net effect size is not of the same magnitude as that of the data in rodents. These data suggest that the complementary effects of α-MSH and insulin may translate to human models. However, the increased GLUT1 present in human myotubes (241) may obscure the true effect size mediated by recruiting additional GLUTs to the plasma membrane, leading to the maximum treatment-induced increase in glucose uptake being reached at a lower "fold-difference" to the basal state.

To further interrogate the translational relevance of the finding in animals that glucose uptake is mediated by MC5R, myotube glucose uptake as assessed following incubation with PG-901, a highly selective peptidomimetic agonist of MC5R. One-hour incubation with 100 nM PG-901 increased resulted in a glucose uptake relative to control, with a similar effect size to that seen with insulin. When initially characterised PG-901 was shown to have an EC_{50} of 0.072nM and demonstrated high specificity for MC5R (273) however, in the myotube experiments described herein a significant increase in glucose uptake was only observed at a concentration of 100nM. This may be due to the faintly detectable levels of MC5R expression in the myotubes used. The cells used in binding assays to establish the pharmacological properties of the newly synthesized PG-901 compound were Chinese hamster ovary cells modified to stably express MC5R at high levels (273), and thus are not biologically equivalent to the primary human myotubes used in this experiment. Therefore, it is possible that with the low receptor abundance observed, PG-901 will only produce significant downstream effects at 100nM in the 1-hour incubation time used in these experiments. In conclusion, these data tentatively suggests that direct agonism of MC5R in human myotubes is capable of eliciting a significant increase in downstream glucose uptake but whether this supports the likelihood of an MCR5 mediated response to α-MSH transients *in vitro* is questionable.

In mice with diet-induced obesity, the glucose tolerising effect of α-MSH during glucose tolerance tests was ablated (205). The lipid-loaded myotube model established in Chapter 3 was employed in an effort to translate these findings to human cells. In an environment where insulin mediated glucose uptake is hampered due to ectopic lipid accumulation, the concentrations of α-MSH used produced no noticeable increase in glucose uptake after 1-hour incubation. In mice, a combination of nonselective phosphodiesterase inhibitors ameliorated the inhibitory effect of obesity on α-MSH induced glucose uptake by blocking the breakdown of cAMP, indicating a failure in signal transduction., It may prove useful in future experiments to demonstrate that insulin resistant human myotubes respond to α-MSH wherein cAMP signalling is restored.

The downstream effects of MCR agonism on glucose uptake was also investigated in human primary adipocytes. Commercially obtained preadipocytes were cultured and differentiated to adipocytes. The melanocortin profile of this cell line was assessed by qRT-PCR and MCR's 1 and 3 were found to be expressed, with no evidence of MC4/5R expression. Following the same glucose uptake assay protocol, differentiated adipocytes were incubated with insulin and a range of doses of α-MSH after being serum and glucose starved. No enhancement of glucose uptake was induced after incubation with α-MSH; thus, the cell type was not used in any subsequent experiments.

This chapter aimed to investigate whether the findings in rodent models that demonstrated direct agonism of skeletal muscle MC5R leads to downstream glucose uptake. Primary human myoblast cell lines were shown to stably express MCR's 1, 3 and 4, with MC5R being faintly detected. The presence of MC5R in human skeletal muscle can be corroborated in the literature however, peer-reviewed data demonstrating whether or not MC1/3R is expressed in human muscle could not be found. A-MSH was shown to significantly increase glucose uptake at concentrations of 10 and 100nM after 1-hour incubation, with this effect size increasing upon co-incubation with insulin. PG-901, a selective MC5R agonist, significantly increased glucose uptake, but only at a concentration of 100nM suggesting that the effect of native hormone at lower dosage is possibly not mediated via signalling downstream of MC5R. This represents a fundamental difference to what has been described

heretofore in rodent studies and has major implications for receptor level drug targeting of this pathway.
In lipid-loaded myotubes α-MSH fails to elicit a glucose uptake response at any of the concentrations used. Whether this can be attributed to a failure in cAMP signalling remains a subject for future experiments. Human primary adipocytes expressing MC1/3R do not demonstrate any increase in glucose uptake in response to α-MSH incubation.

The work described above in primary human culture represents the targeted investigation of the effect of α-MSH on skeletal muscle glucose handling. With evidence of translation of this novel pathway to the human context established, the impact of systemic α-MSH infusion on oral glucose tolerance and skeletal muscle disposal of glucose was investigated in healthy human volunteers as described in the following chapter.

Chapter Four

Investigating the Effect of α-MSH on Glucose Clearance in Healthy Humans

4 Chapter 5: Investigating the Effect of α-MSH on Glucose Clearance in Healthy Humans

4.1 Introduction

Diabetes mellitus is recognized as the fastest growing chronic condition around the globe. In 2021 the International Diabetes Federation estimated that 1 in 10 (537 million) adults are living with diabetes, with diabetes-related healthcare expenditure increasing by 316% over the last 15 years (274). Postprandial hyperglycaemic excursions are a key target for most therapeutic strategies due to glucotoxicity being a major risk factor for the development of diabetic complications (142,275,276). Fortunately, hyperglycaemia is a modifiable risk factor, and a wide array of insulin-centric therapeutics are available.

The primary treatment outcome in patients with both T1DM and T2DM is an improvement in glycaemic control as measured by a reduction in HbA1c. The 2022 update to the Clinical Practice Recommendations of the American Diabetes Association states that adults with Type 1 Diabetes (T1D) should be treated with rapid-acting insulin analogues either prandially or basally. In Type 2 diabetics (T2D), metformin alongside lifestyle modification should be a first-line therapy before progressing to combination therapy with GLP-1 analogues and sulfonylureas The ADA further recommends introduction of insulin to the pharmacotherapeutic strategy if there is no improvement of glycaemic control and/or evidence of ongoing catabolism (277). Progression of disease states in both T1D and T2D can result in the need for intensive insulin therapy to manage hyperglycaemia. This can lead to significant weight gain and the risk of hypoglycaemia in T1D (278), and mortality from cardiovascular causes in T2D (279). As such, there is a need for novel pharmacological approaches which may compliment the glucose-lowering response of insulin thus providing an insulin-sparing effect and may hold promise as use for a future adjunct therapy.

Continuous infusion of α-MSH in mice significantly improves glucose tolerance during a glucose tolerance test and increases the glucose infusion rate during hyperinsulinaemic-euglycaemic clamps mediated by increased glucose uptake in muscle. Additionally, arterial infusions of α-MSH in sheep lead to an increase in muscle temperature, further demonstrating the direct effects on skeletal muscle *in vivo* (205).

As demonstrated in Chapter 4, α-MSH increases glucose uptake in primary human myotubes, with an effect complimentary to insulin. A critical next step in understanding this previously undescribed pathway in humans is validating whether this response *in vitro* translates *in vivo,* in healthy human subjects in the first instance. Therefore, a study in healthy volunteers involving the intravenous infusion of α-MSH during both an oral glucose tolerance test and a euglycaemic-hyperinsulinaemic clamp was designed. Prior to the human study, a mouse study was conducted to validate the batch of peptide to be used in humans. Ten lean mice received bolus injections of 1, 10 and 100ng α-MSH prior to intraperitoneal glucose tolerance test. This was carried out to validate the glucose tolerising effects of the peptide on mice in our own lab, and as previous studies have administered continuous infusions, to investigate whether a single pre-prandial bolus injection of α-MSH would produce a similar effect.

Fifteen participants were then recruited and studied in a double-blind, placebo-controlled crossover manner whilst being infusion with a range of doses of the α-MSH peptide (15, 150 and 1500 ng/kg/hr) and placebo (saline) during OGTT. A reduction in the 0–120-minute iAUC for glucose was investigated as the primary outcome. In the clamp phase of the study, the same cohort of healthy volunteers underwent a hyperinsulinaemic-euglycaemic clamp on two occasions while receiving a saline or α-MSH infusion in a double-blind, placebo-controlled manner crossover manner. Serial blood samples were taken during OGTTs and clamps, and assayed for glucose, insulin, and GLP-1for secondary endpoint analysis.

4.2 Methods

4.2.1 Pre-Clinical Validation in Mice

In a study approved by the UCD Animal Research Ethics Committee (Study ID 18-07-HPRA-P138). Ten C56/B7 mice underwent intraperitoneal (i.p.) glucose tolerance tests four times, one week apart. On week 1 mice were given i.p. saline injections prior to the glucose tolerance test, and on subsequent weeks escalating doses (1, 10 and 100ng) of α-MSH. Mice were euthanised on the final week after 100ng glucose tolerance tests. Gastrocnemius muscle tissue was harvested from each mouse upon euthanasia, RNA isolate and MC5R mRNA assessed by qRT-PCR as previously described.

4.2.2 Study Design and Outcome Measures

4.2.2.1 Study Design

This study was designed to answer the question of whether alpha-MSH increases glucose clearance in healthy humans. This was addressed through the completion of two objectives:

- Objective 1- To identify the concentration of peripherally administered alpha-MSH that increases glucose clearance following an oral glucose load in healthy humans.
- Objective 2- To identify whether changes in skeletal muscle glucose uptake are implicated in alpha-MSH induced enhancement of glucose clearance in healthy humans.

To achieve objective 1, we conducted a prospective randomised double-blinded physiological study recruiting 15 healthy participants from either sex from the community. On each of four study visits, participants underwent a 75g oral glucose tolerance test and were randomized to either a placebo infusion or infusion of α-MSH, at one of three doses (15, 150, 1500 ng/kg/hr). Each participant was studied at least one week apart in a randomized, double blind, placebo-controlled, crossover manner. Following the completion of objective 1, a hyperinsulinaemic euglycaemic clamp was conducted with placebo and the dose of α-MSH observed to induce the maximal change in the area under the curve of glucose OGTT at interim analysis. Each

participant was studied at least one week apart in a randomized, double- blinded, placebo-controlled, crossover manner.

4.2.2.2 Outcome Measures

4.2.2.2.1 Primary Outcome

• Difference in the incremental area under the curve (iAUC) of glucose concentration at an OGTT during saline vs. alpha-MSH infusion between 0 and 120 minutes.

4.2.2.2.2 Secondary Outcomes

- Difference in the area under the incremental curve of insulin (iAUC) concentration at an OGTT during saline vs. alpha-MSH infusion between 0 and 120 minutes.
- Difference in the glucose infusion rate adjusted for insulin at the euglycaemic hyperinsulinaemic clamp during saline vs. alpha-MSH infusion between 270-300 minutes.
- Difference in the incremental area under the curve (iAUC) of GLP-1 concentrations at an OGTT during saline vs. the highest effect dose of alpha-MSH infusion between -30 and 180 minutes.

4.2.3 Ethical Approval and Recruitment

This clinical investigation did not fall under the scope of a clinical trial and was approved as a physiological study by the London-Fulham Research Ethics Committee (IRAS ID; 275910, REC Ref; 20/LO/0355) in March 2020. Formal recruitment began in October 2020.

Posters were distributed and placed throughout the community, and a recruitment email was circulated through the Imperial College healthy volunteer database.

4.2.4 Participant Screening

Potential participants attended a screening visit after an overnight fast. The study was explained, and the participant given a copy of the participant information sheet and consent form, then given ample time to ask questions. Anthropometric measurements of heigh, weight, and bio-electric impedance analysis used to calculate body

composition was taken. A medical professional then took medical history, sampled blood for glucose, HbA1c, liver function and clotting and performed an electrocardiogram. Inclusion and exclusion criteria are detailed below.

4.2.4.1 Inclusion Criteria

- 18-50 years old
- Normal fasting glucose (< 5.6 mmol/L)
- Stable body weight for at least 3 months
- BMI ≥18 < 30 Kg/m2
- The participant is capable of giving written informed consent
- The participant is able to read, comprehend and record information written in English

4.2.4.2 Exclusion Criteria

- Previous or current psychiatric diagnosis listed in DSM-V Axis 1.
- Significant current or past medical or psychiatric history that, in the opinion of the investigators, contraindicates their participation.
- History of type 1 or type 2 diabetes mellitus.
- History of endocrine disorder.
- History of ischaemic heart disease, hypertension, heart failure, cardiac arrhythmia, peripheral vascular or cerebrovascular disease.
- History or presence of significant respiratory, gastrointestinal, hepatic, oncological, neurological or renal disease or other condition that in the opinion of the Investigators may affect participant safety or outcome measures.
- Unwillingness or inability to follow the procedures outlined in the protocol.
- History of sensitivity to any of the peptides, or components thereof, or a history of drug or other allergy that, in the opinion of the investigators, contraindicates their participation.
- Use of current regular prescription or over-the-counter medications that in the opinion of the Investigators may affect participant safety or outcome measures.
- Clinically significant abnormalities in screening electrocardiogram (ECG) or blood tests abnormalities which in the opinion of the study physician, is clinically significant and represents a safety risk.

- Current pregnancy or breast-feeding in female participants (the investigators would advise using contraception for the duration of the study).
- Pulse rate <40 or >100 beats per minute OR systolic blood pressure >160 and <100 and a diastolic blood pressure >95 and <50 in the semi-supine position.
- The participant has participated in a clinical trial and has received an investigational product within the following time period prior to the first experimental visit in the current study: 90 days, 5 half-lives or twice the duration of the biological effect of the investigational product (whichever is longer).
- Exposure to more than 3 new investigational medicinal products within 12 months prior to the screening.
- Participants who have donated, or intend to donate, blood within three months before the screening visit or following study visit completion.

4.2.5 Preparation of Infusions

Infusion syringes were prepared by a qualified medical professional in a controlled environment dedicated to drug preparation. Pharmaceutical grade α-MSH custom synthesized by Auspep Clinical Peptides Australia was diluted in saline supplemented with 4% gelofusine to prevent peptide adhesion to the syringe and infusion lines. Corresponding to the dose increment of α-MSH to be given, concentrations of the syringes were made up to 150, 1500, or 15000 ng/mL.

To deliver a weight (kg) adjusted dose corresponding to one of the three doses (15, 150 or 1500 ng/kg/hr) the infusion pump was set to deliver an infusion rate of 0.1 mL/hr per kilogram of body weight. For example, a 70kg participant would have an infusion rate of 7 mL/hour regardless of the dose which was administered using syringe concentrations of 150, 1500 or 15000 ng/mL to deliver doses of 15, 150 or 1500 ng/kg/hr respectively. The infusion rate remaining the same across all visits allowed the blinded researchers to remain unbiased even if they were to set up the infusion pumps.

4.2.6 Oral Glucose Tolerance Tests

Participants were asked to refrain from alcohol and strenuous physical activity for 48 hours before the study. They were also asked to consume a standardised meal the evening before the study and only consume fluids from 10pm onwards. Participants attended the Imperial NIHR clinical research facility on the day of the visit. Two venous catheters were inserted. The first cannula was used for infusions and the other for

blood sampling. Female participants will be studied in the follicular stage of their menstrual cycle.

The sequence of work-up of each study visit was as follows:

- Pregnancy test for females. If positive, they were excluded from the study.
- Anthropometric Measurements (height, weight, body composition using bioimpedance)
- Record medications and any changes in health
- Cannulation
- Infusion of study solution (α-MSH at one of three concentrations or saline)
- Oral Glucose Tolerance Test (OGTT)

The saline visit involved infusion of pharmaceutical GMP-grade sterile 4% gelofusine (dissolved in saline) obtained from Imperial College Healthcare NHS Trust. Peptide solutions were made up in saline supplemented with 4% gelofusine as detailed in Section 2.17. To reduce binding of peptides to infusion lines, 4% gelofusine dissolved in saline was used to prime the infusion lines prior to infusion of the peptides or placebo solutions.

The participants were cannulated then allowed to rest for 30 minutes, after which they received an infusion of either saline or one of three doses (15, 150, 1500 ng/kg/hr) of α-MSH. Thirty minutes after the infusion started patients underwent a standard OGTT. They were asked to consume a liquid containing 75g glucose within 5 minutes. After the 150-minute infusion had ceased, the participants remained cannulated for an additional 30 minutes where a final sample was drawn, and the participant discharged. Blood samples were collected at the following time points relative to initiation ofthe glucose tolerance test at: -30, 0, 15, 30, 60, 90, 120, 150, 180 minutes.

4.2.7 Hyperinsulinaemic-Euglycaemic Clamps

Once glucose tolerance test infusion visits were completed in 10 participants and an interim unblinding carried out, a hyperinsulinaemic euglycaemic clamp was carried out with placebo and 150 ng/kg/hr α-MSH which was observed to induce the maximal change in the area under the curve of glucose concentration during interim unblinding

of OGTTs. Female participants were studied during the follicular stage of their menstrual cycle.

The sequence of work-up of each study visit was as follows:

- Pregnancy test for females. If positive, they were excluded from the study.
- Anthropometric Measurements (height, weight, body composition using bioimpedance)
- Record medications and any changes in health
- Cannulation
- Infusion of study solution (α-MSH or saline)
- Euglycaemic Hyperinsulinaemic Clamp

The participants received an infusion of either saline or α-MSH. One hundred and twenty minutes after the alpha-MSH infusion has started patients underwent clamp studies. Insulin was infused at a dose depending on patient's weight/body surface area for 3 hours. Euglycaemia was maintained by infusing 20% dextrose at a variable rate. The rate of variable dextrose infusion was calculated using a 200mg/mL solution of dextrose in saline with the participants bodyweight (kg) to deliver a glucose infusion rate in mg/kg/hr that was adjusted continuously to maintain euglycaemia. Blood samples were taken every 10 minutes to measure blood glucose concentration and the dextrose infusion adjusted accordingly to maintain the participant at ±0.5 mmol/L blood glucose within their baseline level. Additional blood was also drawn at timepoints 0, 30, 60, 90, 120, 150, 180, 210, 270, 280, 290, and 300 minutes for further plasma analysis. After all infusions were completed, the participant was offered a meal and monitored for 30 minutes before they left the research facility. Plasma/serum was separated immediately by centrifugation at 4°C and then stored at -80°C until analysis.

4.2.8 Biochemical Analysis

During the OGTTs, blood taken for glucose measurements were immediately sent to the Hammersmith Hospital biochemistry lab to be assayed for glucose oxidase. Plasma samples were assayed for insulin at the UCD Clinical Research Facility (Alinity Ci Series-00192). GLP-1 was measured by ELISA according to manufacturer's protocol (Mercodia 10-1278-01).

4.2.9 Calculation of Sample Size

We defined the minimally important physiological effect of α-MSH to detect as being a reduction in 2-hour area under the curve for glucose during OGTT of 20%, occurring in the context of a standard deviation of 10% of the mean on saline treated day. To detect this reduction with 90% power and a low type 1 error rate (1%) and factoring in 6 pairwise comparisons between the saline treated and three doses result in a predicted sample size of 10. We recruited at 150% power to mitigate for drop-out and hence the study included 15 individuals studied in repeated measure.

4.2.10 Data Handling and Statistical Analysis

Data were tested for evidence of non-normality using the Shapiro-Wilk test and summarised using appropriate descriptive statistics. Incremental area under the curves were calculated by trapezoid analysis using the mean of timepoints t=-30 and t=0 and baseline. Differences in metabolic outcomes between saline and three doses of α-MSH were compared using either two-way ANOVA with the Šidák correction for multiple comparisons, one-way repeated measures ANOVA with Dunnett's correction for multiple comparisons, or paired t-tests as appropriate. $P<0.05$ was considered statistically significant. Analyses were performed with GraphPad Prism 9.0.

4.3 Results

4.3.1 Peptide Validation in Mice

Ten C56/B7 mice underwent intraperitoneal (i.p.) glucose tolerance testing as described. Serial blood samples were taken for glucose measurement and RNA isolated from gastrocnemius muscle samples for MCR5 expression analysis upon euthanasia.

Melanocortin receptor 5 was confirmed as being expressed in mouse skeletal muscle **(Fig. 4.1 A overleaf)**. Bolus injections of 1, 10 and 100ng α-MSH prior to i.p. glucose tolerance tests significantly reduced glucose area under the curve compared to saline **(Fig. 4.2 B overleaf)**.

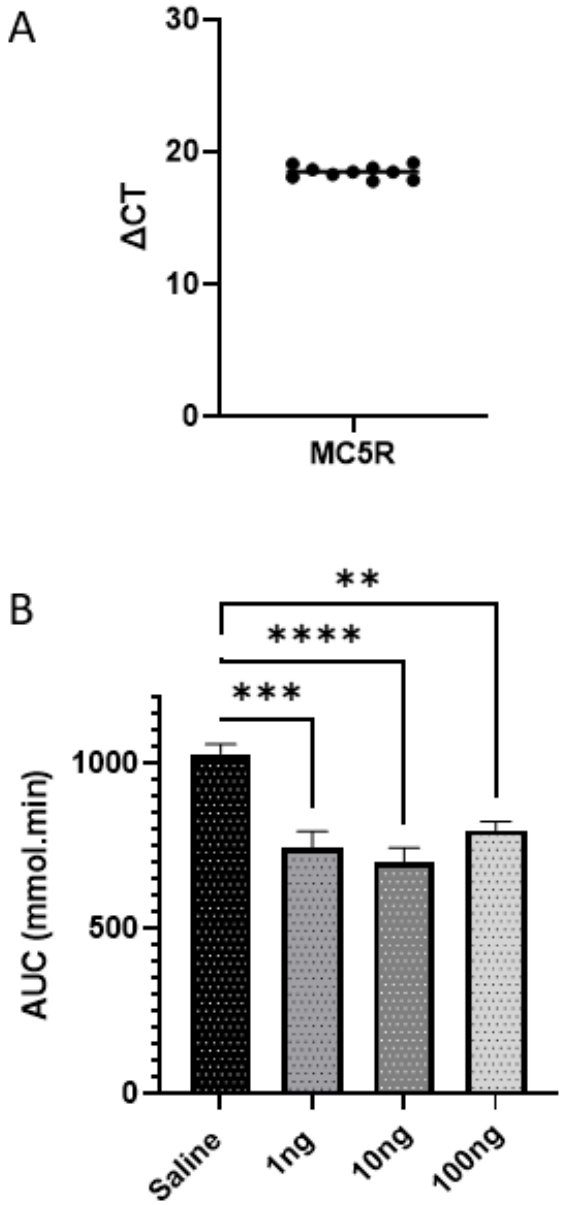

Figure 4.1 MCR5 expression in mice gastrocnemius muscle and glucose AUC during i.p. glucose tolerance tests.

*MC5R gastrocnemius mRNA expression and AUC of i.p glucose tolerance tests following bolus injections in C56/B7 mice. A) MC5R is highly expressed in mouse gastrocnemius muscle (mean 18.49 ± 0.47 ΔCT, n=10). 18S used as internal control. Each data point is a sample from a discrete mouse assayed in duplicate. B) Area under the curve of glucose from 60 minute i.p glucose tolerance tests following bolus injections of saline, 1ng, 10ng and 100ng α-MSH. **p<0.005, ***p<0.0005, ****p<0.00005 vs. Saline. Data are presented as mean ± SD. Statistical analysis was performed with mixed-effects analysis and Dunnett's multiple comparison test.*

4.3.2 Healthy Volunteer Cohort Characteristics

This clinical investigation did not fall under the scope of a clinical trial and was approved as a physiological study by the London-Fulham Research Ethics Committee (IRAS ID; 275910, REC Ref; 20/LO/0355) in March 2020. Formal recruitment began in October 2020.

Fifteen healthy volunteers over 18 years of age and with no major medical conditions successfully passed screening and were entered into the study. The cohort consisted of 8 male and 7 female participants. All participants were metabolically healthy, with a BMI ≥18 <30 Kg/m2, normal fasting glucose (<5.6 mmol/L) and HbA1c (<48 mmol/mol) **(Table 4.1)**.

Measurement	Mean	SD
Age (years)	28	8.4
Height (cm)	174	12
Weight (kg)	73	15
Body fat (%)	24	5.9
Fat mass (kg)	28	40
Fat free mass (kg)	53	11
Resting metabolic rate (kcal)	1663	337
BMI (kg/m^2)	24	3
Fasting glucose (mmol/L)	4.5	0.32
HbA1c (mmol/mol)	32	4.1
Sex	8M,7F	

Table 4.1 Anthropometric and metabolic characteristics of healthy participants who successfully passed screening and were entered into the study (n=15).

4.3.3 Oral Glucose Tolerance Tests

Using a randomized double-blinded, cross-over design, fifteen healthy volunteers completed four oral glucose tolerance tests each while receiving either infusions of saline, 15, 150 and 1500 ng/kg/hr α-MSH. Infusions of saline or α-MSH began 30 minutes prior to consumption of the oral glucose load (T=-30). Plasma samples were collected at timepoints -30, 0, 15, 30, 60, 120 and 180 minutes (**Fig. 4.2**).

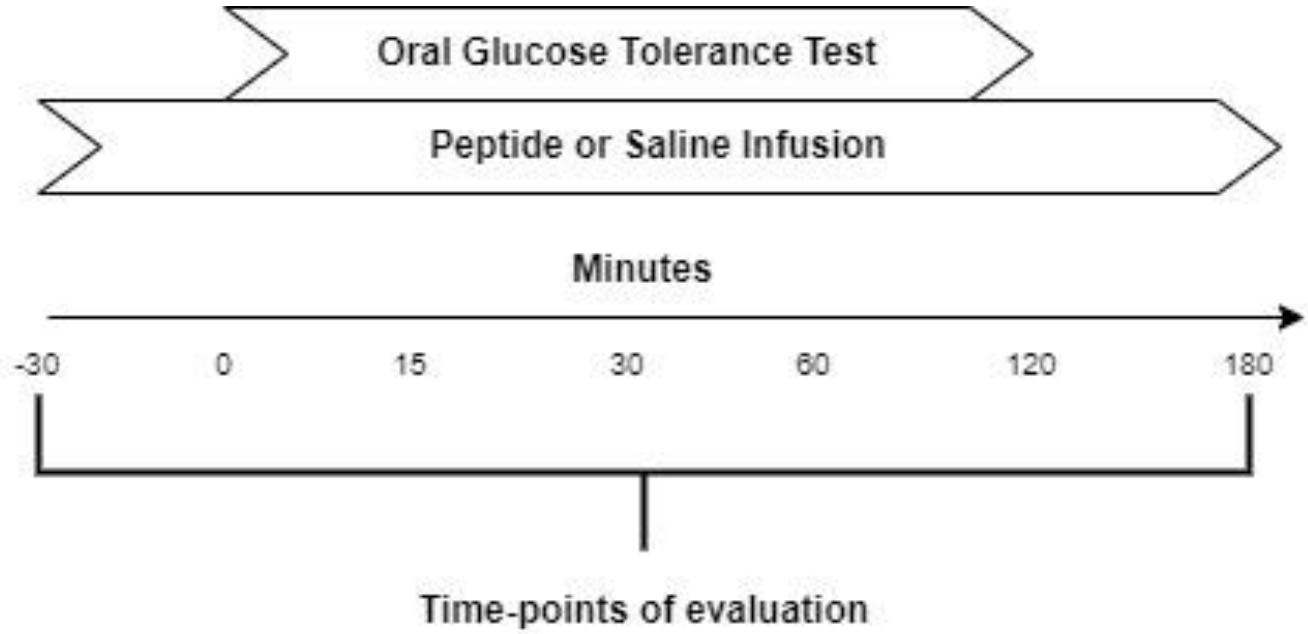

Figure 4.2 Study schematic of oral glucose tolerance test visits.

Blood samples were taken at the time points of evaluation indicated.

4.3.3.1 Glucose Clearance during OGTT α-MSH Infusions

Plasma glucose in blood samples taken at timepoints of evaluation were assessed by clinical biochemistry services at ICL.

Due to the small sample size of the study, a Shapiro-Wilk test was performed to test for non-normality. Glucose and insulin data did not show evidence of non-normality (**Appendix 8.7**). No significant reduction in glucose was observed in a two-way ANOVA analysis of time and dose (**Table 4.2 overleaf**). Incremental area under the curve (iAUC) during the OGTT (0-120 minutes) was calculated for each participant by using their individual fasting blood glucose reading as baseline for area under the curve calculations. Blood glucose iAUC trended downwards with escalating doses of α-MSH, with the highest dose of 1500 ng/kg/hr having the largest effect compared to saline (187.2 ± 31.01 mmol.min vs. 250.4 ± 28.63 mmol.min, p=0.09) **(Fig. 4.3 B overleaf)**.

Exploratory analysis was conducted and the difference in blood glucose during each infusion of α-MSH compared to saline at each timepoint was calculated. The largest reductions in blood glucose occurred during the hyperglycaemic peak of the OGTT, at timepoints 30 and 60 minutes **(Fig. 4.4 overleaf)**. Narrowing the iAUC analysis to timepoints 0-60 minutes, 1500 ng/kg/hr infusions of α-MSH significant reduced iAUC for blood glucose compared to saline in a post-hoc analysis of the data set (92.47 ± 11.81 mmol.min vs. 126.5 ± 11.25 mmol.min, p=0.03) **(Fig. 4.5 overleaf)**.

	F (DFn, DFd)	P value
Time	F (2.157, 30.19) = 35.02	P<0.0001
Dose	F (2.586, 36.21) = 2.560	P=0.0780
Time x Dose	F (5.208, 72.92) = 1.314	P=0.2665

Table 4.2 Two-way ANOVA analysis of glucose time x dose during OGTT infusions. n=15.

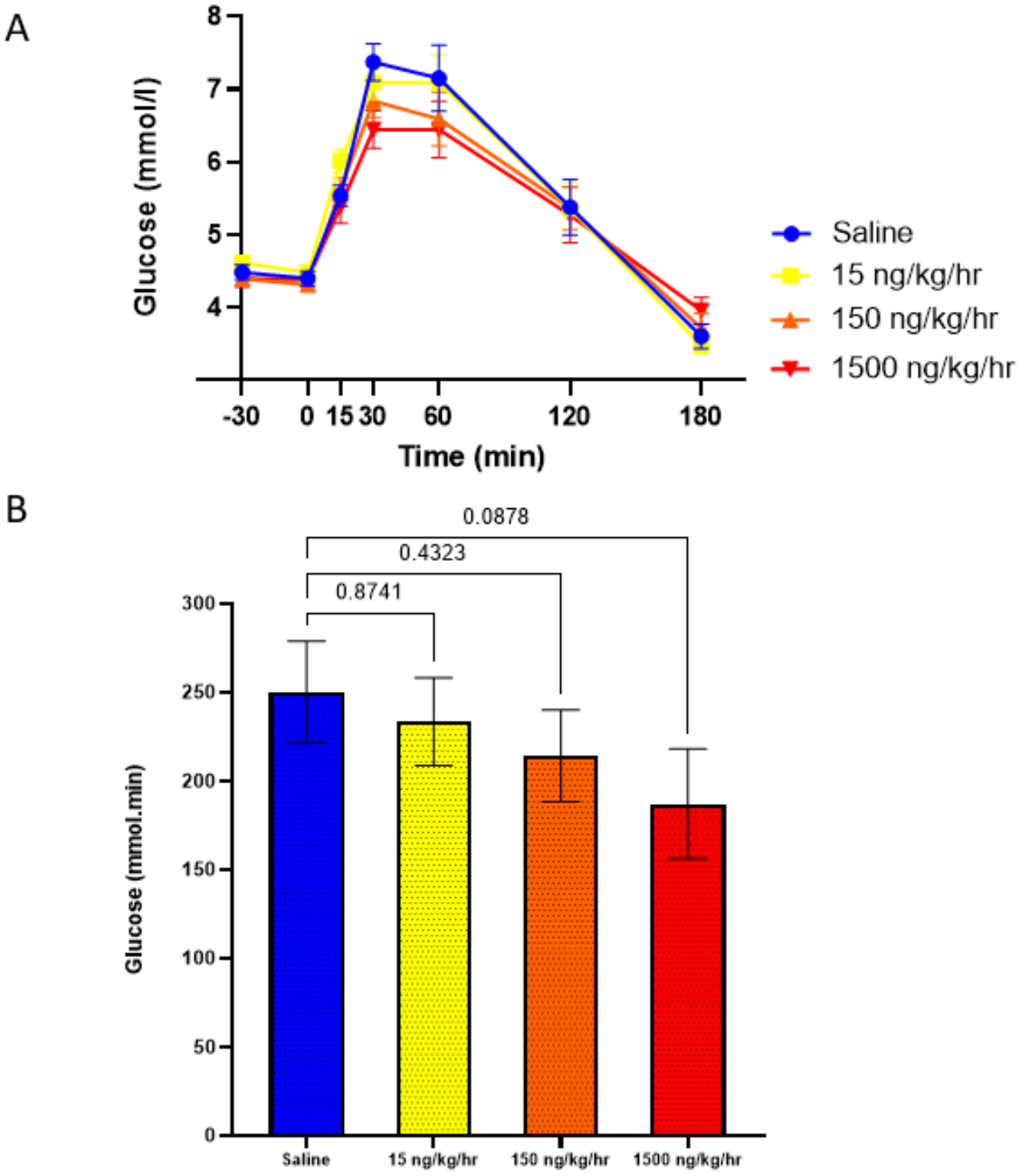

Figure 4.3 Glucose measurements during oral glucose tolerance tests.

Blood glucose (mmol/l) measured during oral glucose tolerance tests (n=15) Two-way ANOVA p=0.26. Data shown as mean ± SEM. B). iAUC of blood glucose levels (mmol.min) from timepoints 0 to 120 minutes of OGTTs (n=15). Data are presented as mean ± SEM. One-way ANOVA p=0.09.

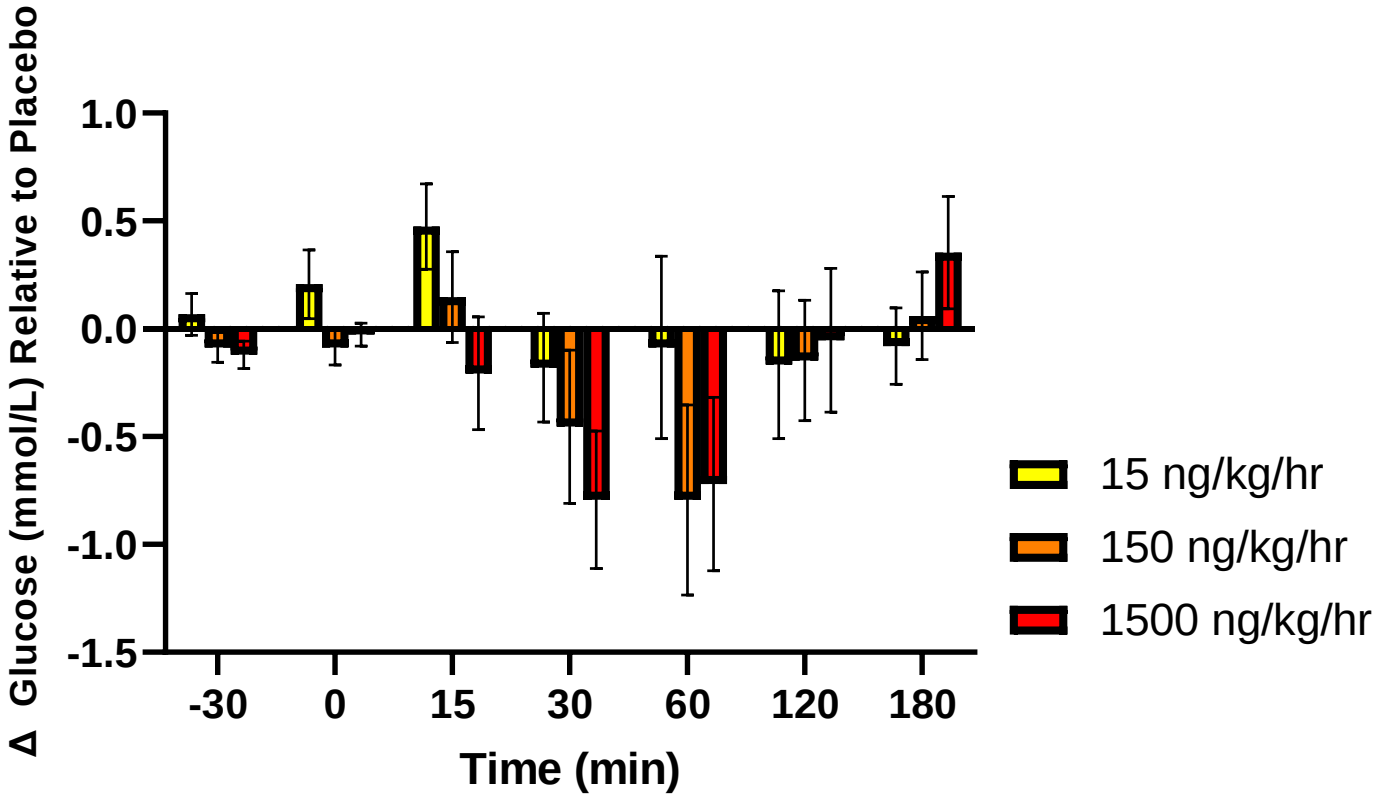

Figure 4.4 Delta glucose measurements during α-MSH infusions.

Change in blood glucose (mmol/L) during α-MSH infusions relative to placebo at timepoints indicated (n=15). Data shown as mean ± SEM.

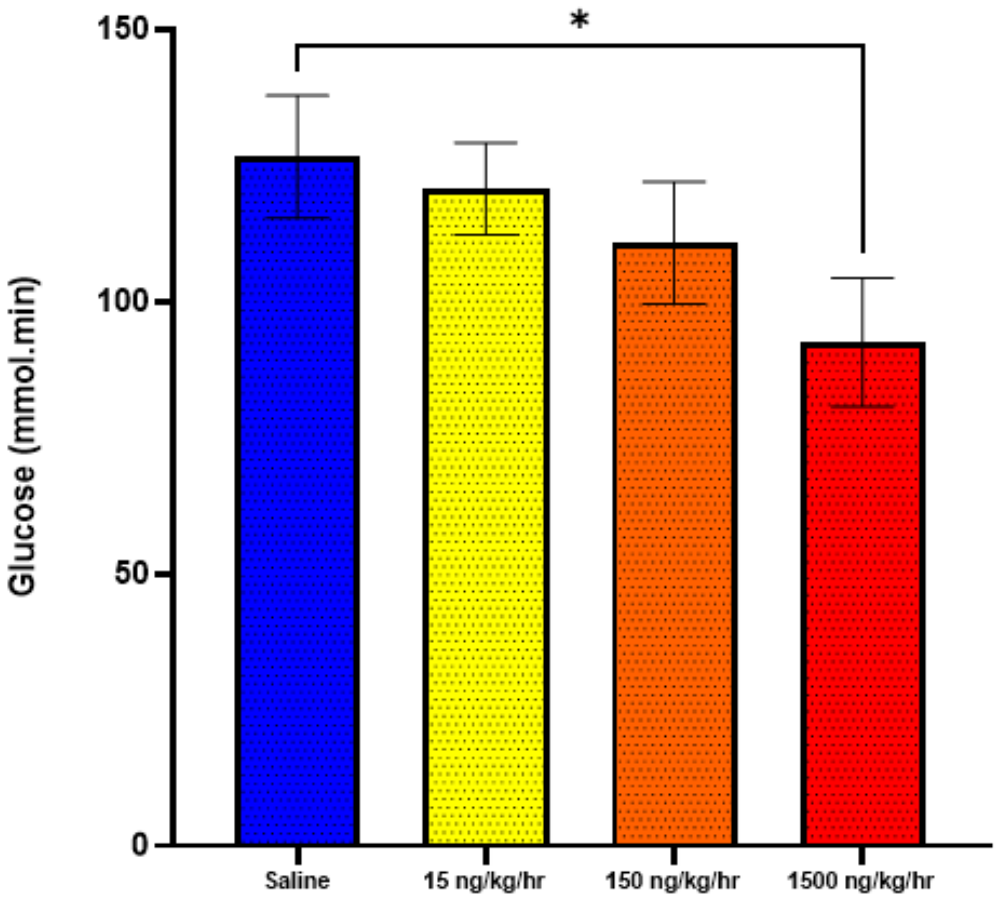

Figure 4.5 Sixty-minute glucose iAUC during OGTTs.

*iAUC of blood glucose levels (mmol.min) from timepoints 0 to 60 minutes of OGTTs (n=15). *p<0.05 vs. Saline. Data are presented as mean ± SEM. Statistical analysis was performed with one-way ANOVA with post-hoc Dunnett's multiple comparison test.*

4.3.3.2 Total GLP-1 levels in responders

Conflicting data has been published on whether α-MSH directly causes enteroendocrine L-cells to secrete GLP-1 (196,197). An enzyme-linked immunoassay (ELISA) was carried out to assess whether increased GLP-1 secretion in response to α-MSH caused a glucose tolerising effect. Plasma samples from six responders, as defined by a <20% reduction in iAUC between Saline and 1500 ng/kg/hr infusions, were chosen to be assayed for total GLP-1.

No significant difference in iAUC of total GLP-1 levels between saline and 1500 ng/kg/hr α-MSH infusions was measured in the six responders (616 ± 91.63 pmol/L.min vs. 593.2 ± 101.5 pmol/L.min, p=0.8) **(Fig. 4.6 overleaf)**.

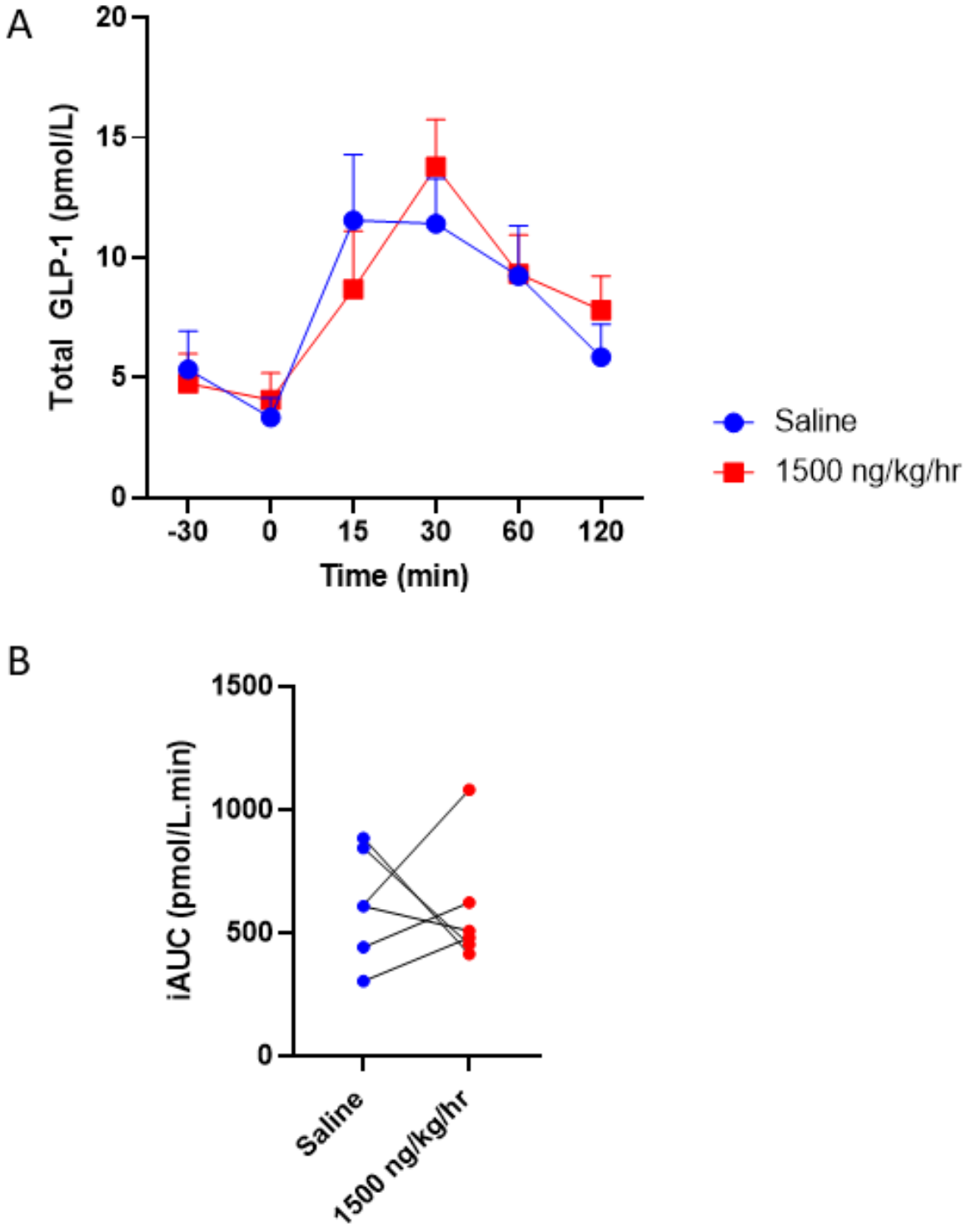

Figure 4.6 Total GLP-1 measurements during oral glucose tolerance tests.

A) Total GLP-1 (pmol/L) measured during oral glucose tolerance tests (n=6) Data shown as mean ± SEM. B) iAUC of total GLP-1 levels (pmol/L) from timepoints -30 to 120 minutes of OGTTs (n=6). Data are presented as mean ± SEM. Paired t-test p=0.08.

4.3.3.3 Plasma Insulin during OGTT α-MSH Infusions

Plasma was harvested from blood samples taken prior (T= -30), during (T=0-120) and after (T=180) the OGTT and assayed for insulin.

No significant reduction in insulin was observed in a two-way ANOVA analysis of time and dose (**Table 4.3**). Incremental area under the curve (iAUC) during the OGTT (0-120 minutes) was calculated for each participant by using their individual fasting insulin reading as baseline for area under the curve calculations. In a similar manner to glucose, insulin iAUC trended downwards with escalating doses of α-MSH, with the highest dose of 1500 ng/kg/hr having the largest effect compared to saline (4455 ± 568 µU/mL vs. 5484 ± 781 µU/mL, p=0.08) **(Fig. 4.7 B overleaf)**.

Exploratory analysis was conducted and the difference in plasma insulin during each infusion of α-MSH compared to saline at each timepoint was calculated. The highest dose of 1500 ng/kg/hr α-MSH consistently had the lowest maximum insulin levels during the hyperinsulinaemic peak of the OGTT (timepoints 15, 30 and 60 minutes). At 60 minutes, a similar insulin sparing effect was observed at all doses of α-MSH **(Fig. 4.8 overleaf)**. Similar to glucose, narrowing the iAUC to timepoints 0-60 minutes in post-hoc analysis, 1500 ng/kg/hr infusions of α-MSH significant reduced iAUC for blood glucose compared to saline (2137 ± 359.3 µU/mL vs. 2773 ± 472.8 µU/mL, p=0.006) **(Fig. 4.9 overleaf)**.

The ratio of plasma insulin to blood glucose (µU/mmol) was calculated at each timepoint. Insulin/glucose ratios were reduced following the glucose load at 15, 30 and 60 minutes **(Fig. 4.10 overleaf)**.

	F (DFn, DFd)	P value
Time	F (2.584, 36.18) = 24.80	P<0.0001
Dose	F (2.095, 29.34) = 3.842	P=0.03
Time x Dose	F (3.804, 53.26) = 2.164	P=0.09

Table 4.3 Two-way ANOVA analysis of insulin time x dose during OGTT infusions. n=15

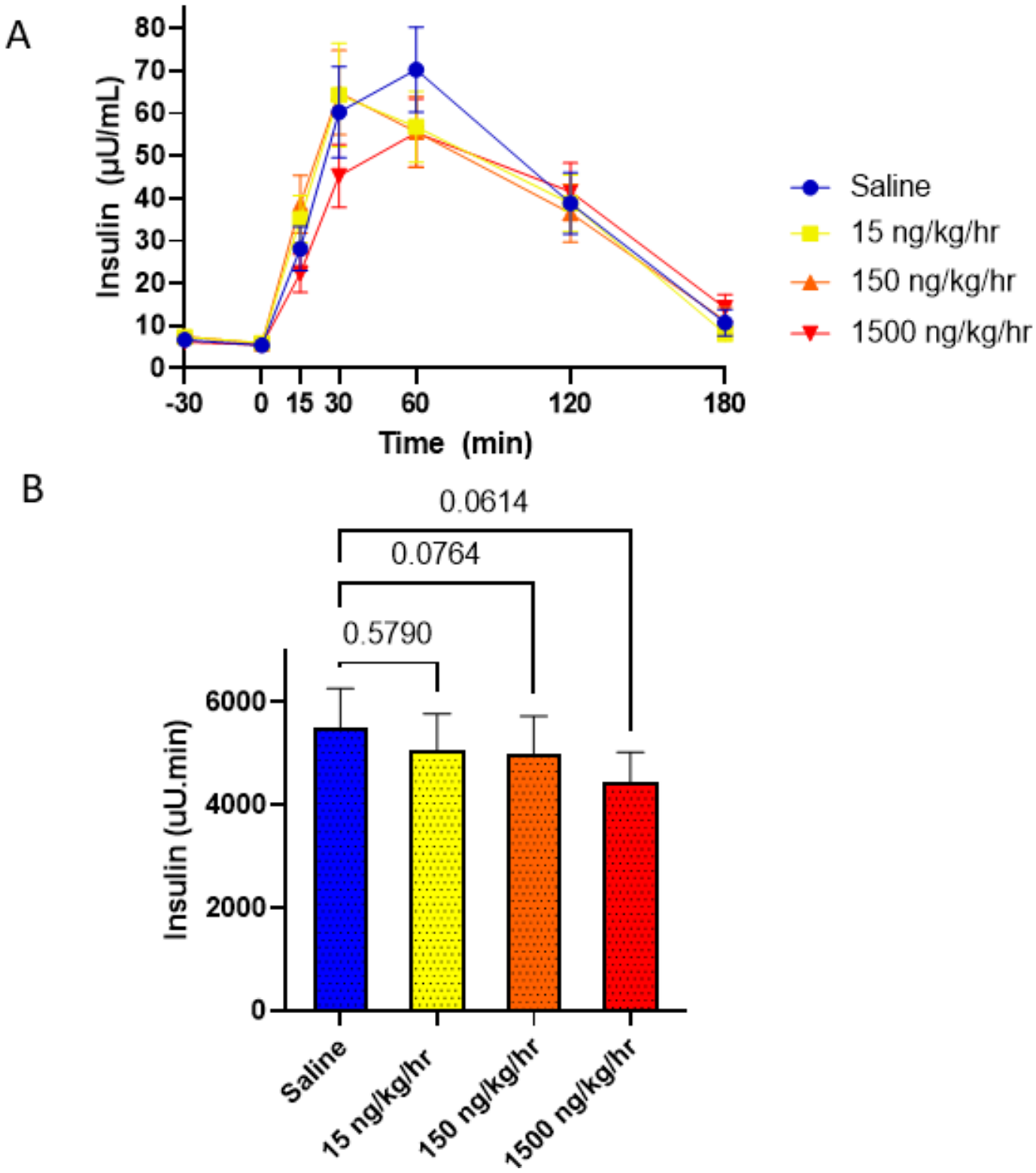

Figure 4.7 Insulin measurements during oral glucose tolerance tests.

A) Plasma insulin (µU/mL) measured during oral glucose tolerance tests (n=15).Two-way ANOVA p=0.09. Data shown as mean ± SEM. B) iAUC of plasma insulin levels (µU/mL) from timepoints 0 to 120 minutes of OGTTs (n=15). Data are presented as mean ± SEM. One-way ANOVA p=0.08.

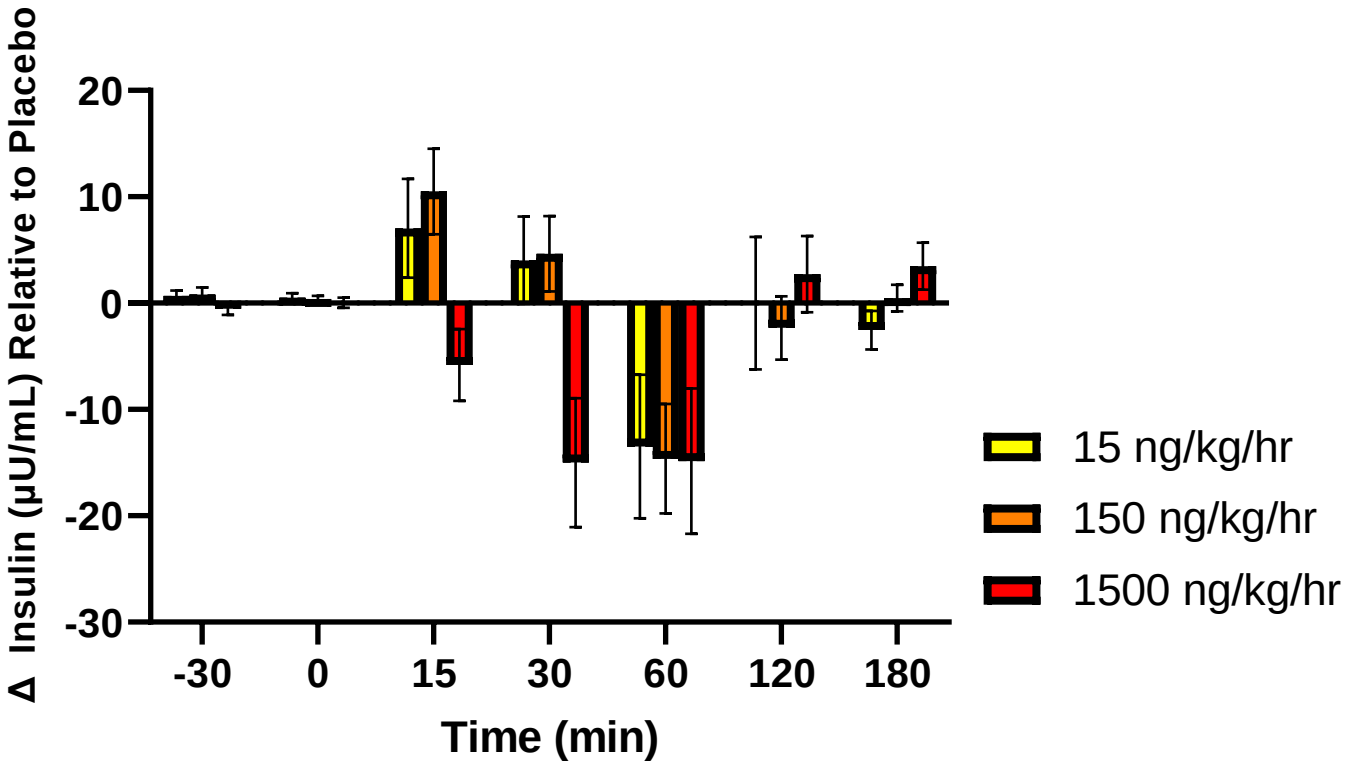

Figure 4.8 Delta plasma insulin measurements during α-MSH infusions.

Change in plasma insulin (μU/mL) during α-MSH infusions relative to placebo at timepoints indicated (n=15). Data shown as mean ± SEM.

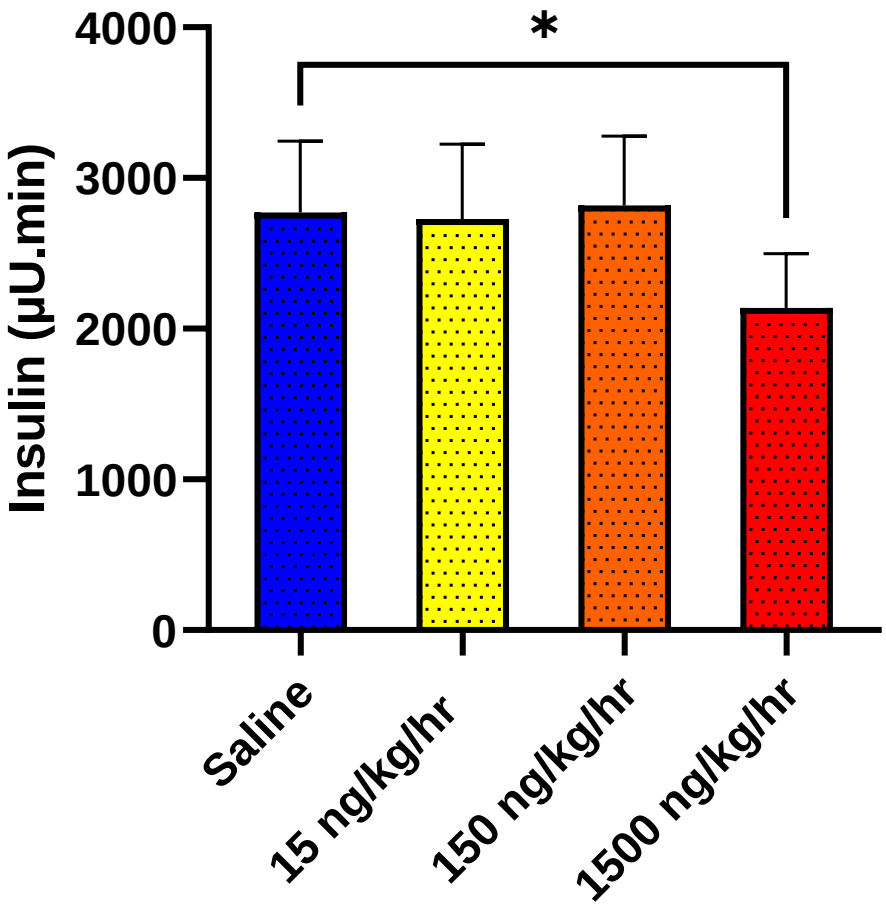

Figure 4.9 60-minute iAUC of plasma insulin during OGTTs.

iAUC of plasma insulin levels (µU/mL) from timepoints 0 to 60 minutes of OGTTs (n=15). Data are presented as mean ± SEM. One-way ANOVA p=0.006, post-hoc Dunnett's comparison test Saline vs. 1500 ng/kg/hr p=0.014).

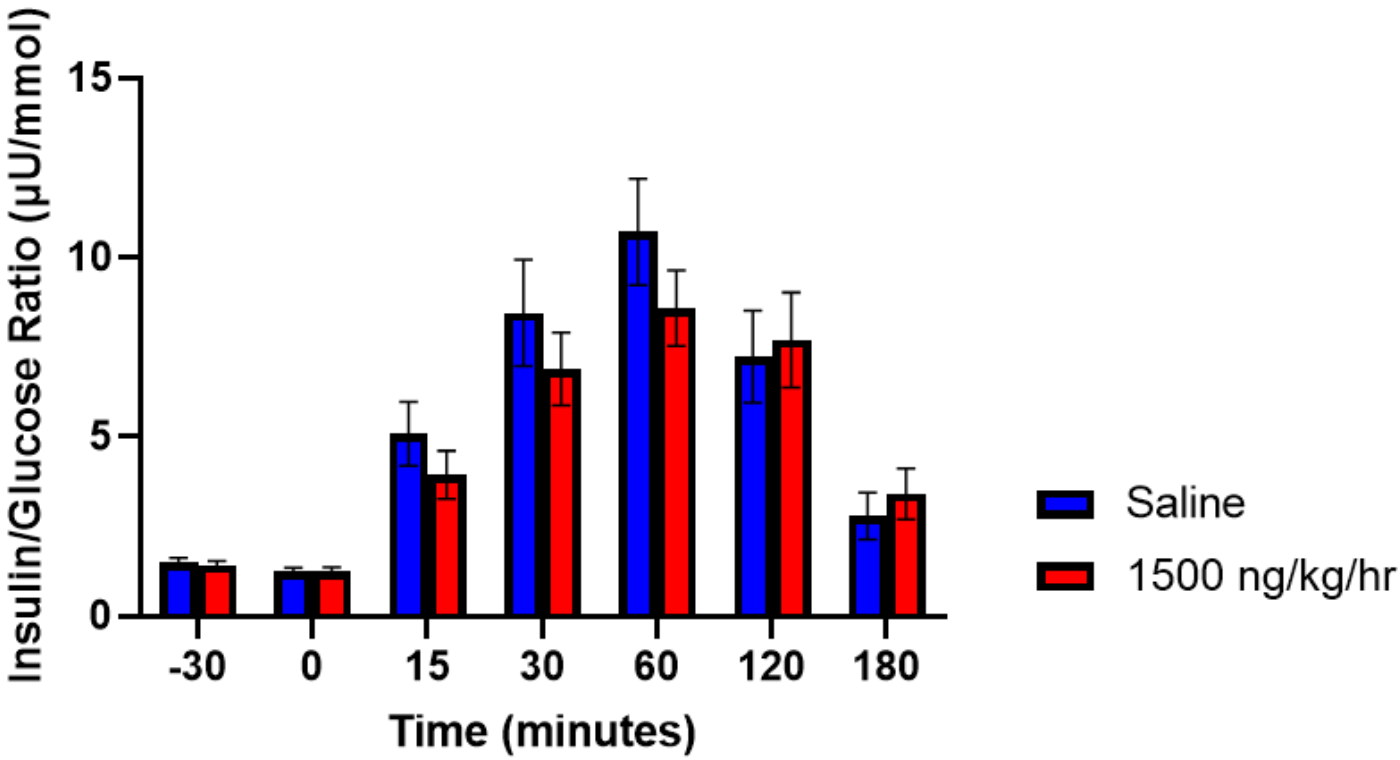

Figure 4.10 Insulin to glucose ratio (µU/mmol) during OGTTs.

Data shown as mean ± SEM. Multiple paired t-tests 1500 ng/kg/hr vs. Saline; -30 minutes p=0..5, 0 minutes p=0.9, 15 minutes p=0.08, 30 minutes p=0.08, 60 minutes p=0.1, 120 minutes p=0.4, 180 minutes p=0.2 (n=15).

4.3.4 Hyperinsulinaemic-Euglycaemic Clamps

Once 10 participants had completed the OGTT phase of the study (infusions of saline and 3 doses of α-MSH) and interim unblinding of the data was carried out, and the most effective dose, as defined by the greatest reduction in glucose iAUC between 0-120 minutes, chosen to proceed with in hyperinsulinaemic-euglycaemic clamps. Demonstrating the largest reduction in glucose iAUC, a dose of 150 ng/kg/hr was chosen to administer during clamps in a double-blinded, placebo controlled randomized design. However, as shown ultimately 150 ng/kg/hr rather than 150 ng/kg/hr was the most effective dose in OGTT upon analysis of the complete data set.

Fasting blood glucose was measured at baseline (0 minutes), and a range of ± 0.5 mmol from this measurement was used as a target to maintain euglycaemia. A modified design of a traditional hyperinsulinaemic-euglycaemic clamp experiment was employed, separated into two stages **(Fig 4.11 overleaf**). Stage 1 (0 to 120 minutes) consisted of an infusion of either saline or 150 ng/kg/hr α-MSH. Blood glucose was measured every 10 minutes and an intravenous infusion of 20% dextrose was initiated as necessary to maintain the defined euglycaemic range. At 120 minutes an intravenous infusion of insulin was initiated at a dose of 1 μU/kg/hr for 180 minutes alongside α-MSH or saline. The glucose infusion rate (GIR) of 20% dextrose was increased as necessary to maintain euglycaemia. Fourteen participants completed both clamp visits, with one drop-out.

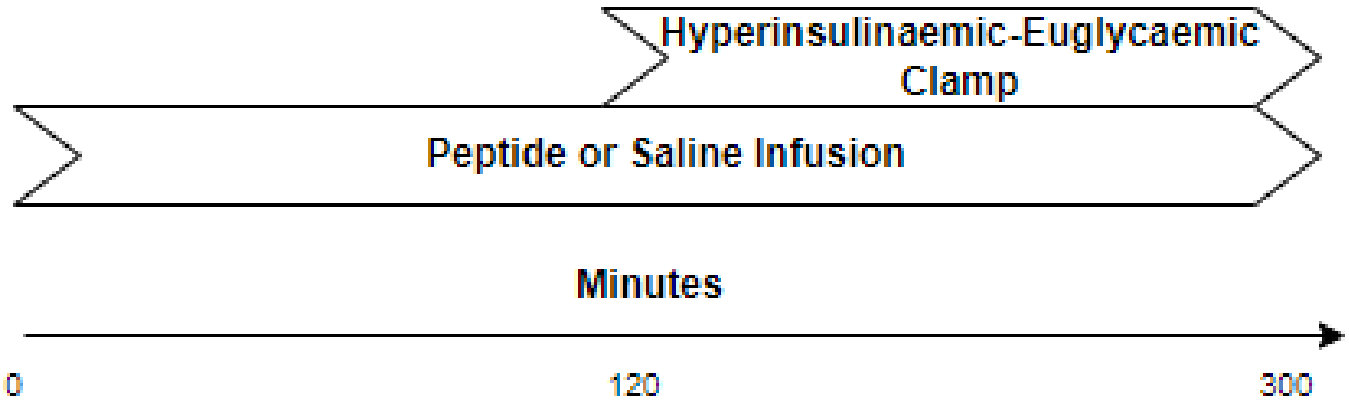

Figure 4.11 Study schematic of clamp visits.

Peptide or α-MSH infusion was initiated 120 minutes prior to beginning the insulin infusion and subsequent clamp. Blood glucose was measured every 10 minutes for 300 minutes. Plasma was collected at 0, 30, 60, 90, 110, 120, 150, 240, 270, 290, and 300 minutes.

During Stage 1, α-MSH marginally increased the GIR needed to maintain the euglycaemic range (t=90-100 minutes, 0.47 mg/kg/min vs. 0.26 mg/kg/min) **(Fig. 4.12 overleaf)**. However, both the low levels of glucose needed to maintain euglycaemia during α-MSH infusions and the magnitude of effect compared to placebo were not considered physiologically relevant. Additionally, in some participants the glucose needed to be initiated during saline infusions, possibly confounded by the extended fasting time.

Area under the curve for the duration of Stage 2 (120-300 minutes) was increased during α-MSH infusions (610.3 ± 79.03 mg/kg vs. 520.8 ± 66.03 mg/kg, p=0.1). This increase in GIR was not observed to the same extent by the time the plateau phase (270-300 minutes) of the clamp was reached (insulin adjusted GIR 0.1297 ± 0.01 mg/kg vs. 0.1229 ± 0.01 mg/kg) **(Fig. 4.13 overleaf)**.

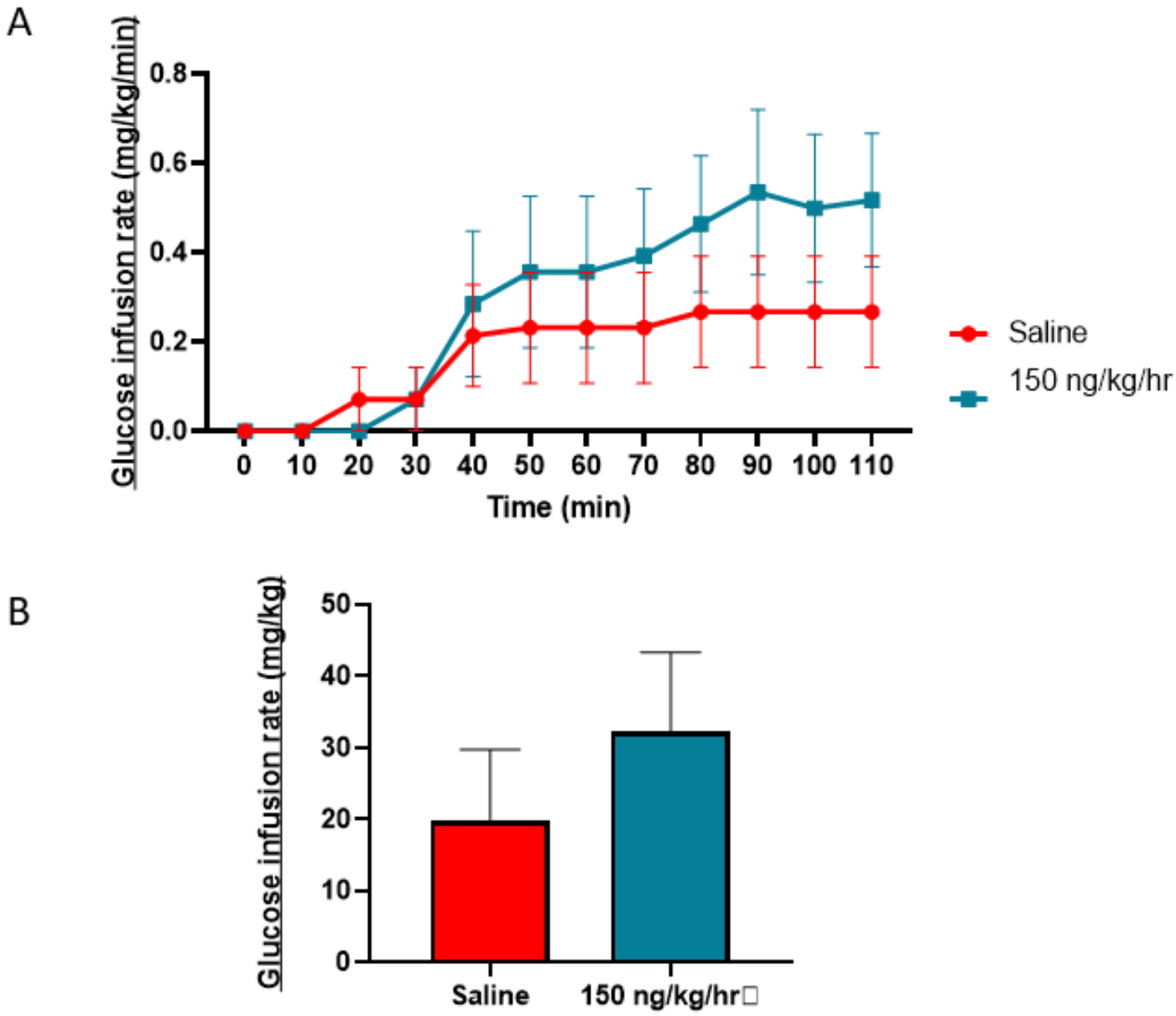

Figure 4.12 Glucose infusion rate (GIR) during the first stage of hyperinsulinaemic-euglycaemic clamps.

A) GIR from timepoints 0 to 110 minutes. Data presented as mean ± SEM B) iAUC of GIR during the first stage. Data presented as mean ± SEM. Statistical analysis was performed using paired t-test, p=0.4.

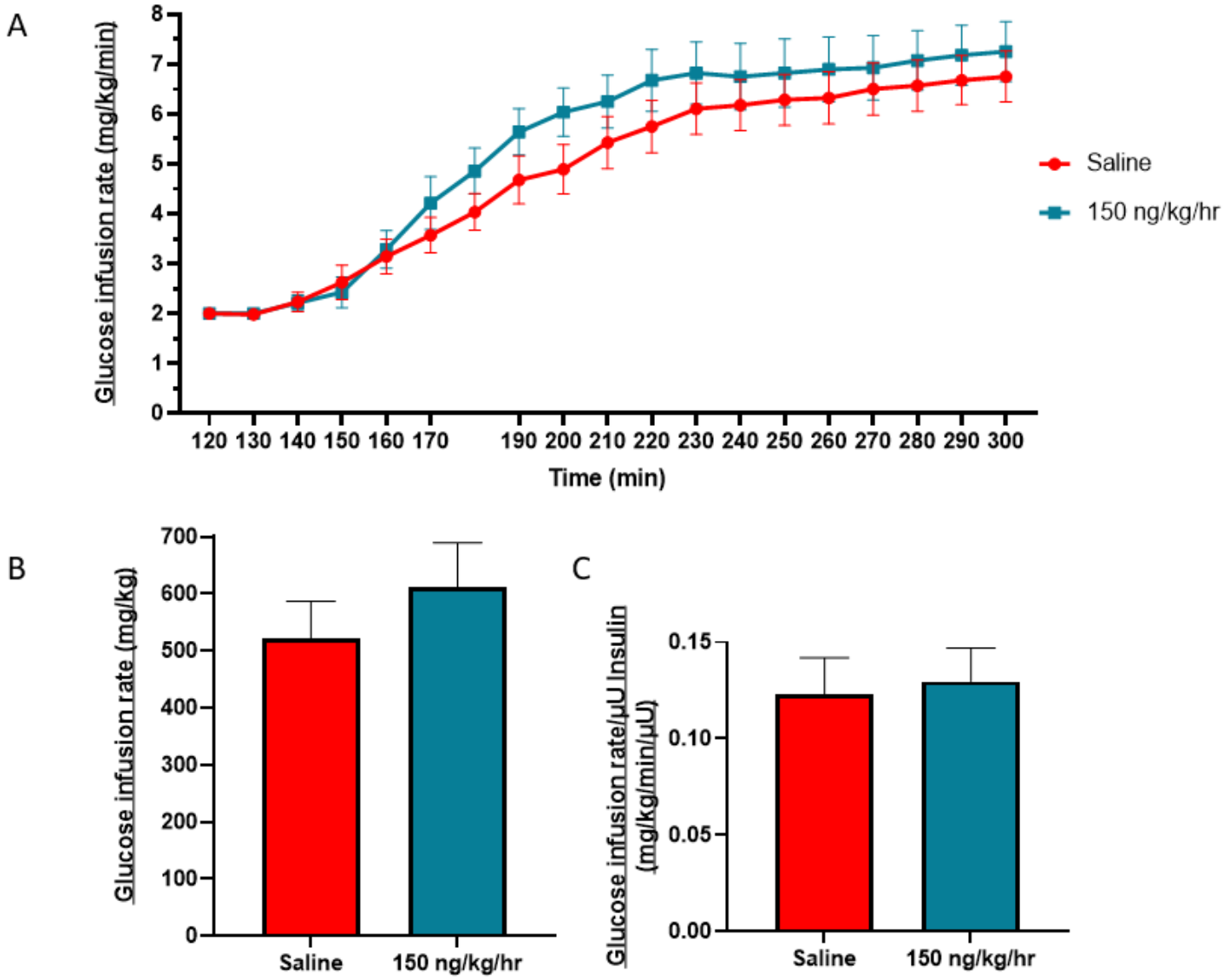

Figure 4.13 Glucose infusion rate (GIR) during the second stage of hyperinsulinaemic-euglycaemic clamps.

A) GIR from timepoints 120 to 300 minutes. Data presented as mean ± SEM. B) iAUC of GIR during the second stage. Data presented as mean ± SEM. Statistical analysis was performed using paired t-test, p=0.1. C) GIR adjusted to plasma insulins levels during the stage state (270-300 minutes). Data presented as mean ± SEM. Statistical analysis was performed using paired t-test, p=0.3.

4.4 Adverse Events

The peptide was well tolerated with the exceptions of facial flushing in two participants during OGTT infusions of 1500 ng/kg/hr α-MSH. Nausea was reported by one participant during the insulin phase of the clamp while receiving a saline infusion.

4.5 Discussion

The aim of this chapter was to carry out a first of its kind physiological response study in healthy volunteers in which the effects of α-MSH on glucose tolerance and uptake was investigated.

Prior to commencing the clinical study, an *in vivo* investigation administering bolus injections of α-MSH during an intraperitoneal glucose tolerance test was conducted. Ten mice were administered i.p. glucose tolerance tests after receiving injections of saline, following by subsequent escalating doses (1, 10 and 100ng) of α-MSH, each one week apart. These doses were chosen to reflect the total exposure mice had received to the peptide during previous infusions which were found effective (205). All doses of the peptide produced a significant improvement in glucose tolerance in mice. Whilst this physiological effect has been recorded previously during infusions, this presents novel data that pre-prandial bolus injections, as well as continuous infusions, can lead to increases in glucose tolerance in mice. Gastrocnemius muscle samples were taken upon euthanasia and expression of MC5R measured by qRT-PCR. MC5R was found to be highly abundant, consistent with published data (187,200,205).

Fifteen healthy volunteers were recruited to take part in a physiological study in Hammersmith Hospital, part of the Imperial College London Healthcare Trust (REC reference 20/LO/0355). Due to the novelty of this investigation, strict inclusion and exclusion criteria were employed to ensure participants were of sound metabolic health. All participants were between 18-50 years old, with a healthy BMI, stable body weight for 3 months, and a normal fasting blood glucose with no history of endocrine disorders. Allometric scaling, a method preferred for inter-species dose conversions of short half-life peptides(280,281), was used to convert the effective dose range observed in mice (205), to humans (**Appendix 6.5**). Three ten-fold increments beginning at the lower end of this dose range (15 ng/kg/hr) were chosen to employ in human infusions. Unpublished data from Prof. Michael Cowley has demonstrated that in primates, allometrically scaled doses at the upper end of the range previously used causes a counterregulatory response of unknown mechanism, reversing the glucose tolerising effects seen at lower doses. Thus, doses at the lower end of the allometrically scaled effective range were chosen for this first-in-human investigation. Additionally,

establishing ineffective lower doses in humans may be beneficial for the design of future studies.

Using a randomized double-blinded, cross-over design, the fifteen healthy volunteers that passed screening then completed four oral glucose tolerance tests each while receiving infusions of saline, 15, 150 and 1500 ng/kg/hr α-MSH. Infusions of saline or α-MSH began 30 minutes prior to consumption of the oral glucose load (T=-30). This 30-minute pre-infusion of the peptide before the OGTT began was to allow for circulating α-MSH to equilibrate.

Analysis of the primary endpoint (0-120 minute glucose iAUC) revealed improvements in glucose tolerance during infusions of 15 and 150 ng/kg/hr, with the greatest effect size observed at a dose of 1500 ng/kg/hr. Exploratory analysis of the data calculating the delta blood glucose between placebo and each dose across each timepoint, it is apparent that instead of lowering blood glucose across all timepoints, α-MSH is having its impact during the hyperglycaemic peak of the OGTT (15, 30 and 60 minutes) by blunting post-prandial glucose excursions. Upon narrowing down the iAUC analysis to the timeframe this effect is observed at (0-60 minutes) during post-hoc analysis, 1500 ng/kg/hr produces a significant reduction in the average glucose iAUC of approximately 27%.

In a study by Panaro et al. in 2014, it was shown that MC4R is diffusely expressed across the human GI system, and that infusion of a MC4R receptor agonist in mice rapidly elevated plasma GLP-1 (196). In a pilot experiment investigating whether this improvement in glucose tolerance observed in humans was mediated by increased GLP-1 release leading to amplified insulin secretion, plasma samples from six responders (as defined by a 20% reduction in iAUC during 1500 ng/kg/hr OGTT infusions) were assayed for total GLP-1. No change in total GLP-1 was observed between saline and α-MSH infusions in these samples. In August of 2021, a study failing to corroborate Panaro et al. was published in which it was demonstrated that MC4R expression is marginal in the small intestine of mice and humans, and that MC4R agonism in mice and rats does not stimulate GLP-1 secretion (197). *In vitro* data as described in Chapter 4 supports the hypothesis that systemic α-MSH is improving

glucose tolerance in humans during an OGTT by acting directly on the skeletal muscle, causing glucose uptake and clearance from the blood

Plasma insulin was measured in samples taken at all timepoints during OGTT visits for secondary endpoint analysis. The effect of α-MSH infusions on insulin levels was similar to glucose in that while the reduction in insulin during the 0–120-minute iAUC was marginal, during post-hoc analysis profound decreases in insulin levels at timepoints 15, 30 and 60 minutes were observed, with a dose of 1500 ng/kg/hr α-MSH reducing the 0–60-minute iAUC by an average of 23%. As demonstrated in **Fig. 5.7**, at 60 minutes all doses of α-MSH lead to a reduction in insulin levels which does not necessarily reflect the effect size in glucose reduction at each timepoint, particularly at a dose of 15 ng/kg/hr. Upon further examination comparing individual glucose and insulin curves within the same participant, in several cases insulin levels are drastically reduced in response to α-MSH without a concomitant reduction in glucose levels. This suggests that glucose levels may not be the primary outcome measure of a “response” to the peptide infusions, as in some participants where glucose levels remained unchanged between saline and α-MSH, there was a significant reduction in insulin.
Thus, we hypothesise the glucose tolerising effects of α-MSH during an OGTT appears to manifest a physiological response by reducing hyperglycaemic excursions after a glucose challenge thereby blunting insulin secretion in during the time points measured.

In the same cohort of participants, a hyperinsulinaemic-euglycaemic clamp was performed with infusions of saline or α-MSH as part of a secondary study objective. The purpose of this widely applied clinical research method (72,282) is to obtain a quantitative measure of whole body insulin sensitivity by measuring the rate at which intravenous glucose is required to maintain euglycaemia. In the basal state, glucose homeostasis is maintained by a balance of endogenous glucose production and glucose (both insulin dependent and independent) uptake in tissue. The value of the clamp technique lies in that during these conditions, endogenous glucose production is greatly supressed thus allowing the relationship between endogenous glucose production and uptake of exogenously administered glucose to be teased apart. Insulin sensitivity during the clamp is expressed as a mean of the GIR once steady state (a balance between glucose uptake and exogenous glucose infusion after a prolonged

period of hyperinsulinaemia) is achieved, usually in the final 30 minutes of the experiment. Although muscle specific glucose uptake was not measured, which is typically done via tracer molecules and muscle biopsies, skeletal muscle accounts for 80% of glucose uptake in the hyperinsulinaemic steady state (21,72). This steady-state GIR is then normalized by the plasma insulin level at the time to provide an accurate assessment of whole-body insulin sensitivity and glucose uptake.

Prior to commencement of the clamp phase of the study, an interim unblinding was carried out once 10 participants completed OGTTs with saline and all three doses of the peptide. This data set showed that the middle dose of 150 ng/kg/hr was the most effective at reducing glucose iAUC, therefor was chosen as the dose to use during the clamps.

A modified design of the traditional single-stage, high-dose insulin clamp was employed in which a monitoring period, which we termed 1st Stage, preceding the initiation of an insulin infusion was carried out for 120 minutes. During this 1st Stage, the infusion of saline or α-MSH was initiated whilst blood glucose was measured every 10 minutes and a 20% dextrose bag was connected to an intravenous line as per standard clamp protocol. If necessary, if a participant's blood glucose began to fall below the clamped euglycaemic range, the dextrose infusion was started. The purpose of this augmentation to the clamp protocol was to investigate whether an infusion of α-MSH would reduce blood glucose levels in the basal state. Although a minor increase in the glucose infusion rate (GIR) was observed in α-MSH infusions during this phase, this was physiologically insignificant and confounded by the fact that glucose infusions were occasionally required during placebo, potentially owing to the extended period of fasting. This matches pre-clinical findings in mice, where basal euglycaemia was unaffected by continuous α-MSH infusion (205).

At 120 minutes from the initiation of either saline or α-MSH infusions, insulin was administered at a rate of 1 μU/kg/hr for 180 minutes and the GIR increased as necessary to maintain the euglycaemic clamp. While 150 ng/kg/hr α-MSH led to a noticeable increase in the GIR needed to maintain euglycaemia during the equilibration phase (180-270 minutes) of the clamp, by the time the glucose infusion was equilibrated with whole body glucose uptake the difference, although still present, had lessened. This may be attributed partly to receptor desensitization to the peptide, as

by the time the equilibration phase was reached the participant had been receiving a continuous infusion of α-MSH for almost 5 hours. Although an insulin reducing effect was seen across all doses during OGTTs, future studies in which a dose of 1500 ng/kg/hr and muscle biopsies are taken before and after the clamp will be invaluable in elucidating whether a higher dose of α-MSH can further increase whole body glucose uptake, and if a continuous infusion of this length can lead to desensitization to the peptide.

This study represents the first time α-MSH has been continuously infused into humans and its impact on glucose homeostasis assessed. Although the primary outcome of the trial (0-120 minute glucose iAUC analysis) did not reveal any statistically significant results, post-hoc analysis tentatively suggest a previously undiscovered mechanism in which peripheral melanocortin receptor agonism can improve post-prandial glucose tolerance as demonstrated by a reduction in glucose iAUC during oral glucose tolerance tests. In the context of a concomitant reduction in insulin levels alongside this increase in glucose clearance alongside the direct action of α-MSH on human myotubes *in vitro* inducing glucose uptake via MC5R may be evidence of a novel pathway in which skeletal muscle melanocortin agonism induces an insulin-like physiological response in humans by clearing glucose from the blood via skeletal muscle. During the high-dose (1 μU/kg/hr) insulin infusions of the clamps described herein, a maximal insulin-induced glucose uptake response is occurring in peripheral tissue. In this physiological state, α-MSH appears to further increase this response beyond the maximum response possible with endogenous insulin alone. This suggests a pathway that may be responsible for insulin-independent glucose uptake.
The data generated from this pilot study presents an exciting justification for further clinical investigations, both in healthy and diabetic volunteers.

Chapter Five

General Discussion and Future Research

5 General Discussion and Future Research

5.1 Summary of Findings

- MCR1/3/4 are expressed in both primary human myotubes and skeletal muscle tissue. MCR5 is weakly expressed in myotubes, and not detectable in skeletal muscle tissue.
- α-MSH induces glucose uptake in primary human myotubes at a level comparable to insulin. When co-incubated with insulin this effect size is further increased.
- Incubation with the MCR5 selective agonist PG-901 causes glucose uptake at high concentrations, suggesting the action of α-MSH may be mediated by MCR5.
- Primary human adipocytes express MCR1/3 and do not have a glucose uptake response when incubated with α-MSH.
- Lipid-loaded myotubes demonstrating insulin resistance do not have a glucose uptake response when incubated with α-MSH.
- Mice express MCR5 in skeletal muscle and demonstrate improvements in glucose tolerance when administered a bolus of α-MSH prior to an i.p. GTT.
- Healthy human volunteers infused with α-MSH during an OGTT display a reduced 0-120 minute glucose iAUC compared to placebo. Exploratory post-hoc analysis reveals the greatest difference to lie in the initial 60 minutes of the OGTT.
- GLP-1 is unchanged between placebo and 1500 ng/kg/hr α-MSH infusions in participants who showed improvements in glucose tolerance during α-MSH administration.
- Insulin is reduced concomitant to glucose with infusions of α-MSH during OGTTs.
- During hyperinsulinaemic-euglycaemic clamps, participants infused with 150 ng/kg/hr α-MSH required a nonsignificant increase in GIR in order to maintain euglycaemia compared to placebo.

5.2 General Discussion

The aim of this research project was threefold; to establish validated and characterized human primary *in vitro* models in which glucose uptake could be quantified, to use these *in vitro* models to quantify glucose uptake in response to melanocortin receptor agonism, and finally to conduct a first-in-human infusion study investigating whether α-MSH improves post-prandial glycaemic control and increases whole-body glucose uptake.

Whilst pre-clinical animal studies conducted by Prof. Michael Cowley have clearly demonstrated the insulin-independent role of MC5R agonism on glucose uptake in skeletal muscle, to date there has been no investigations into the translational relevance of this novel pathway to human biology.

The aim of Chapter 2 was to establish multiple characterized and validated primary human myoblast cell lines derived from healthy volunteer muscle biopsies, with the purpose of using this model in further experiments examining the direct actions of α-MSH on skeletal muscle. Establishment of these cell lines proved challenging, as even with pooled biopsy samples satellite cell yield was extremely low yielding to failed cultures. After several optimisations of both the digestion and isolation protocol itself and the culture reagents used, six cell lines were successfully established. Through differential attachment to uncoated culture surfaces, fibroblast contamination was eliminated from each culture at early passages and purity was confirmed by desmin staining. Normal differentiation into multinucleated myotubes was confirmed by observation of morphological changes and confirmation of contractile protein expression.

Once the presence of the insulin receptor was validated by qRT-PCR, a radiometric based assay was employed to measure glucose uptake *in vitro*. Published literature shows that due to high GLUT1 levels, the insulin induced glucose uptake reaches a maximum effect size approximately 2-3 fold above basal levels (234,241,242). This effect size was observed in the primary human myotubes that were established, validating a functioning insulin signalling pathway.

Thus, by establishing a validated *in vitro* model of human skeletal muscle in Chapter 2, followed by measuring the effects of melanocortin receptor agonism on glucose uptake in this model in Chapter 3 and finally, conducting a first-in-human α-MSH infusion study in Chapter 4, this project aimed to provide the first evidence that skeletal muscle melanocortin receptor agonism improves post-prandial glucose tolerance in humans.

Elevated levels of circulating free fatty acids are linked to metabolic disorders such as obesity and Type 2 diabetes, and lead to defects in skeletal muscle insulin signalling mediated by intramuscular lipid accumulation (124,125,256). An *in vitro* model commonly employed to study these lipotoxic effects on glucose uptake is one in which intracellular lipid accumulation is induced by extended incubation in media supplemented with high levels of free fatty acids(257–259). This leads to accumulation of neutral lipids in particular ceramides and diacylglycerols (258,260) which then leads to downstream defects in Akt/PKB activation and inhibited GLUT4 trafficking to the plasma membrane (260). A model in which this resistance to insulin-mediated glucose uptake was established using the primary human myotube cultures and was then used to investigate whether there is a concomitant resistance to α-MSH in this state.

In Chapter 3, the myotube models previously detailed were then used as a foundation for the investigation of the direct effects α-MSH has on glucose uptake in human skeletal muscle. Cell lines were assayed for melanocortin receptors 1, 3, 4 and 5. MC2R was not investigated as α-MSH has no binding properties at this receptor. MC1R was found in high abundance and in consistent levels across all cell lines. MC3/4R were expressed at lower levels but easily detectable. MC5R was faintly detected. This melanocortin profile differs significantly from that of rodents, where MC5R is highly abundant and MC4R is faintly detected (205,206).

Using concentrations previously found to induce glucose uptake in rat and mice myotubes (205,206), myotubes were incubated with insulin and 1, 10 and 100nM α-MSH for one hour and glucose uptake measured. At 10 and 100nM α-MSH, there was a statistically significant increase in glucose uptake compared to basal. This effect size was similar, although less consistent to the response to insulin. These data are the first

evidence of a novel pathway in which α-MSH acts directly on human skeletal muscle to stimulate glucose uptake.

In myotubes this glucose uptake can be further increased by co-incubation of insulin. While all doses of α-MSH when co-incubated with insulin showed a trend to increase the average glucose uptake over insulin alone, 10nM α-MSH generated a statistically significant response. Data in rodent models has shown that glucose uptake mediated by MC5R activation is independent of insulin signalling, and that the glucose uptake effect size of combined incubation is additive (205,206). While further research in human myotubes needs to be done to validate the insulin-independence of the α-MSH pathway, these results suggest that similar to rodents, these effects may be independent and complementary to insulin. Additionally, the increased GLUT1 present in human myotubes (241) may obscure the true effect size mediated by recruiting additional GLUTs to the plasma membrane in response to co-incubation of the peptides, leading to the maximum treatment-induced increase in glucose uptake being reached at a lower “fold-difference” to the basal state.

PG-901, a highly selective MC5R agonist, was used in a first step to identify which of the melanocortin receptors found in the myotubes could be responsible for the glucose uptake observed. In animals, blockade of MC5R signalling abolished the effects of α-MSH *in vivo* and *in vitro* and further experiments treating with PG-901 confirmed the glucoregulatory effects were mediated by MC5R. In human myotubes, 100nM PG-901 induced a significant increase in glucose uptake over basal. Published data shows PG-901 to have an EC_{50} of 0.072nM and demonstrate high specificity for MC5R (273). However, in these myotube experiments a significant increase in glucose uptake was only observed at a concentration of 100nM. This may be due to the faintly detectable levels of MC5R expression in the myotubes used. The cells used in bindings assays to establish the pharmacological properties of the newly synthesized PG-901 compound were Chinese hamster ovary cells modified to stably express MC5R at high levels (273), and thus are not biologically equivalent to the primary human myotubes used in this experiment. Therefore, it is possible that with the low receptor abundance observed, PG-901 will only produce significant downstream effects at 100nM in the 1-hour incubation time used in these experiments. This result suggests that MC5R is responsible for downstream glucose uptake.

In mice with diet-induced obesity, the glucose tolerising effect of α-MSH during glucose tolerance tests was ablated (205). The lipid-loaded myotube model previously described was employed to translate these findings to human cells. In an environment where insulin mediated glucose uptake is hampered due to ectopic lipid accumulation, the concentrations of α-MSH used produced no noticeable increase in glucose uptake after 1-hour incubation. In mice, a combination of nonselective phosphodiesterase inhibitors ameliorated the inhibitory effect of obesity on α-MSH induced glucose uptake by blocking the breakdown of cAMP, indicating a failure in signal transduction. Access to phosphodiesterase inhibitors was not logistically possible at the time of these experiments. However, this lipid-loaded myotube model may prove useful in future experiment that continue to translate these pre-clinical findings and may demonstrate that insulin resistant human myotubes respond to α-MSH where cAMP signalling is restored.

The downstream effects of melanocortin agonism on glucose uptake was also investigated in another insulin-sensitive cell type, human primary adipocytes. Commercially obtained preadipocytes were cultured and differentiated to adipocytes. The melanocortin profile of this cell line was assessed by qRT-PCR and MCR's 1 and 3 were found to be expressed, with no evidence of MC4/5R expression. Following the same glucose uptake assay protocol, differentiated adipocytes were incubated with insulin and a range of doses of α-MSH after being serum and glucose starved. No noticeable glucose uptake was induced after incubation with α-MSH; thus, the cell type was not used in any subsequent experiments.

Chapter 3 generated novel data demonstrating that α-MSH can act directly on human skeletal muscle to produce a glucose uptake response, likely mediated by MC5R and complimentary to insulin. The *in vitro* data shown is a key step in elucidating this previously unknown pathway in humans. With this discovery *in vitro*, a physiological response study was conducted in healthy volunteers at the Hammersmith Hospital London, in collaboration with Imperial College London. As detailed in Chapter 4, this study aimed to investigate whether continuous infusions of α-MSH improved post-prandial glucose tolerance and whole-body glucose uptake in healthy volunteers.

Fifteen healthy volunteers were screened and accepted into the study which consisted of two parts. The first of which consisted of four oral glucose tolerance test (OGTT) visits in which participants received infusions throughout of saline or one of three (15, 150 and 1500 ng/kg/hr) α-MSH in a randomized, double-blind manner. Infusions began 30 minutes prior to the 75g oral glucose load to equilibrate the peptide in circulation, serial blood samples were taken and assayed for glucose, insulin, and GLP-1. At a dose of 1500 ng/kg/hr, the highest dose used in this study, a marked increase in glucose tolerance was observed although this was not significant during primary outcome analysis. Exploratory analysis revealed this effect primarily manifested itself by blunting hyperglycaemic excursions during the first 60 minutes of the OGTT. This physiological response cannot be attributed to increased insulin secretion as GLP-1 levels remained unchanged between treatments and interestingly, α-MSH reduced insulin levels during the same period of time the glucose lowering effect was observed. In light of *in vitro* data described in Chapter 4, this presents a strong case that α-MSH acts directly on skeletal muscle to improve post-prandial glucose clearance in humans.

Before commencing the second part of this study, in which the same cohort of participants received infusions of saline and α-MSH during a hyperinsulinaemic-euglycaemic clamp, an interim unblinding occurred once 10 participants completed the OGTTs to facilitate the commencement of the clamps phase of the study by unblinding and analysing which dose is most effect to proceed with in clamps. This interim unblinding was necessitated by the study taking place throughout 2020/21 and significant pandemic related pressures on the use of clinical resources for non-therapeutic trials were present, thus prompting us to commence the clamps in a timely manner. At the time of the interim unblinding, 150 ng/kg/hr was observed to have the greatest glucose tolerising effects during the OGTTs and was chosen to use in the clamps. However, once the entire OGTT dataset was analysed 1500 ng/kg/hr was found to be the most effective dose. Further studies are planned in which the clamps are repeated at the higher dose of 1500 ng/kg/hr.

Traditionally, the output of the hyperinsulinaemic-euglycaemic clamp is a quantitative measurement of whole-body glucose uptake attributed to specifically the subject's own sensitivity to insulin. However, in the context of this trial where *in vitro* data demonstrates an insulin-independent effect it is more useful to view the glucose

infusion rate (GIR) as an endpoint rather than inputting GIR and insulin into formulae to generate an index for insulin sensitivity. Additionally, glucose tracers and muscle biopsies are commonly employed in clamp studies allowing skeletal muscle-specific sensitivity to be quantified. As this was a pilot study in which the glucoregulatory effects of α-MSH was being investigated for the first time in humans, it was decided more reliable novel data could be obtained if there was no additional stress placed on the participant as a result of biopsies before and after clamps thus leading to confounding effects of stress-induced changes in glucose homeostasis.

Prior to beginning the high-dose insulin infusions of the clamp, subjects received a 120-minute infusion of α-MSH or saline whilst blood glucose was measured every 10 minutes and a 20% dextrose bag was connected to an intravenous line as per standard clamp protocol. If necessary, if a participant's blood glucose began to fall below the clamped euglycaemic range, the dextrose infusion was started. The purpose of this augmentation to the clamp protocol was to investigate whether an infusion of α-MSH would reduce blood glucose levels in the basal state. Although a minor increase in the glucose infusion rate (GIR) was observed in α-MSH infusions during this phase, this was physiologically insignificant and confounded by the fact that glucose infusions were occasionally required during placebo, potentially owing to the extended period the participant was fasting for. This matches pre-clinical findings in mice, where basal euglycaemia was unaffected by continuous α-MSH infusion (205).

At 120 minutes from the initiation of either saline or α-MSH infusions, insulin was administered at a rate of 1 μU/kg/hr for 180 minutes and the GIR increased as necessary to maintain the euglycaemic clamp. While 150 ng/kg/hr α-MSH led to a noticeable increase in the GIR needed to maintain euglycaemia during the equilibration phase (180-270 minutes) of the clamp, by the time the glucose infusion was equilibrated with whole body glucose uptake the difference, although still present, had lessened. At this high dose of insulin, a healthy, non-insulin resistant person will have a maximal peripheral glucose uptake response to insulin. It can be inferred that any increase in GIR during α-MSH infusions is leading to an increase over this maximal response. Confirmation whether this is due to sensitization of the insulin signalling pathway or by an independent pathway mediated by melanocortin receptor signalling will be the subject of future studies. Furthermore, the reduction in effect size of an

increase in GIR during α-MSH infusions may be attributed partly to receptor desensitization to the peptide, as by the time the equilibration phase was reached the participant had been receiving a continuous infusion of α-MSH for almost 5 hours. More importantly however, upon completion of the OGTTs it was a dose of 1500, not 150 ng/kg/hr, that was found to be most effective at improving glucose tolerance. Future studies in which a dose of 1500 ng/kg/hr and muscle biopsies are taken before and after the clamp will be invaluable in elucidating whether a higher dose of α-MSH can further increase whole body glucose uptake, and if a continuous infusion of this length can lead to desensitization to the peptide.

5.3 The Opportunity for Insulin-Independent Pharmacotherapy in Diabetes Mellitus

As detailed in Section 1.2.3, pharmacological management of diabetes mellitus is heavily reliant on the targeting of insulin release and action. Intensive therapy carries significant risk to the patient in the form of increased incidence of hypoglycaemic episodes and weight gain. The data presented in this thesis suggests skeletal muscle glucose uptake can be stimulated by MCR agonism to improve post-prandial glucose tolerance in healthy humans. Importantly, fasted participants infused with 150 ng/kg/hr α-MSH for 120 minutes (prior to commencing the insulin clamp) showed no evidence of hypoglycaemia. We hypothesize the reason for this may be the presence an endocrine counter-regulatory pathway, which there is some unsubstantiated evidence for in published literature. In POMC-null mice, lacking central and peripheral melanocortin peptides, administration of an insulin tolerance tests results in fatal hypoglycaemic episodes (269). Upon administration of an α-MSH analogue prior to the insulin tolerance test, POMC-null mounted a counterregulatory response to defend against hypoglycaemia with glucagon levels rising by 130%. Additionally, in a study conducted in 1984 by J. Knudtzon, intravenous injections of α-MSH increased plasma levels of glucagon in rabbits (283). However, Enriori et al. found no upregulation of gluconeogenic enzymes following α-MSH infusions during a clamp in mice (205). Further investigations into human biology, such as measuring glucagon in the fasted and post-prandial state during α-MSH infusions, must be carried out before the merit of this hypothesis can be established.

In insulin resistant primary human myotubes (**Fig. 3.5)** and mice with diet-induced obesity (205), no improvements in glucose uptake or tolerance are observed. This may limit the therapeutic potential of α-MSH in obese patients with insulin-resistant diabetes. However, with the increasing stratification of subtypes of diabetes mellitus (as outlined by Ahlqvist et al., (107) and outlined in Section 1.2.1) the efficacy of α-MSH may not be binary between insulin-resistant and insulin-dependent disease states as it has been demonstrated α-MSH "resistance" in muscle is mediated by cAMP signalling defects and thus does not have the same point-of-failure as in insulin resistant skeletal muscle. Alpha-MSH may improve glucose tolerance in patients from Cluster 1 and 2, those that are insulin-deficient and of low BMI. Additionally, patients in Cluster 5 in which metabolic dysfunctions are age-related may also respond. Although current *in vitro* suggest it may be ineffective in patients with severe insulin resistance due to obesity (Cluster 2), and those with obesity and metabolic dysfunctions without significant insulin resistant (Cluster 3), this remains inconclusive in the absence of physiological data obtained from humans in these disease states.

5.4 Limitations

The *in vitro* myotube models described herein presented significant challenges due to their morphological and metabolic behaviour. Unlike their immortalized murine counterparts, myoblasts could not be differentiated to myotubes in 96-well plate culture vessels. Multiple attempts were made to change the basal protein coating, plastics, and seeding densities used but these optimisations were unsuccessful. This phenomenon has not been reported in the literature however, this limitation could possibly be due to the limited surface area (0.32 cm^2) inhibiting myotube formation which can be several millimetres long *in vitro*. Normal differentiation was observed in vessels with larger surface areas such as, 24-well plates, and flasks. This led to the myotubes not being compatible with multiple biochemical analysis platforms such as the Agilent Seahorse system which has cartridges for cell culture fixed at a size of 0.16 cm^2. In terms of metabolic limitations, whereas insulin and α-MSH had a clear additive effect on glucose uptake in rodent myotubes (205), the combined effect size was significantly weaker in primary human myotubes. This could be due to the increased GLUT1, and therefor total glucose uptake, in human myotubes obfuscating the

combined contribution of the two hormones to glucose uptake. The glucose analogue, 2-deoxy-D-glucose is phosphorylated to 2-deoxy-D-glucose-6-phosphate (analogous to glucose-6-phosphate) upon entering the cell but cannot be further metabolized. As phosphorylated glucose is an allosteric inhibitor of hexokinase, a maximum amount of glucose uptake could have taken place before the end of the 10-minute incubation, leading to inactivation of hexokinase by a build-up of 2-DG-6-phosphate and an excess of unphosphorylated glucose which may have been lost by diffusion out of the cell in the downstream washing steps and thus not quantified.

The human infusion study was powered to detect a 20% reduction in iAUC with a standard deviation of 10%, 90% power and 1% type 1 error rate. Although statistical significance was achieved in post-hoc analysis of the truncated 0-60 minute OGTT curve where the peptide was imparting its glucose tolerising effect, these sample size calculation parameters may have been too stringent to detect a significant difference in the complete 0–120-minute OGTT. This may be due to the standard deviation being drastically higher than anticipated, upwards of 40% depending on the treatment, despite a substantial mean effect size of a 27% iAUC reduction at the 1500 ng/kg/hr dose. Using the measured standard deviation from this study as an input into sample size calculations with a 5% type 1 error rate and 80% power, a total sample size of 22 participants is calculated. Future studies will employ more facilitative study powering, and a validation cohort is planned as detailed in the following section. During the course of the clinical investigation, COVID-19 related logistical restraints led to an interim unblinding being amended into the study protocol. This facilitated commencement of the hyperinsulinaemic-euglycaemic clamps once 10 participants had completed the OGTTs and an effective dose found, instead of all 15 participants. At the time of the unblinding, the intermediate dose of 150 ng/kg/hr caused the greatest reduction in glucose AUC and thus was infused during the clamps. Although an increase in GIR was observed at this dose compared to placebo, it was not significant during the steady state.

5.5 Future Research

The data generated in this thesis represents the first step in establishing the role of the peripheral melanocortin system in glucose homeostasis in humans and provides a strong foundation for further research. There is strong justification for further exploring the glucoregulatory mechanism both *in vitro* and *in vivo* in addition to gaining insight into the therapeutic potential for this pathway in various diabetic disease states.

With respect to additional analysis of samples, valuable data can be obtained through biochemical analysis given additional resources. In plasma samples obtained from human infusions, glucagon could be measured both in the post-prandial state and fasted state, shedding light into a possible counterregulatory endocrine mechanism that prevents the peptide from causing hypoglycaemia. Using the principle of radioimmunoassay, which UCD does not have the facilities for, the low levels of plasma α-MSH can be quantified. This would provide an insight into whether or not the circulating levels of α-MSH during infusions are still within the physiological range and establish a kinetic profile of when stable levels of the hormone are reached in circulation.

Employing mass spectrometry, the as of yet unknown signalling pathway leading to skeletal muscle glucose uptake can be explored. Using stable isotope labelling by amino acids (SILAC) in myotube cell culture the GLUT transporters, which are hydrophobic and cannot prepared for mass spectrometry using traditional methods, can be analysed in plasma membrane extracts. This will allow us to identify which GLUT is being translocated in response to α-MSH and corroborate animals studies showing an insulin independent mechanism. Additionally, phosphoproteomic analysis of both cell and muscle biopsy lysates can be used to establish the intracellular signalling mechanism downstream of the MCR. Due to the novel and unknown nature of this pathway, it would be infeasible to target individual proteins and phosphorylation events using traditional methods such as Western Blots.

Further experiments in the clinical setting are being planned, with recruitment of a validation cohort of an additional 10 participants for OGTT infusions already underway. Repeating the clamps using the high dose, ultimately shown to be the most effective in OGTTs, is a critical next step. The gathering of muscle biopsies before and after α-

MSH infusions in volunteers would provide valuable data on tissue-specific responses to the peptide. Finally, oral glucose tolerance tests and clamps with α-MSH infusions in patients with varying degrees of diabetes would aid in assessing the therapeutic potential of this mechanism in different diabetic disease states.

In conclusion, the data described in this thesis details highly promising results which mark the first steps of the discovery of a novel glucoregulatory pathway in humans. Possibly mediated by MC5R, it is evident that α-MSH acts directly on skeletal muscle to produce a glucose uptake response leading to an improvement in post-prandial glucose tolerance which may be complimentary to the effects of insulin as demonstrated by hyperinsulinaemic clamps and co-incubation of α-MSH with insulin *in vitro*. This research will lay the foundations for a future drug development pipeline in which the therapeutic benefits of peripheral melanocortin receptor agonism in both insulin resistant and insulin sensitive diabetics.

Appendix

6 Appendix

6.1 Reagents and materials used

Methods Section	Reagent	Supplier	Code
2.2.1.2.3	Bio-feather Coaxial Needle 14G	Medax Srl	BF1416002
	DPBS	ThermoFIsher	14040141
2.2.2.1	Collagenase D	Merck	11088858001
	Dispase II	Merck	D4693-1G
	Calcium Chloride	Merck	10035-04-8
2.2.2.3	Skeletal Muscle Growth Medium	Cell Applications Inc.	151-500
	70µm Cell Strainer	Falcon	352350
	Collagen Coating Solution	Cell Applications Inc.	125-50
	TrypLE Express	ThermoFisher	12604013
2.2.3.2	Dimethyl sulfoxide solution	Merck	MFCD00002089
2.2.3.3	Skeletal Muscle Differentiation medium	Promocell	C-23061
2.2.3.4	Human Preadipocytes	Merck	S802S-05A
	Human Preadipocyte Growth Medium	Merck	811-500
	Human Adipocyte Differentiation Medium	Merck	811D-250
2.2.4.1	Formaldehyde solution 4%	Merck	1004968350
	MHC3 Antibody	Abcam	Ab124205

	Desmin Antibody	Abcam	Ab15200
	AlexFluor 488	Thermofisher	A-11008
	DAPI	Abcam	Ab228549
2.2.5	RNEasy Mini Kit	Qiagen	74104
	Dnase	Qiagen	79254
2.2.7	Superscript III Reverse Transcriptase	ThermoFisher	18080093
2.2.8	Human melanocortin receptor 1 probe	ThermoFisher	Hs00267167_s1
	Human melanocortin receptor 3 probe	ThermoFisher	Hs01562847_s1
	Human melanocortin receptor 4 probe	ThermoFisher	Hs00271877_s1
	Human melanocortin receptor 5 probe	ThermoFisher	Hs00271882_s1
	Human insulin receptor probe	ThermoFisher	Hs00961557_m1
	Human myosin heavy chain 3 probe	ThermoFisher	Hs01074230_m1
	Human GAPDH probe	ThermoFisher	Hs02786624_g1
	PCR Master Mix	ThermoFisher	K0171
2.2.9	Palmitic Acid	Merck	258725
	BSA	Merck	A1595-50ML
2.2.10	10% Formalin Solution	Merck	HT501128-4L
	Oil Red O Solution	Merck	O1391

	2-propanol	Merck	109634
2.2.11	Recombinant Human Insulin	Merck	I19278
	Tritiated 2-deoxy-D-glucose	PerkinElmer	NET549250UC
	2-deoxy-D-glucose	Merck	D8375-10MG
2.2.12.1	1 g/L glucose DMEM	Lonza	BE12-707F
	Glucose free DMEM	Lonza	BE12-604F
	Cell Lytic MT	Merck	C3228-50ML
	Ultima Gold Scintillation Fluid	Merck	L8286-5L
2.2.12.2	Pierce BCA Protein Assay	ThermoFisher	23225
4.2.8	Insulin Assay		
	Total GLP-1 ELISA	Mercodia	10-1278-01

Table 6.1 Reagents and materials used.

6.2 Dose-response of insulin induced glucose uptake in myotubes.

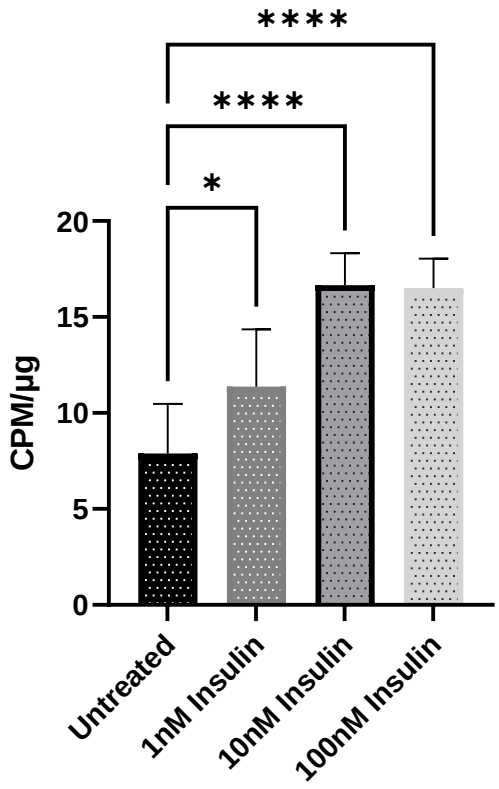

Figure 6.1 Insulin induced glucose uptake in myotubes.

*Glucose uptake represented as counts per minute (CPM) of cell lysates as measured by liquid scintillation counting normalized by protein content (n=3). *p<0.05, ****p<0.0005 vs Untreated. Data are presented as mean ± standard deviation with each data point shown as a mean of duplicates. Statistical analysis was performed with one-way ANOVA with post-hoc Dunnett's multiple comparison test*

6.3 Impact of palmitic acid on insulin induced glucose uptake in myotubes.

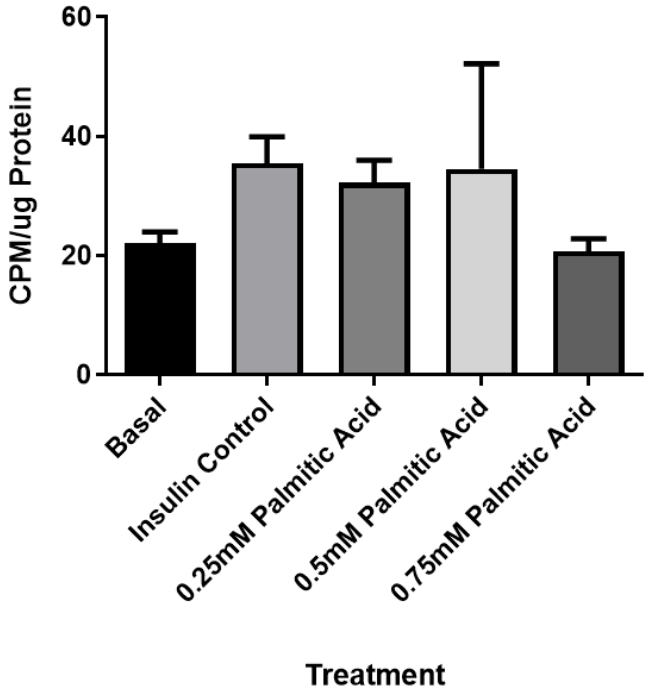

Figure 6.2 Resistance to insulin induced glucose uptake in response to palmitic acid incubation.

Glucose uptake represented as counts per minute (CPM) of cell lysates as measured by liquid scintillation counting normalized by protein content (n=3). 0.75 mM palmitic acid (20.71 ±2.1 cpm/µG) produced the greatest reduction in glucose uptake over insulin control (35.45 ±4.4 cpm/µg) in comparison to 0.25mM and 0.50 mM palmitic acid (32.25±3.7 cpm/µg and 34.5±17.6 cpm/µg respectively). Data are presented as mean ± standard deviation with each data point shown as a mean of triplicates. Statistical analysis was performed with one-way ANOVA.

6.4 Assessment of RNA Quality

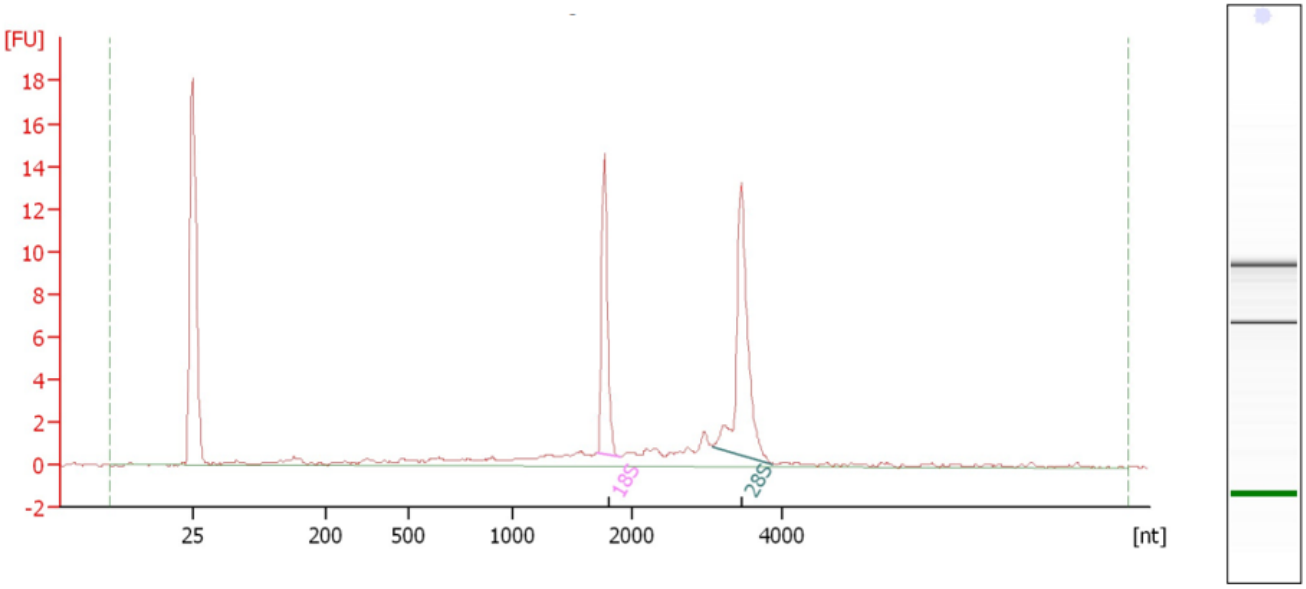

Figure 6.3 Representative bioanalyzer results of RNA isolated during in vitro experiments. RNA with integrity values over 1.8 were exclusively used.

6.5 MCR5 Expression in myotubes cultured in high glucose

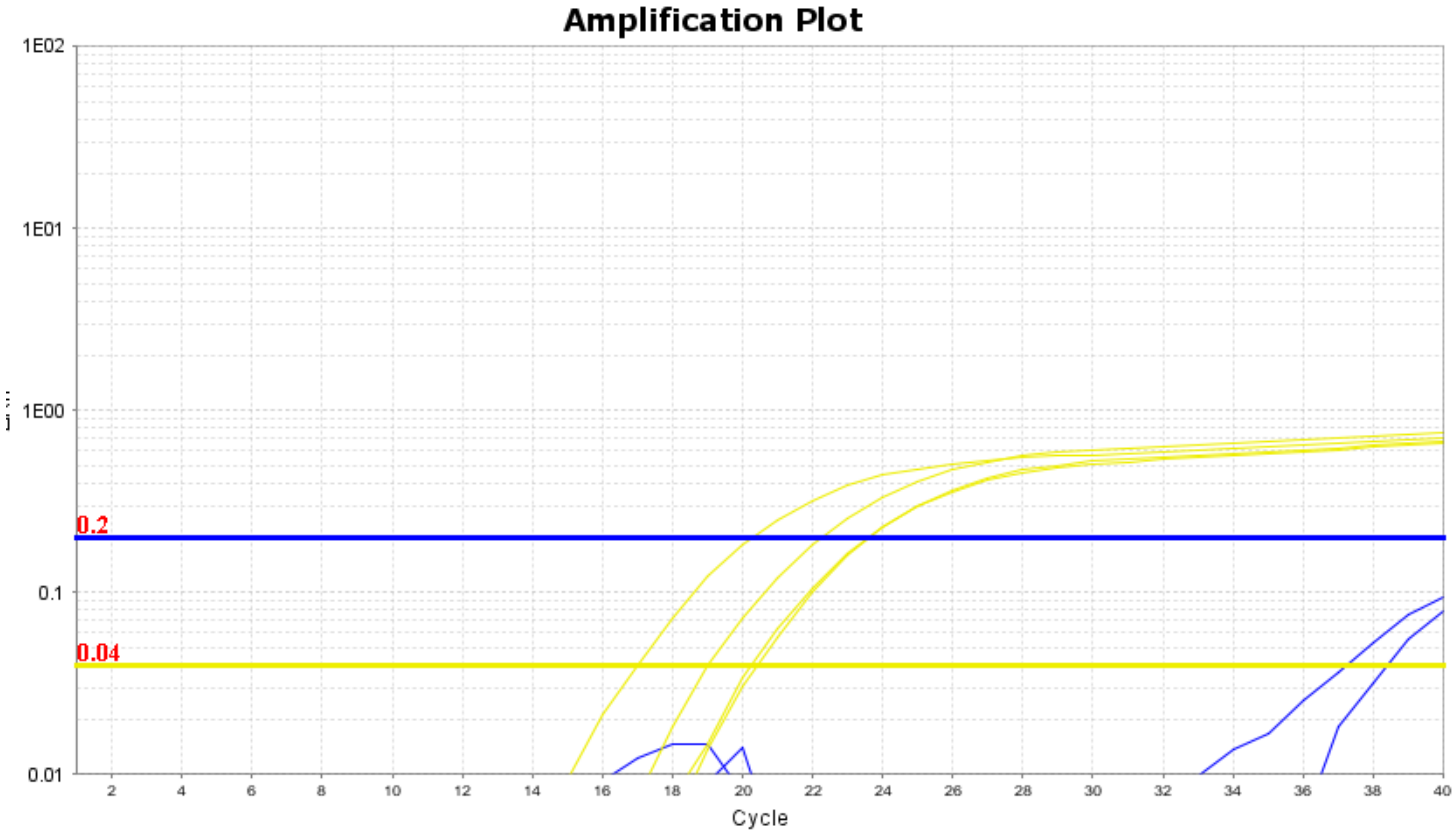

Figure 6.4 RT-qPCR amplification plot of GAPDH and MCR5 expression in myotubes cultured in high glucose. GAPDH amplification curves shown in yellow and MCR5 in blue (n=4).

6.6 Human Infusion Dose Calculation

Human Equivalent Dose (mg / kg) = Animal does (mg / kg) × (Animal K_m / Human K_m)

Using 0.001 ug/hr=0.000001 mg/hr

Assuming 20g mouse= 0.00005 mg/kg/hr

Mouse K_m=3

Human K_m=37

Rhesus Macaque K_m=12

HED= (0.00005 mg/kg/hr) x (3/37)

HED= 0.000004 mg/kg /hr

HED of Lowest Effective Dose in Mice =4 ng/kg/hr

6.7 Data Normality Tests

Glucose x Treatment Curves - 30 to 180 minutes.				
	Saline	15 ng/kg/hr	150 ng/kg/hr	1500 ng/kg/hr
W	0.92	0.93	0.94	0.9
P value	0.53	0.61	0.69	0.38
Glucose iAUC 0-120 minutes				
	Saline	15 ng/kg/hr	150 ng/kg/hr	1500 ng/kg/hr
W	0.95	0.89	0.93	0.94
P value	0.67	0.056	0.36	0.48
Insulin x Treatment Curves- 30 to 180 minutes				
	Saline	15 ng/kg/hr	150 ng/kg/hr	1500 ng/kg/hr
W	0.89	0.87	0.89	0.9
P value	0.27	0.18	0.29	0.33
Insulin iAUC 0-120 minutes				
	Saline	15 ng/kg/hr	150 ng/kg/hr	1500 ng/kg/hr
W	0.91	0.89	0.93	0.94
P value	0.43	0.38	0.57	0.61
Clamp 2nd Stage Insulin Adjusted GIR				
	Saline		150 ng/kg/hr	
W	0.96		0.93	
P value	0.82		0.31	

Table 6.2 Shapiro-Wilk test of glucose and insulin data sets during OGTT (n=15) and clamp (n=14) experiments.

References

7 References

1. Maran A, Lomas J, Macdonald IA, Amiel SA. Lack of preservation of higher brain function during hypoglycaemia in patients with intensively-treated IDDM. Diabetologia. 1995 Dec 1;38(12):1412–8.

2. Dienel GA. Brain Glucose Metabolism: Integration of Energetics with Function. Physiological Reviews. 2019 Jan;99(1):949–1045.

3. Navale AM, Paranjape AN. Glucose transporters: physiological and pathological roles. Biophys Rev. 2016 Jan 19;8(1):5–9.

4. Sansbury FH, Flanagan SE, Houghton JAL, Shuixian Shen FL, Al-Senani AMS, Habeb AM, et al. SLC2A2 mutations can cause neonatal diabetes, suggesting GLUT2 may have a role in human insulin secretion. Diabetologia. 2012 Sep 1;55(9):2381–5.

5. Karim S, Adams DH, Lalor PF. Hepatic expression and cellular distribution of the glucose transporter family. World J Gastroenterol. 2012 Dec 14;18(46):6771–81.

6. Chadt A, Al-Hasani H. Glucose transporters in adipose tissue, liver, and skeletal muscle in metabolic health and disease. Pflugers Arch. 2020;472(9):1273–98.

7. Radziuk J, Pye S. Hepatic glucose uptake, gluconeogenesis and the regulation of glycogen synthesis. Diabetes/Metabolism Research and Reviews. 2001;17(4):250–72.

8. Gomis RR, Ferrer JC, Guinovart JJ. Shared control of hepatic glycogen synthesis by glycogen synthase and glucokinase. Biochem J. 2000 Nov 1;351 Pt 3:811–6.

9. von Wilamowitz-Moellendorff A, Hunter RW, García-Rocha M, Kang L, López-Soldado I, Lantier L, et al. Glucose-6-phosphate-mediated activation of liver glycogen synthase plays a key role in hepatic glycogen synthesis. Diabetes. 2013 Dec;62(12):4070–82.

10. Petersen MC, Vatner DF, Shulman GI. Regulation of hepatic glucose metabolism in health and disease. Nat Rev Endocrinol. 2017 Oct;13(10):572–87.

11. Roach PJ, Depaoli-Roach AA, Hurley TD, Tagliabracci VS. Glycogen and its metabolism: some new developments and old themes. Biochem J. 2012 Feb 1;441(3):763–87.

12. Führing JI, Cramer JT, Schneider J, Baruch P, Gerardy-Schahn R, Fedorov R. A Quaternary Mechanism Enables the Complex Biological Functions of Octameric Human UDP-glucose Pyrophosphorylase, a Key Enzyme in Cell Metabolism. Sci Rep. 2015 Apr 10;5(1):9618.

13. Goldsmith E, Sprang S, Fletterick R. Structure of maltoheptaose by difference Fourier methods and a model for glycogen. J Mol Biol. 1982 Apr 5;156(2):411–27.

14. Strable MS, Ntambi JM. Genetic control of de novo lipogenesis: role in diet-induced obesity. Crit Rev Biochem Mol Biol. 2010 Jun;45(3):199–214.

15. Ameer F, Scandiuzzi L, Hasnain S, Kalbacher H, Zaidi N. De novo lipogenesis in health and disease. Metabolism - Clinical and Experimental. 2014 Jul 1;63(7):895–902.

16. Witters LA, Kemp BE. Insulin activation of acetyl-CoA carboxylase accompanied by inhibition of the 5'-AMP-activated protein kinase. J Biol Chem. 1992 Feb 15;267(5):2864–7.

17. Witters LA, Watts TD, Daniels DL, Evans JL. Insulin stimulates the dephosphorylation and activation of acetyl-CoA carboxylase. Proc Natl Acad Sci U S A. 1988 Aug;85(15):5473–7.

18. Luo L, Liu M. Adipose tissue in control of metabolism. Journal of Endocrinology. 2016 Dec 1;231(3):R77–99.

19. Thiebaud D, Jacot E, DeFronzo RA, Maeder E, Jequier E, Felber JP. The effect of graded doses of insulin on total glucose uptake, glucose oxidation, and glucose storage in man. Diabetes. 1982 Nov;31(11):957–63.

20. Marette A, Liu Y, Sweeney G. Skeletal muscle glucose metabolism and inflammation in the development of the metabolic syndrome. Rev Endocr Metab Disord. 2014 Dec;15(4):299–305.

21. Henry RR, Abrams L, Nikoulina S, Ciaraldi TP. Insulin action and glucose metabolism in nondiabetic control and NIDDM subjects. Comparison using human skeletal muscle cell cultures. Diabetes. 1995 Aug;44(8):936–46.

22. Huang S, Czech MP. The GLUT4 Glucose Transporter. Cell Metabolism. 2007 Apr 4;5(4):237–52.

23. Rowland AF, Fazakerley DJ, James DE. Mapping Insulin/GLUT4 Circuitry. Traffic. 2011;12(6):672–81.

24. Coderre L, Kandror KV, Vallega G, Pilch PF. Identification and characterization of an exercise-sensitive pool of glucose transporters in skeletal muscle. J Biol Chem. 1995 Nov 17;270(46):27584–8.

25. Kjøbsted R, Munk-Hansen N, Birk JB, Foretz M, Viollet B, Björnholm M, et al. Enhanced Muscle Insulin Sensitivity After Contraction/Exercise Is Mediated by AMPK. Diabetes. 2017 Mar;66(3):598–612.

26. Whitfield J, Paglialunga S, Smith BK, Miotto PM, Simnett G, Robson HL, et al. Ablating the protein TBC1D1 impairs contraction-induced sarcolemmal glucose transporter 4 redistribution but not insulin-mediated responses in rats. J Biol Chem. 2017 Oct 6;292(40):16653–64.

27. Fujii N, Hayashi T, Hirshman MF, Smith JT, Habinowski SA, Kaijser L, et al. Exercise induces isoform-specific increase in 5'AMP-activated protein kinase activity in human skeletal muscle. Biochem Biophys Res Commun. 2000 Jul 14;273(3):1150–5.

28. Hawley SA, Pan DA, Mustard KJ, Ross L, Bain J, Edelman AM, et al. Calmodulin-dependent protein kinase kinase-beta is an alternative upstream kinase for AMP-activated protein kinase. Cell Metab. 2005 Jul;2(1):9–19.

29. Sakamoto K, McCarthy A, Smith D, Green KA, Grahame Hardie D, Ashworth A, et al. Deficiency of LKB1 in skeletal muscle prevents AMPK activation and glucose uptake during contraction. EMBO J. 2005 May 18;24(10):1810–20.

30. Turban S, Stretton C, Drouin O, Green CJ, Watson ML, Gray A, et al. Defining the contribution of AMP-activated protein kinase (AMPK) and protein kinase C (PKC) in regulation of glucose uptake by metformin in skeletal muscle cells. J Biol Chem. 2012 Jun 8;287(24):20088–99.

31. Shulman GI, Rothman DL, Jue T, Stein P, DeFronzo RA, Shulman RG. Quantitation of muscle glycogen synthesis in normal subjects and subjects with non-insulin-dependent diabetes by 13C nuclear magnetic resonance spectroscopy. N Engl J Med. 1990 Jan 25;322(4):223–8.

32. Nielsen J, Holmberg HC, Schrøder HD, Saltin B, Ørtenblad N. Human skeletal muscle glycogen utilization in exhaustive exercise: role of subcellular localization and fibre type. J Physiol. 2011 Jun 1;589(Pt 11):2871–85.

33. Jensen J, Lai YC. Regulation of muscle glycogen synthase phosphorylation and kinetic properties by insulin, exercise, adrenaline and role in insulin resistance. Archives of Physiology and Biochemistry. 2009 Feb 1;115(1):13–21.

34. Jensen J, Rustad PI, Kolnes AJ, Lai YC. The Role of Skeletal Muscle Glycogen Breakdown for Regulation of Insulin Sensitivity by Exercise. Front Physiol. 2011 Dec 30;2:112.

35. van Loon LJC, Greenhaff PL, Constantin-Teodosiu D, Saris WHM, Wagenmakers AJM. The effects of increasing exercise intensity on muscle fuel utilisation in humans. The Journal of Physiology. 2001;536(1):295–304.

36. Hargreaves M, Spriet LL. Skeletal muscle energy metabolism during exercise. Nat Metab. 2020 Sep;2(9):817–28.

37. Parolin ML, Chesley A, Matsos MP, Spriet LL, Jones NL, Heigenhauser GJ. Regulation of skeletal muscle glycogen phosphorylase and PDH during maximal intermittent exercise. Am J Physiol. 1999 Nov;277(5):E890-900.

38. Medbø JI, Tabata I. Anaerobic energy release in working muscle during 30 s to 3 min of exhausting bicycling. J Appl Physiol (1985). 1993 Oct;75(4):1654–60.

39. Conley KE, Blei ML, Richards TL, Kushmerick MJ, Jubrias SA. Activation of glycolysis in human muscle in vivo. American Journal of Physiology-Cell Physiology. 1997 Jul 1;273(1):C306–15.

40. Consoli A, Nurjhan N, Reilly JJ, Bier DM, Gerich JE. Contribution of liver and skeletal muscle to alanine and lactate metabolism in humans. Am J Physiol. 1990 Nov;259(5 Pt 1):E677-684.

41. Gladden LB. Lactate metabolism: a new paradigm for the third millennium. J Physiol. 2004 Jul 1;558(Pt 1):5–30.

42. Da Silva Xavier G. The Cells of the Islets of Langerhans. J Clin Med. 2018 Mar 12;7(3):E54.

43. Müller A, Mziaut H, Neukam M, Knoch KP, Solimena M. A 4D view on insulin secretory granule turnover in the β-cell. Diabetes Obes Metab. 2017 Sep;19 Suppl 1:107–14.

44. De Meyts P. Insulin and its receptor: structure, function and evolution. Bioessays. 2004 Dec;26(12):1351–62.

45. Vakilian M, Tahamtani Y, Ghaedi K. A review on insulin trafficking and exocytosis. Gene. 2019 Jul 20;706:52–61.

46. Orci L, Vassalli JD, Perrelet A. The insulin factory. Sci Am. 1988 Sep;259(3):85–94.

47. De Vos A, Heimberg H, Quartier E, Huypens P, Bouwens L, Pipeleers D, et al. Human and rat beta cells differ in glucose transporter but not in glucokinase gene expression. J Clin Invest. 1995 Nov;96(5):2489–95.

48. Matschinsky FM. Regulation of pancreatic beta-cell glucokinase: from basics to therapeutics. Diabetes. 2002 Dec;51 Suppl 3:S394-404.

49. Gauthier BR, Wollheim CB. Synaptotagmins bind calcium to release insulin. Am J Physiol Endocrinol Metab. 2008 Dec;295(6):E1279-1286.

50. Gustavsson N, Lao Y, Maximov A, Chuang JC, Kostromina E, Repa JJ, et al. Impaired insulin secretion and glucose intolerance in synaptotagmin-7 null mutant mice. Proc Natl Acad Sci U S A. 2008 Mar 11;105(10):3992–7.

51. Drucker DJ. The biology of incretin hormones. Cell Metabolism. 2006 Mar 1;3(3):153–65.

52. Holst JJ. The physiology of glucagon-like peptide 1. Physiol Rev. 2007 Oct;87(4):1409–39.

53. Gloerich M, Bos JL. Epac: defining a new mechanism for cAMP action. Annu Rev Pharmacol Toxicol. 2010;50:355–75.

54. Skelin M, Rupnik M. cAMP increases the sensitivity of exocytosis to Ca^{2}+ primarily through protein kinase A in mouse pancreatic beta cells. Cell Calcium. 2011 Feb;49(2):89–99.

55. Effects of meal size and composition on incretin, α-cell, and β-cell responses. Metabolism. 2010 Apr 1;59(4):502–11.

56. Vilsbøll T, Krarup T, Madsbad S, Holst JJ. Both GLP-1 and GIP are insulinotropic at basal and postprandial glucose levels and contribute nearly equally to the

incretin effect of a meal in healthy subjects. Regul Pept. 2003 Jul 15;114(2–3):115–21.

57. Mari A, Bagger JI, Ferrannini E, Holst JJ, Knop FK, Vilsbøll T. Mechanisms of the Incretin Effect in Subjects with Normal Glucose Tolerance and Patients with Type 2 Diabetes. PLOS ONE. 2013 Sep 3;8(9):e73154.

58. Fast insulin secretion reflects exocytosis of docked granules in mouse pancreatic B-cells - PubMed [Internet]. [cited 2022 Jan 19]. Available from: https://pubmed.ncbi.nlm.nih.gov/11976915/

59. Henquin JC. Regulation of insulin secretion: a matter of phase control and amplitude modulation. Diabetologia. 2009 May;52(5):739–51.

60. Luzi L, DeFronzo RA. Effect of loss of first-phase insulin secretion on hepatic glucose production and tissue glucose disposal in humans. Am J Physiol. 1989 Aug;257(2 Pt 1):E241-246.

61. Ottensmeyer FP, Beniac DR, Luo RZT, Yip CC. Mechanism of Transmembrane Signaling: Insulin Binding and the Insulin Receptor. Biochemistry. 2000 Oct 1;39(40):12103–12.

62. Tatulian SA. Structural Dynamics of Insulin Receptor and Transmembrane Signaling. Biochemistry. 2015 Sep 15;54(36):5523–32.

63. White MF. IRS proteins and the common path to diabetes. Am J Physiol Endocrinol Metab. 2002 Sep;283(3):E413-422.

64. Versteyhe S, Blanquart C, Hampe C, Mahmood S, Christeff N, De Meyts P, et al. Insulin receptor substrates-5 and -6 are poor substrates for the insulin receptor. Mol Med Rep. 2010 Feb;3(1):189–93.

65. Kohn AD, Barthel A, Kovacina KS, Boge A, Wallach B, Summers SA, et al. Construction and characterization of a conditionally active version of the serine/threonine kinase Akt. J Biol Chem. 1998 May 8;273(19):11937–43.

66. Bradley H, Shaw CS, Bendtsen C, Worthington PL, Wilson OJ, Strauss JA, et al. Visualization and quantitation of GLUT4 translocation in human skeletal muscle following glucose ingestion and exercise. Physiol Rep [Internet]. 2015 May 11 [cited 2019 Aug 11];3(5). Available from: https://www.ncbi.nlm.nih.gov/pmc/articles/PMC4463815/

67. Wasserman DH, Kang L, Ayala JE, Fueger PT, Lee-Young RS. The physiological regulation of glucose flux into muscle in vivo. J Exp Biol. 2011 Jan 15;214(2):254–62.

68. Kang ES, Yun YS, Park SW, Kim HJ, Ahn CW, Song YD, et al. Limitation of the validity of the homeostasis model assessment as an index of insulin resistance in Korea. Metabolism. 2005 Feb;54(2):206–11.

69. American Diabetes Association Professional Practice Committee. 2. Classification and Diagnosis of Diabetes: Standards of Medical Care in Diabetes—2022. Diabetes Care. 2021 Dec 16;45(Supplement_1):S17–38.

70. Patarrão RS, Wayne Lautt W, Paula Macedo M. Assessment of methods and indexes of insulin sensitivity. Rev Port Endocrinol Diabetes Metab. 2014 Jan 1;9(1):65–73.

71. Muniyappa R, Madan R, Varghese RT. Assessing Insulin Sensitivity and Resistance in Humans. In: Feingold KR, Anawalt B, Boyce A, Chrousos G, de Herder WW, Dhatariya K, et al., editors. Endotext [Internet]. South Dartmouth (MA): MDText.com, Inc.; 2000 [cited 2022 Jul 25]. Available from: http://www.ncbi.nlm.nih.gov/books/NBK278954/

72. DeFronzo RA, Tobin JD, Andres R. Glucose clamp technique: a method for quantifying insulin secretion and resistance. Am J Physiol. 1979 Sep;237(3):E214-223.

73. Del Prato S, Tiengo A. The importance of first-phase insulin secretion: implications for the therapy of type 2 diabetes mellitus. Diabetes Metab Res Rev. 2001 Jun;17(3):164–74.

74. Bingley PJ. Interactions of Age, Islet Cell Antibodies, Insulin Autoantibodies, and First-Phase Insulin Response in Predicting Risk of Progression to IDDM in ICA+ Relatives: The ICARUS Data Set. Diabetes. 1996 Dec 1;45(12):1720–8.

75. DeFronzo RA, Tripathy D. Skeletal Muscle Insulin Resistance Is the Primary Defect in Type 2 Diabetes. Diabetes Care. 2009 Nov;32(Suppl 2):S157–63.

76. Campostano A, Altomonte F, Bessarione D, Casu M, Triolo A, Lamedica G. A new glucose clamp algorithm: clinical validation. Int J Artif Organs. 1991 Jul;14(7):441–7.

77. Matthews DR, Edge JA, Dunger DB. An unbiased glucose clamp method using a variable insulin infusion: its application in diabetic adolescents. Diabet Med. 1990 Apr;7(3):246–51.

78. Rothman DL, Magnusson I, Katz LD, Shulman RG, Shulman GI. Quantitation of hepatic glycogenolysis and gluconeogenesis in fasting humans with 13C NMR. Science. 1991 Oct 25;254(5031):573–6.

79. Sutherland EW, Robison GA. The role of cyclic AMP in the control of carbohydrate metabolism. Diabetes. 1969 Dec;18(12):797–819.

80. Lin HV, Accili D. Hormonal regulation of hepatic glucose production in health and disease. Cell Metab. 2011 Jul 6;14(1):9–19.

81. Philippe J. Structure and Pancreatic Expression of the Insulin and Glucagon Genes*. Endocrine Reviews. 1991 Aug 1;12(3):252–71.

82. MacDonald PE, De Marinis YZ, Ramracheya R, Salehi A, Ma X, Johnson PRV, et al. A K ATP channel-dependent pathway within alpha cells regulates glucagon

release from both rodent and human islets of Langerhans. PLoS Biol. 2007 Jun;5(6):e143.

83. Cheng-Xue R, Gómez-Ruiz A, Antoine N, Noël LA, Chae HY, Ravier MA, et al. Tolbutamide controls glucagon release from mouse islets differently than glucose: involvement of K(ATP) channels from both α-cells and δ-cells. Diabetes. 2013 May;62(5):1612–22.

84. Banarer S, McGregor VP, Cryer PE. Intraislet hyperinsulinemia prevents the glucagon response to hypoglycemia despite an intact autonomic response. Diabetes. 2002 Apr;51(4):958–65.

85. Havel PJ, Veith RC, Dunning BE, Taborsky GJ. Pancreatic noradrenergic nerves are activated by neuroglucopenia but not by hypotension or hypoxia in the dog. Evidence for stress-specific and regionally selective activation of the sympathetic nervous system. J Clin Invest. 1988 Nov;82(5):1538–45.

86. Gerich JE, Karam JH, Forsham PH. Stimulation of glucagon secretion by epinephrine in man. J Clin Endocrinol Metab. 1973 Sep;37(3):479–81.

87. De Marinis YZ, Salehi A, Ward CE, Zhang Q, Abdulkader F, Bengtsson M, et al. GLP-1 inhibits and adrenaline stimulates glucagon release by differential modulation of N- and L-type Ca2+ channel-dependent exocytosis. Cell Metab. 2010 Jun 9;11(6):543–53.

88. Gonzalez GA, Montminy MR. Cyclic AMP stimulates somatostatin gene transcription by phosphorylation of CREB at serine 133. Cell. 1989 Nov 17;59(4):675–80.

89. Hoffer LJ. Cori cycle contribution to plasma glucose appearance in man. JPEN J Parenter Enteral Nutr. 1990 Dec;14(6):646–8.

90. Cori CF. The glucose-lactic acid cycle and gluconeogenesis. Curr Top Cell Regul. 1981;18:377–87.

91. Shah AM, Wondisford FE. Tracking the carbons supplying gluconeogenesis. Journal of Biological Chemistry. 2020 Oct 16;295(42):14419–29.

92. Okun JG, Rusu PM, Chan AY, Wu Y, Yap YW, Sharkie T, et al. Liver alanine catabolism promotes skeletal muscle atrophy and hyperglycaemia in type 2 diabetes. Nat Metab. 2021 Mar;3(3):394–409.

93. Sarabhai T, Roden M. Hungry for your alanine: when liver depends on muscle proteolysis. J Clin Invest. 2019 Nov 1;129(11):4563–6.

94. Stumvoll M, Perriello G, Meyer C, Gerich J. Role of glutamine in human carbohydrate metabolism in kidney and other tissues. Kidney International. 1999 Mar 1;55(3):778–92.

95. Baba H, Zhang XJ, Wolfe RR. Glycerol gluconeogenesis in fasting humans. Nutrition. 1995 Apr;11(2):149–53.

96. Sugden MC, Holness MJ. Mechanisms underlying regulation of the expression and activities of the mammalian pyruvate dehydrogenase kinases. Arch Physiol Biochem. 2006 Jul;112(3):139–49.

97. Adina-Zada A, Zeczycki TN, St Maurice M, Jitrapakdee S, Cleland WW, Attwood PV. Allosteric regulation of the biotin-dependent enzyme pyruvate carboxylase by acetyl-CoA. Biochem Soc Trans. 2012 Jun 1;40(3):567–72.

98. El-Maghrabi MR, Haston WS, Flockhart DA, Claus TH, Pilkis SJ. Studies on the phosphorylation and dephosphorylation of L-type pyruvate kinase by the catalytic subunit of cyclic AMP-dependent protein kinase. J Biol Chem. 1980 Jan 25;255(2):668–75.

99. Engström L. The regulation of liver pyruvate kinase by phosphorylation--dephosphorylation. Curr Top Cell Regul. 1978;13:28–51.

100. Chakravarty K, Cassuto H, Reshef L, Hanson RW. Factors that control the tissue-specific transcription of the gene for phosphoenolpyruvate carboxykinase-C. Crit Rev Biochem Mol Biol. 2005 Jun;40(3):129–54.

101. Park EA, Roesler WJ, Liu J, Klemm DJ, Gurney AL, Thatcher JD, et al. The role of the CCAAT/enhancer-binding protein in the transcriptional regulation of the gene for phosphoenolpyruvate carboxykinase (GTP). Mol Cell Biol. 1990 Dec;10(12):6264–72.

102. Hatting M, Tavares CDJ, Sharabi K, Rines AK, Puigserver P. Insulin regulation of gluconeogenesis. Ann N Y Acad Sci. 2018 Jan;1411(1):21–35.

103. Lu M, Wan M, Leavens KF, Chu Q, Monks BR, Fernandez S, et al. Insulin regulates liver metabolism in vivo in the absence of hepatic Akt and Foxo1. Nat Med. 2012 Feb 19;18(3):388–95.

104. Lin J, Handschin C, Spiegelman BM. Metabolic control through the PGC-1 family of transcription coactivators. Cell Metab. 2005 Jun;1(6):361–70.

105. Skyler JS, Bakris GL, Bonifacio E, Darsow T, Eckel RH, Groop L, et al. Differentiation of Diabetes by Pathophysiology, Natural History, and Prognosis. Diabetes. 2017 Feb;66(2):241–55.

106. Dabelea D, Pihoker C, Talton JW, D'Agostino RB, Fujimoto W, Klingensmith GJ, et al. Etiological approach to characterization of diabetes type: the SEARCH for Diabetes in Youth Study. Diabetes Care. 2011 Jul;34(7):1628–33.

107. Ahlqvist E, Storm P, Käräjämäki A, Martinell M, Dorkhan M, Carlsson A, et al. Novel subgroups of adult-onset diabetes and their association with outcomes: a data-driven cluster analysis of six variables. The Lancet Diabetes & Endocrinology. 2018 May 1;6(5):361–9.

108. Martins AR, Nachbar RT, Gorjao R, Vinolo MA, Festuccia WT, Lambertucci RH, et al. Mechanisms underlying skeletal muscle insulin resistance induced by fatty acids: importance of the mitochondrial function. Lipids in Health and Disease. 2012 Feb 23;11(1):30.

109. Petersen KF, Dufour S, Savage DB, Bilz S, Solomon G, Yonemitsu S, et al. The role of skeletal muscle insulin resistance in the pathogenesis of the metabolic syndrome. Proc Natl Acad Sci U S A. 2007 Jul 31;104(31):12587–94.

110. DeFronzo RA. Pathogenesis of type 2 diabetes mellitus. Med Clin North Am. 2004 Jul;88(4):787–835, ix.

111. Samuel VT. Fructose induced lipogenesis: from sugar to fat to insulin resistance. Trends Endocrinol Metab. 2011 Feb;22(2):60–5.

112. Krssak M, Falk Petersen K, Dresner A, DiPietro L, Vogel SM, Rothman DL, et al. Intramyocellular lipid concentrations are correlated with insulin sensitivity in humans: a 1H NMR spectroscopy study. Diabetologia. 1999 Jan 1;42(1):113–6.

113. Kase ET, Wensaas AJ, Aas V, Højlund K, Levin K, Thoresen GH, et al. Skeletal Muscle Lipid Accumulation in Type 2 Diabetes May Involve the Liver X Receptor Pathway. Diabetes. 2005 Apr 1;54(4):1108–15.

114. Shulman GI. Ectopic Fat in Insulin Resistance, Dyslipidemia, and Cardiometabolic Disease. N Engl J Med. 2014 Sep 18;371(12):1131–41.

115. Kim JK, Gavrilova O, Chen Y, Reitman ML, Shulman GI. Mechanism of insulin resistance in A-ZIP/F-1 fatless mice. J Biol Chem. 2000 Mar 24;275(12):8456–60.

116. Kim JK, Fillmore JJ, Chen Y, Yu C, Moore IK, Pypaert M, et al. Tissue-specific overexpression of lipoprotein lipase causes tissue-specific insulin resistance. Proc Natl Acad Sci U S A. 2001 Jun 19;98(13):7522–7.

117. Ferreira LD, Pulawa LK, Jensen DR, Eckel RH. Overexpressing human lipoprotein lipase in mouse skeletal muscle is associated with insulin resistance. Diabetes. 2001 May;50(5):1064–8.

118. Kim JY, Hickner RC, Cortright RL, Dohm GL, Houmard JA. Lipid oxidation is reduced in obese human skeletal muscle. American Journal of Physiology-Endocrinology and Metabolism. 2000 Nov;279(5):E1039–44.

119. Ukropcova B, McNeil M, Sereda O, de Jonge L, Xie H, Bray GA, et al. Dynamic changes in fat oxidation in human primary myocytes mirror metabolic characteristics of the donor. J Clin Invest. 2005 Jul 1;115(7):1934–41.

120. Erion DM, Shulman GI. Diacylglycerol-mediated insulin resistance. Nat Med. 2010 Apr;16(4):400–2.

121. Roden M, Price TB, Perseghin G, Petersen KF, Rothman DL, Cline GW, et al. Mechanism of free fatty acid-induced insulin resistance in humans. J Clin Invest. 1996 Jun 15;97(12):2859–65.

122. Dresner A, Laurent D, Marcucci M, Griffin ME, Dufour S, Cline GW, et al. Effects of free fatty acids on glucose transport and IRS-1-associated phosphatidylinositol 3-kinase activity. J Clin Invest. 1999 Jan;103(2):253–9.

123. Itani SI, Ruderman NB, Schmieder F, Boden G. Lipid-induced insulin resistance in human muscle is associated with changes in diacylglycerol, protein kinase C, and IkappaB-alpha. Diabetes. 2002 Jul;51(7):2005–11.

124. Griffin ME, Marcucci MJ, Cline GW, Bell K, Barucci N, Lee D, et al. Free fatty acid-induced insulin resistance is associated with activation of protein kinase C theta and alterations in the insulin signaling cascade. Diabetes. 1999 Jun;48(6):1270–4.

125. Yu C, Chen Y, Cline GW, Zhang D, Zong H, Wang Y, et al. Mechanism by which fatty acids inhibit insulin activation of insulin receptor substrate-1 (IRS-1)-associated phosphatidylinositol 3-kinase activity in muscle. J Biol Chem. 2002 Dec 27;277(52):50230–6.

126. Morino K, Neschen S, Bilz S, Sono S, Tsirigotis D, Reznick RM, et al. Muscle-Specific IRS-1 Ser→Ala Transgenic Mice Are Protected From Fat-Induced Insulin Resistance in Skeletal Muscle. Diabetes. 2008 Oct;57(10):2644–51.

127. Cusi K, Maezono K, Osman A, Pendergrass M, Patti ME, Pratipanawatr T, et al. Insulin resistance differentially affects the PI 3-kinase- and MAP kinase-mediated signaling in human muscle. J Clin Invest. 2000 Feb;105(3):311–20.

128. Krook A, Björnholm M, Galuska D, Jiang XJ, Fahlman R, Myers MG, et al. Characterization of signal transduction and glucose transport in skeletal muscle from type 2 diabetic patients. Diabetes. 2000 Feb;49(2):284–92.

129. Bouzakri K, Roques M, Gual P, Espinosa S, Guebre-Egziabher F, Riou JP, et al. Reduced activation of phosphatidylinositol-3 kinase and increased serine 636 phosphorylation of insulin receptor substrate-1 in primary culture of skeletal muscle cells from patients with type 2 diabetes. Diabetes. 2003 Jun;52(6):1319–25.

130. Freidenberg GR, Reichart D, Olefsky JM, Henry RR. Reversibility of defective adipocyte insulin receptor kinase activity in non-insulin-dependent diabetes mellitus. Effect of weight loss. J Clin Invest. 1988 Oct;82(4):1398–406.

131. Hirabara SM, Silveira LR, Abdulkader F, Carvalho CRO, Procopio J, Curi R. Time-dependent effects of fatty acids on skeletal muscle metabolism. Journal of Cellular Physiology. 2007;210(1):7–15.

132. Hajduch E, Balendran A, Batty IH, Litherland GJ, Blair AS, Downes CP, et al. Ceramide impairs the insulin-dependent membrane recruitment of protein kinase B leading to a loss in downstream signalling in L6 skeletal muscle cells. Diabetologia. 2001 Feb;44(2):173–83.

133. Del Prato S, Bonadonna RC, Bonora E, Gulli G, Solini A, Shank M, et al. Characterization of cellular defects of insulin action in type 2 (non-insulin-dependent) diabetes mellitus. J Clin Invest. 1993 Feb;91(2):484–94.

134. Freymond D, Bogardus C, Okubo M, Stone K, Mott D. Impaired insulin-stimulated muscle glycogen synthase activation in vivo in man is related to low fasting glycogen synthase phosphatase activity. J Clin Invest. 1988 Nov;82(5):1503–9.

135. Mandarino LJ, Printz RL, Cusi KA, Kinchington P, O'Doherty RM, Osawa H, et al. Regulation of hexokinase II and glycogen synthase mRNA, protein, and activity in human muscle. Am J Physiol. 1995 Oct;269(4 Pt 1):E701-708.

136. Vestergaard H, Lund S, Larsen FS, Bjerrum OJ, Pedersen O. Glycogen synthase and phosphofructokinase protein and mRNA levels in skeletal muscle from insulin-resistant patients with non-insulin-dependent diabetes mellitus. J Clin Invest. 1993 Jun;91(6):2342–50.

137. Vestergaard H, Bjørbæk C, Andersen PH, Bak JF, Pedersen O. Impaired Expression of Glycogen Synthase mRNA in Skeletal Muscle of NIDDM Patients. Diabetes. 1991 Dec 1;40(12):1740–5.

138. Gulli G, Ferrannini E, Stern M, Haffner S, DeFronzo RA. The metabolic profile of NIDDM is fully established in glucose-tolerant offspring of two Mexican-American NIDDM parents. Diabetes. 1992 Dec;41(12):1575–86.

139. Bjørbaek C, Vik TA, Echwald SM, Yang PY, Vestergaard H, Wang JP, et al. Cloning of a human insulin-stimulated protein kinase (ISPK-1) gene and analysis of coding regions and mRNA levels of the ISPK-1 and the protein phosphatase-1 genes in muscle from NIDDM patients. Diabetes. 1995 Jan;44(1):90–7.

140. Prochazka M, Mochizuki H, Baier LJ, Cohen PT, Bogardus C. Molecular and linkage analysis of type-1 protein phosphatase catalytic beta-subunit gene: lack of evidence for its major role in insulin resistance in Pima Indians. Diabetologia. 1995 Apr;38(4):461–6.

141. Nathan DM. The Diabetes Control and Complications Trial/Epidemiology of Diabetes Interventions and Complications Study at 30 Years: Overview. Diabetes Care. 2014 Jan;37(1):9–16.

142. The Effect of Intensive Treatment of Diabetes on the Development and Progression of Long-Term Complications in Insulin-Dependent Diabetes Mellitus | NEJM [Internet]. [cited 2022 Jan 7]. Available from: https://www.nejm.org/doi/10.1056/NEJM199309303291401?url_ver=Z39.88-2003&rfr_id=ori:rid:crossref.org&rfr_dat=cr_pub%20%200www.ncbi.nlm.nih.gov

143. American Diabetes Association. Implications of the United Kingdom Prospective Diabetes Study. Diabetes Care. 2000 Jan;23 Suppl 1:S27-31.

144. Bryan J, Crane A, Vila-Carriles WH, Babenko AP, Aguilar-Bryan L. Insulin Secretagogues, Sulfonylurea Receptors and KATP Channels. Current Pharmaceutical Design. 2005 Aug 1;11(21):2699–716.

145. Feingold KR. Oral and Injectable (Non-Insulin) Pharmacological Agents for the Treatment of Type 2 Diabetes. In: Feingold KR, Anawalt B, Boyce A, Chrousos G, de Herder WW, Dhatariya K, et al., editors. Endotext [Internet]. South Dartmouth (MA): MDText.com, Inc.; 2000 [cited 2022 Feb 22]. Available from: http://www.ncbi.nlm.nih.gov/books/NBK279141/

146. Hermann LS, Scherstén B, Bitzén PO, Kjellström T, Lindgärde F, Melander A. Therapeutic comparison of metformin and sulfonylurea, alone and in various

combinations. A double-blind controlled study. Diabetes Care. 1994 Oct;17(10):1100–9.

147. Garber AJ, Larsen J, Schneider SH, Piper BA, Henry D, Glyburide/Metformin Initial Therapy Study Group. Simultaneous glyburide/metformin therapy is superior to component monotherapy as an initial pharmacological treatment for type 2 diabetes. Diabetes Obes Metab. 2002 May;4(3):201–8.

148. Sola D, Rossi L, Schianca GPC, Maffioli P, Bigliocca M, Mella R, et al. Sulfonylureas and their use in clinical practice. Arch Med Sci. 2015 Aug 12;11(4):840–8.

149. Douros A, Dell'Aniello S, Yu OHY, Filion KB, Azoulay L, Suissa S. Sulfonylureas as second line drugs in type 2 diabetes and the risk of cardiovascular and hypoglycaemic events: population based cohort study. BMJ. 2018 Jul 18;362:k2693.

150. Intensive Blood Glucose Control and Vascular Outcomes in Patients with Type 2 Diabetes. N Engl J Med. 2008 Jun 12;358(24):2560–72.

151. Intensive blood-glucose control with sulphonylureas or insulin compared with conventional treatment and risk of complications in patients with type 2 diabetes (UKPDS 33). UK Prospective Diabetes Study (UKPDS) Group. Lancet. 1998 Sep 12;352(9131):837–53.

152. Andersen A, Lund A, Knop FK, Vilsbøll T. Glucagon-like peptide 1 in health and disease. Nat Rev Endocrinol. 2018 Jul;14(7):390–403.

153. Gentilella R, Bianchi C, Rossi A, Rotella CM. Exenatide: a review from pharmacology to clinical practice. Diabetes Obes Metab. 2009 Jun;11(6):544–56.

154. Kolterman OG, Buse JB, Fineman MS, Gaines E, Heintz S, Bicsak TA, et al. Synthetic exendin-4 (exenatide) significantly reduces postprandial and fasting plasma glucose in subjects with type 2 diabetes. J Clin Endocrinol Metab. 2003 Jul;88(7):3082–9.

155. Lingvay I, Catarig AM, Frias JP, Kumar H, Lausvig NL, Roux CW le, et al. Efficacy and safety of once-weekly semaglutide versus daily canagliflozin as add-on to metformin in patients with type 2 diabetes (SUSTAIN 8): a double-blind, phase 3b, randomised controlled trial. The Lancet Diabetes & Endocrinology. 2019 Nov 1;7(11):834–44.

156. Marso SP, Daniels GH, Brown-Frandsen K, Kristensen P, Mann JFE, Nauck MA, et al. Liraglutide and Cardiovascular Outcomes in Type 2 Diabetes. New England Journal of Medicine. 2016 Jul 28;375(4):311–22.

157. Marso SP, Bain SC, Consoli A, Eliaschewitz FG, Jódar E, Leiter LA, et al. Semaglutide and Cardiovascular Outcomes in Patients with Type 2 Diabetes. New England Journal of Medicine. 2016 Nov 10;375(19):1834–44.

158. Mentlein R. Dipeptidyl-peptidase IV (CD26)--role in the inactivation of regulatory peptides. Regul Pept. 1999 Nov 30;85(1):9–24.

159. Aroda VR, Henry RR, Han J, Huang W, DeYoung MB, Darsow T, et al. Efficacy of GLP-1 Receptor Agonists and DPP-4 Inhibitors: Meta-Analysis and Systematic Review. Clinical Therapeutics. 2012 Jun 1;34(6):1247-1258.e22.

160. Kurtzhals P. Pharmacology of insulin detemir. Endocrinol Metab Clin North Am. 2007 Aug;36 Suppl 1:14–20.

161. Heinemann L, Linkeschova R, Rave K, Hompesch B, Sedlak M, Heise T. Time-action profile of the long-acting insulin analog insulin glargine (HOE901) in comparison with those of NPH insulin and placebo. Diabetes Care. 2000 May;23(5):644–9.

162. Bolli GB, Porcellati F, Lucidi P, Fanelli CG, Owens DR. One-hundred year evolution of prandial insulin preparations: From animal pancreas extracts to rapid-acting analogs. Metabolism. 2022 Jan 1;126:154935.

163. Skrivarhaug T, Bangstad HJ, Stene LC, Sandvik L, Hanssen KF, Joner G. Long-term mortality in a nationwide cohort of childhood-onset type 1 diabetic patients in Norway. Diabetologia. 2006 Feb;49(2):298–305.

164. Feltbower RG, Bodansky HJ, Patterson CC, Parslow RC, Stephenson CR, Reynolds C, et al. Acute complications and drug misuse are important causes of death for children and young adults with type 1 diabetes: results from the Yorkshire Register of diabetes in children and young adults. Diabetes Care. 2008 May;31(5):922–6.

165. The Diabetes Control and Complications Trial Research Group. Hypoglycemia in the Diabetes Control and Complications Trial. Diabetes. 1997 Feb 1;46(2):271–86.

166. UK Hypoglycaemia Study Group. Risk of hypoglycaemia in types 1 and 2 diabetes: effects of treatment modalities and their duration. Diabetologia. 2007 Jun;50(6):1140–7.

167. American Diabetes Association Professional Practice Committee. 6. Glycemic Targets: Standards of Medical Care in Diabetes—2022. Diabetes Care. 2021 Dec 16;45(Supplement_1):S83–96.

168. Towler DA, Havlin CE, Craft S, Cryer P. Mechanism of awareness of hypoglycemia. Perception of neurogenic (predominantly cholinergic) rather than neuroglycopenic symptoms. Diabetes. 1993 Dec;42(12):1791–8.

169. DeRosa MA, Cryer PE. Hypoglycemia and the sympathoadrenal system: neurogenic symptoms are largely the result of sympathetic neural, rather than adrenomedullary, activation. American Journal of Physiology-Endocrinology and Metabolism. 2004 Jul;287(1):E32–41.

170. Cryer PE, Axelrod L, Grossman AB, Heller SR, Montori VM, Seaquist ER, et al. Evaluation and management of adult hypoglycemic disorders: an Endocrine Society Clinical Practice Guideline. J Clin Endocrinol Metab. 2009 Mar;94(3):709–28.

171. Cryer PE. Mechanisms of Hypoglycemia-Associated Autonomic Failure in Diabetes. N Engl J Med. 2013 Jul 25;369(4):362–72.

172. Fanelli CG, Paramore DS, Hershey T, Terkamp C, Ovalle F, Craft S, et al. Impact of nocturnal hypoglycemia on hypoglycemic cognitive dysfunction in type 1 diabetes. Diabetes. 1998 Dec;47(12):1920–7.

173. Dagogo-Jack SE, Craft S, Cryer PE. Hypoglycemia-associated autonomic failure in insulin-dependent diabetes mellitus. Recent antecedent hypoglycemia reduces autonomic responses to, symptoms of, and defense against subsequent hypoglycemia. J Clin Invest. 1993 Mar;91(3):819–28.

174. Purnell JQ, Zinman B, Brunzell JD, DCCT/EDIC Research Group. The effect of excess weight gain with intensive diabetes mellitus treatment on cardiovascular disease risk factors and atherosclerosis in type 1 diabetes mellitus: results from the Diabetes Control and Complications Trial/Epidemiology of Diabetes Interventions and Complications Study (DCCT/EDIC) study. Circulation. 2013 Jan 15;127(2):180–7.

175. Nathan DM, Cleary PA, Backlund JYC, Genuth SM, Lachin JM, Orchard TJ, et al. Intensive diabetes treatment and cardiovascular disease in patients with type 1 diabetes. N Engl J Med. 2005 Dec 22;353(25):2643–53.

176. Mäkimattila S, Nikkilä K, Yki-Järvinen H. Causes of weight gain during insulin therapy with and without metformin in patients with Type II diabetes mellitus. Diabetologia. 1999 Apr;42(4):406–12.

177. Harno E, Gali Ramamoorthy T, Coll AP, White A. POMC: The Physiological Power of Hormone Processing. Physiological Reviews. 2018 Oct 1;98(4):2381–430.

178. Pritchard LE, Turnbull AV, White A. Pro-opiomelanocortin processing in the hypothalamus: impact on melanocortin signalling and obesity. J Endocrinol. 2002 Mar;172(3):411–21.

179. Raffin-Sanson ML, de Keyzer Y, Bertagna X. Proopiomelanocortin, a polypeptide precursor with multiple functions: from physiology to pathological conditions. Eur J Endocrinol. 2003 Aug;149(2):79–90.

180. Cone RD. Anatomy and regulation of the central melanocortin system. Nature Neuroscience. 2005 May;8(5):571.

181. Gibson S, Crosby SR, Stewart MF, Jennings AM, McCall E, White A. Differential release of proopiomelanocortin-derived peptides from the human pituitary: evidence from a panel of two-site immunoradiometric assays. J Clin Endocrinol Metab. 1994 Apr;78(4):835–41.

182. Zhou A, Bloomquist BT, Mains RE. The prohormone convertases PC1 and PC2 mediate distinct endoproteolytic cleavages in a strict temporal order during proopiomelanocortin biosynthetic processing. Journal of Biological Chemistry. 1993 Jan 25;268(3):1763–9.

183. Hahn TM, Breininger JF, Baskin DG, Schwartz MW. Coexpression of Agrp and NPY in fasting-activated hypothalamic neurons. Nat Neurosci. 1998 Aug;1(4):271–2.

184. Ollmann MM, Wilson BD, Yang YK, Kerns JA, Chen Y, Gantz I, et al. Antagonism of Central Melanocortin Receptors in Vitro and in Vivo by Agouti-Related Protein. Science. 1997 Oct 3;278(5335):135–8.

185. Creemers JWM, Pritchard LE, Gyte A, Le Rouzic P, Meulemans S, Wardlaw SL, et al. Agouti-Related Protein Is Posttranslationally Cleaved by Proprotein Convertase 1 to Generate Agouti-Related Protein (AGRP)83–132: Interaction between AGRP83–132 and Melanocortin Receptors Cannot Be Influenced by Syndecan-3. Endocrinology. 2006 Apr 1;147(4):1621–31.

186. Falls BA, Zhang Y. Insights into the Allosteric Mechanism of Setmelanotide (RM-493) as a Potent and First-in-Class Melanocortin-4 Receptor (MC4R) Agonist To Treat Rare Genetic Disorders of Obesity through an in Silico Approach. ACS Chem Neurosci. 2019 Mar 20;10(3):1055–65.

187. Mountjoy KG, Robbins LS, Mortrud MT, Cone RD. The cloning of a family of genes that encode the melanocortin receptors. Science. 1992 Aug 28;257(5074):1248–51.

188. Gantz I, Miwa H, Konda Y, Shimoto Y, Tashiro T, Watson SJ, et al. Molecular cloning, expression, and gene localization of a fourth melanocortin receptor. J Biol Chem. 1993 Jul 15;268(20):15174–9.

189. Chen M, Aprahamian CJ, Kesterson RA, Harmon CM, Yang Y. Molecular identification of the human melanocortin-2 receptor responsible for ligand binding and signaling. Biochemistry. 2007 Oct 9;46(40):11389–97.

190. Chakraborty A, Slominski A, Ermak G, Hwang J, Pawelek J. Ultraviolet B and Melanocyte-Stimulating Hormone (MSH) Stimulate mRNA Production for ∝MSH Receptors and Proopiomelanocortin-Derived Peptides in Mouse Melanoma Cells and Transformed Keratinocytes. Journal of Investigative Dermatology. 1995 Nov 1;105(5):655–9.

191. Luger TA, Schwarz T, Kalden H, Scholzen T, Schwarz A, Brzoska T. Role of epidermal cell-derived alpha-melanocyte stimulating hormone in ultraviolet light mediated local immunosuppression. Ann N Y Acad Sci. 1999 Oct 20;885:209–16.

192. Chhajlani V. Distribution of cDNA for melanocortin receptor subtypes in human tissues. Biochem Mol Biol Int. 1996 Feb;38(1):73–80.

193. Suzuki I, Cone RD, Im S, Nordlund J, Abdel-Malek ZA. Binding of melanotropic hormones to the melanocortin receptor MC1R on human melanocytes stimulates proliferation and melanogenesis. Endocrinology. 1996 May 1;137(5):1627–33.

194. Abdel-Malek ZA. Melanocortin receptors: their functions and regulation by physiological agonists and antagonists. CMLS, Cell Mol Life Sci. 2001 Mar 1;58(3):434–41.

195. Yang Y. Structure, function and regulation of the melanocortin receptors. European Journal of Pharmacology. 2011 Jun 11;660(1):125–30.

196. Panaro BL, Tough IR, Engelstoft MS, Matthews RT, Digby GJ, Møller CL, et al. The Melanocortin-4 Receptor Is Expressed in Enteroendocrine L Cells and Regulates the Release of Peptide YY and Glucagon-like Peptide 1 In Vivo. Cell Metabolism. 2014 Dec 2;20(6):1018–29.

197. Kuhre RE, Modvig IM, Jepsen SL, Kizilkaya HS, Bæch-Laursen C, Smith CA, et al. L-Cell Expression of Melanocortin-4-Receptor Is Marginal in Most of the Small Intestine in Mice and Humans and Direct Stimulation of Small Intestinal Melanocortin-4-Receptors in Mice and Rats Does Not Affect GLP-1 Secretion. Frontiers in Endocrinology. 2021;12:813.

198. González-Jiménez E, Aguilar Cordero MJ, Padilla López CA, García García I. [Monogenic human obesity: role of the leptin-melanocortin system in the regulation of food intake and body weight in humans]. An Sist Sanit Navar. 2012 May 1;35(2):285–93.

199. Hainerová IA, Lebl J. Treatment options for children with monogenic forms of obesity. World Rev Nutr Diet. 2013;106:105–12.

200. Fathi Z, Iben LG, Parker EM. Cloning, expression, and tissue distribution of a fifth melanocortin receptor subtype. Neurochem Res. 1995 Jan 1;20(1):107–13.

201. Trotta MC, Maisto R, Alessio N, Hermenean A, D'Amico M, Di Filippo C. The Melanocortin MC5R as a New Target for Treatment of High Glucose-Induced Hypertrophy of the Cardiac H9c2 Cells. Front Physiol [Internet]. 2018 [cited 2019 Mar 20];9. Available from: https://www.frontiersin.org/articles/10.3389/fphys.2018.01475/full

202. Zhang L, Li WH, Anthonavage M, Eisinger M. Melanocortin-5 receptor: A marker of human sebocyte differentiation. Peptides. 2006 Feb 1;27(2):413–20.

203. Zhang L, Li WH, Anthonavage M, Pappas A, Rossetti D, Cavender D, et al. Melanocortin-5 receptor and sebogenesis. European Journal of Pharmacology. 2011 Jun 11;660(1):202–6.

204. Thiboutot D, Sivarajah A, Gilliland K, Cong Z, Clawson G. The Melanocortin 5 Receptor is Expressed in Human Sebaceous Glands and Rat Preputial Cells. Journal of Investigative Dermatology. 2000 Oct 1;115(4):614–9.

205. Enriori PJ, Chen W, Garcia-Rudaz MC, Grayson BE, Evans AE, Comstock SM, et al. α-Melanocyte stimulating hormone promotes muscle glucose uptake via melanocortin 5 receptors. Molecular Metabolism. 2016 Oct 1;5(10):807–22.

206. Møller CL, Kjøbsted R, Enriori PJ, Jensen TE, Garcia-Rudaz C, Litwak SA, et al. α-MSH Stimulates Glucose Uptake in Mouse Muscle and Phosphorylates Rab-GTPase-Activating Protein TBC1D1 Independently of AMPK. PLoS ONE. 2016 Jul 28;11(7):1–18.

207. Yeo GS, Farooqi IS, Aminian S, Halsall DJ, Stanhope RG, O'Rahilly S. A frameshift mutation in MC4R associated with dominantly inherited human obesity. Nat Genet. 1998 Oct;20(2):111–2.

208. Cone RD, Cowley MA, Butler AA, Fan W, Marks DL, Low MJ. The arcuate nucleus as a conduit for diverse signals relevant to energy homeostasis. Int J Obes Relat Metab Disord. 2001 Dec;25 Suppl 5:S63-67.

209. Cowley MA, Smart JL, Rubinstein M, Cerdán MG, Diano S, Horvath TL, et al. Leptin activates anorexigenic POMC neurons through a neural network in the arcuate nucleus. Nature. 2001 May 24;411(6836):480–4.

210. Niswender KD, Baskin DG, Schwartz MW. Insulin and its evolving partnership with leptin in the hypothalamic control of energy homeostasis. Trends in Endocrinology & Metabolism. 2004 Oct 1;15(8):362–9.

211. Brüning JC, Gautam D, Burks DJ, Gillette J, Schubert M, Orban PC, et al. Role of brain insulin receptor in control of body weight and reproduction. Science. 2000 Sep 22;289(5487):2122–5.

212. Elias CF, Aschkenasi C, Lee C, Kelly J, Ahima RS, Bjorbaek C, et al. Leptin differentially regulates NPY and POMC neurons projecting to the lateral hypothalamic area. Neuron. 1999 Aug;23(4):775–86.

213. Bariohay B, Roux J, Tardivel C, Trouslard J, Jean A, Lebrun B. Brain-Derived Neurotrophic Factor/Tropomyosin-Related Kinase Receptor Type B Signaling Is a Downstream Effector of the Brainstem Melanocortin System in Food Intake Control. Endocrinology. 2009 Jun 1;150(6):2646–53.

214. Wan S, Browning KN, Coleman FH, Sutton G, Zheng H, Butler A, et al. Presynaptic Melanocortin-4 Receptors on Vagal Afferent Fibers Modulate the Excitability of Rat Nucleus Tractus Solitarius Neurons. J Neurosci. 2008 May 7;28(19):4957–66.

215. Butler AA, Kesteson RA, Khong K, Cullen MJ, Pelleymounter MA, Dekoning J, et al. A Unique Metalolic Sysdrone Causes Obesity in the Melanocortin-3 Receptor-Deficient Mouse. Endocrinology. 2000 Sep 1;141(9):3518–21.

216. EMA. Imcivree [Internet]. European Medicines Agency. 2021 [cited 2022 Feb 12]. Available from: https://www.ema.europa.eu/en/medicines/human/EPAR/imcivree

217. Clément K, Akker E van den, Argente J, Bahm A, Chung WK, Connors H, et al. Efficacy and safety of setmelanotide, an MC4R agonist, in individuals with severe obesity due to LEPR or POMC deficiency: single-arm, open-label, multicentre, phase 3 trials. The Lancet Diabetes & Endocrinology. 2020 Dec 1;8(12):960–70.

218. Miltenberger RJ, Mynatt RL, Wilkinson JE, Woychik RP. The Role of the agouti Gene in the Yellow Obese Syndrome. The Journal of Nutrition. 1997 Sep 1;127(9):1902S-1907S.

219. Wolff GL, Roberts DW, Mountjoy KG. Physiological consequences of ectopic agouti gene expression: the yellow obese mouse syndrome. Physiol Genomics. 1999 Nov 11;1(3):151–63.

220. Aponte Y, Atasoy D, Sternson SM. AGRP neurons are sufficient to orchestrate feeding behavior rapidly and without training. Nat Neurosci. 2011 Mar;14(3):351–5.

221. Liu T, Kong D, Shah BP, Ye C, Koda S, Saunders A, et al. Fasting activation of AgRP neurons requires NMDA receptors and involves spinogenesis and increased excitatory tone. Neuron. 2012 Feb 9;73(3):511–22.

222. Ariyasu H, Takaya K, Tagami T, Ogawa Y, Hosoda K, Akamizu T, et al. Stomach is a major source of circulating ghrelin, and feeding state determines plasma ghrelin-like immunoreactivity levels in humans. J Clin Endocrinol Metab. 2001 Oct;86(10):4753–8.

223. Tschöp M, Wawarta R, Riepl RL, Friedrich S, Bidlingmaier M, Landgraf R, et al. Post-prandial decrease of circulating human ghrelin levels. J Endocrinol Invest. 2001 Jun;24(6):RC19-21.

224. Willesen MG, Kristensen P, Rømer J. Co-localization of growth hormone secretagogue receptor and NPY mRNA in the arcuate nucleus of the rat. Neuroendocrinology. 1999 Nov;70(5):306–16.

225. Shintani M, Ogawa Y, Ebihara K, Aizawa-Abe M, Miyanaga F, Takaya K, et al. Ghrelin, an endogenous growth hormone secretagogue, is a novel orexigenic peptide that antagonizes leptin action through the activation of hypothalamic neuropeptide Y/Y1 receptor pathway. Diabetes. 2001 Feb;50(2):227–32.

226. Shishioh-Ikejima N, Ogawa T, Yamaguti K, Watanabe Y, Kuratsune H, Kiyama H. The increase of alpha-melanocyte-stimulating hormone in the plasma of chronic fatigue syndrome patients. BMC Neurology. 2010 Aug 23;10(1):73.

227. Gavrila A, Chan JL, Miller LC, Heist K, Yiannakouris N, Mantzoros CS. Circulating Melanin-Concentrating Hormone, Agouti-Related Protein, and α-Melanocyte-Stimulating Hormone Levels in Relation to Body Composition: Alterations in Response to Food Deprivation and Recombinant Human Leptin Administration. The Journal of Clinical Endocrinology & Metabolism. 2005 Feb 1;90(2):1047–54.

228. Zelent D, Golson ML, Koeberlein B, Quintens R, Lommel L van, Buettger C, et al. A Glucose Sensor Role for Glucokinase in Anterior Pituitary Cells. Diabetes. 2006 Jul 1;55(7):1923–9.

229. An JJ, Rhee Y, Kim SH, Kim DM, Han DH, Hwang JH, et al. Peripheral Effect of α-Melanocyte-stimulating Hormone on Fatty Acid Oxidation in Skeletal Muscle. J Biol Chem. 2007 Feb 2;282(5):2862–70.

230. Cardasis CA, Cooper GW. An analysis of nuclear numbers in individual muscle fibers during differentiation and growth: a satellite cell-muscle fiber growth unit. J Exp Zool. 1975 Mar;191(3):347–58.

231. Collins CA, Olsen I, Zammit PS, Heslop L, Petrie A, Partridge TA, et al. Stem Cell Function, Self-Renewal, and Behavioral Heterogeneity of Cells from the Adult Muscle Satellite Cell Niche. Cell. 2005 Jul 29;122(2):289–301.

232. Blau HM, Webster C. Isolation and characterization of human muscle cells. Proc Natl Acad Sci U S A. 1981 Sep;78(9):5623–7.

233. MANGNALL D, BRUCE C, FRASER RB. Insulin-stimulated glucose uptake in C2C12 myoblasts. Biochemical Society Transactions. 1993 Nov 1;21(4):438S.

234. Chanon S, Durand C, Vieille-Marchiset A, Robert M, Dibner C, Simon C, et al. Glucose Uptake Measurement and Response to Insulin Stimulation in In Vitro Cultured Human Primary Myotubes. J Vis Exp [Internet]. 2017 Jun 25 [cited 2020 Feb 11];(124). Available from: https://www.ncbi.nlm.nih.gov/pmc/articles/PMC5608504/

235. Sarabia V, Ramlal T, Klip A. Glucose uptake in human and animal muscle cells in culture. Biochem Cell Biol. 1990 Feb 1;68(2):536–42.

236. McIntyre EA, Halse R, Yeaman SJ, Walker M. Cultured muscle cells from insulin-resistant type 2 diabetes patients have impaired insulin, but normal 5-amino-4-imidazolecarboxamide riboside-stimulated, glucose uptake. J Clin Endocrinol Metab. 2004 Jul;89(7):3440–8.

237. Gaster M, Kristensen SR, Beck-Nielsen H, Schrøder HD. A cellular model system of differentiated human myotubes. APMIS. 2001;109(11):735–44.

238. Dohm GL, Tapscott EB, Pories WJ, Dabbs DJ, Flickinger EG, Meelheim D, et al. An in vitro human muscle preparation suitable for metabolic studies. Decreased insulin stimulation of glucose transport in muscle from morbidly obese and diabetic subjects. J Clin Invest. 1988 Aug;82(2):486–94.

239. Wong CY, Al-Salami H, Dass CR. C2C12 cell model: its role in understanding of insulin resistance at the molecular level and pharmaceutical development at the preclinical stage. Journal of Pharmacy and Pharmacology. 2020 Dec 1;72(12):1667–93.

240. Hoffman NJ, Parker BL, Chaudhuri R, Fisher-Wellman KH, Kleinert M, Humphrey SJ, et al. Global Phosphoproteomic Analysis of Human Skeletal Muscle Reveals a Network of Exercise-Regulated Kinases and AMPK Substrates. Cell Metab. 2015 Nov 3;22(5):922–35.

241. Abdelmoez AM, Sardón Puig L, Smith JAB, Gabriel BM, Savikj M, Dollet L, et al. Comparative profiling of skeletal muscle models reveals heterogeneity of transcriptome and metabolism. American Journal of Physiology-Cell Physiology. 2020 Mar 1;318(3):C615–26.

242. Al-Khalili L, Chibalin AV, Kannisto K, Zhang BB, Permert J, Holman GD, et al. Insulin action in cultured human skeletal muscle cells during differentiation: assessment of cell surface GLUT4 and GLUT1 content. Cell Mol Life Sci. 2003 May;60(5):991–8.

243. Sarabia V, Lam L, Burdett E, Leiter LA, Klip A. Glucose transport in human skeletal muscle cells in culture. Stimulation by insulin and metformin. J Clin Invest. 1992 Oct 1;90(4):1386–95.

244. Baj A, Bettaccini AA, Casalone R, Sala A, Cherubino P, Toniolo AQ. Culture of skeletal myoblasts from human donors aged over 40 years: dynamics of cell growth and expression of differentiation markers. J Transl Med. 2005 May 12;3(1):21.

245. Hindi L, McMillan J, Afroze D, Hindi S, Kumar A. Isolation, Culturing, and Differentiation of Primary Myoblasts from Skeletal Muscle of Adult Mice. BIO-PROTOCOL [Internet]. 2017 [cited 2019 Apr 9];7(9). Available from: https://bio-protocol.org/e2248

246. Shahini A, Vydiam K, Choudhury D, Rajabian N, Nguyen T, Lei P, et al. Efficient and high yield isolation of myoblasts from skeletal muscle. Stem Cell Research. 2018 Jul 1;30:122–9.

247. Berggren JR, Tanner CJ, Houmard JA. Primary cell cultures in the study of human muscle metabolism. Exerc Sport Sci Rev. 2007 Apr;35(2):56–61.

248. Soriano-Arroquia A, Clegg PD, Molloy AP, Goljanek-Whysall K. Preparation and Culture of Myogenic Precursor Cells/Primary Myoblasts from Skeletal Muscle of Adult and Aged Humans. JoVE (Journal of Visualized Experiments). 2017 Feb 16;(120):e55047.

249. Christov C, Chrétien F, Abou-Khalil R, Bassez G, Vallet G, Authier FJ, et al. Muscle satellite cells and endothelial cells: close neighbors and privileged partners. Mol Biol Cell. 2007 Apr;18(4):1397–409.

250. Agley CC, Rowlerson AM, Velloso CP, Lazarus NR, Harridge SDR. Human skeletal muscle fibroblasts, but not myogenic cells, readily undergo adipogenic differentiation. J Cell Sci. 2013 Dec 15;126(Pt 24):5610–25.

251. Nehlin JO, Just M, Rustan AC, Gaster M. Human myotubes from myoblast cultures undergoing senescence exhibit defects in glucose and lipid metabolism. Biogerontology. 2011 Aug 1;12(4):349–65.

252. Hildyard JCW, Wells DJ. Identification and Validation of Quantitative PCR Reference Genes Suitable for Normalizing Expression in Normal and Dystrophic Cell Culture Models of Myogenesis. PLoS Curr [Internet]. 2014 Mar 6 [cited 2020 Jan 31];6. Available from: https://www.ncbi.nlm.nih.gov/pmc/articles/PMC3948689/

253. Zammit PS, Golding JP, Nagata Y, Hudon V, Partridge TA, Beauchamp JR. Muscle satellite cells adopt divergent fates: a mechanism for self-renewal? J Cell Biol. 2004 Aug 2;166(3):347–57.

254. Zammit PS, Heslop L, Hudon V, Rosenblatt JD, Tajbakhsh S, Buckingham ME, et al. Kinetics of Myoblast Proliferation Show That Resident Satellite Cells Are Competent to Fully Regenerate Skeletal Muscle Fibers. Experimental Cell Research. 2002 Nov 15;281(1):39–49.

255. Al-Khalili L, Cartee GD, Krook A. RNA interference-mediated reduction in GLUT1 inhibits serum-induced glucose transport in primary human skeletal muscle cells. Biochemical and Biophysical Research Communications. 2003 Jul 18;307(1):127–32.

256. Paolisso G, Tataranni PA, Foley JE, Bogardus C, Howard BV, Ravussin E. A high concentration of fasting plasma non-esterified fatty acids is a risk factor for the development of NIDDM. Diabetologia. 1995 Oct;38(10):1213–7.

257. Jeon JY, Choi SE, Ha ES, Lee HB, Kim TH, Han SJ, et al. GLP-1 improves palmitate-induced insulin resistance in human skeletal muscle via SIRT1 activity. International Journal of Molecular Medicine. 2019 Sep 1;44(3):1161–71.

258. Abildgaard J, Henstridge DC, Pedersen AT, Langley KG, Scheele C, Pedersen BK, et al. In Vitro Palmitate Treatment of Myotubes from Postmenopausal Women Leads to Ceramide Accumulation, Inflammation and Affected Insulin Signaling. PLOS ONE. 2014 Jul 7;9(7):e101555.

259. Haghani K, Pashaei S, Vakili S, Taheripak G, Bakhtiyari S. TNF-α knockdown alleviates palmitate-induced insulin resistance in C2C12 skeletal muscle cells. Biochemical and Biophysical Research Communications. 2015 May 15;460(4):977–82.

260. Chavez JA, Knotts TA, Wang LP, Li G, Dobrowsky RT, Florant GL, et al. A Role for Ceramide, but Not Diacylglycerol, in the Antagonism of Insulin Signal Transduction by Saturated Fatty Acids *. Journal of Biological Chemistry. 2003 Mar 21;278(12):10297–303.

261. Thody AJ, Graham A. Does α-MSH Have a Role in Regulating Skin Pigmentation in Humans? Pigment Cell Research. 1998;11(5):265–74.

262. Luger TA, Scholzen T, Grabbe S. The Role of α-Melanocyte-Stimulating Hormone in Cutaneous Biology. Journal of Investigative Dermatology Symposium Proceedings. 1997 Jan;2(1):87–93.

263. Budry L, Lafont C, El Yandouzi T, Chauvet N, Conéjero G, Drouin J, et al. Related pituitary cell lineages develop into interdigitated 3D cell networks. Proc Natl Acad Sci U S A. 2011 Jul 26;108(30):12515–20.

264. Hoggard N, Johnstone AM, Faber P, Gibney ER, Elia M, Lobley G, et al. Plasma concentrations of alpha-MSH, AgRP and leptin in lean and obese men and their relationship to differing states of energy balance perturbation. Clin Endocrinol (Oxf). 2004 Jul;61(1):31–9.

265. Baltatzi M, Hatzitolios A, Tziomalos K, Iliadis F, Zamboulis C. Neuropeptide Y and alpha-melanocyte-stimulating hormone: interaction in obesity and possible role in the development of hypertension. International Journal of Clinical Practice. 2008;62(9):1432–40.

266. Fatima MT, Ahmed I, Fakhro KA, Akil AAS. Melanocortin-4 receptor complexity in energy homeostasis/obesity and drug development strategies. Diabetes,

Obesity and Metabolism [Internet]. [cited 2022 Jan 3];n/a(n/a). Available from: https://onlinelibrary.wiley.com/doi/abs/10.1111/dom.14618

267. Liu T, Ji RL, Tao YX. Naturally occurring mutations in G protein-coupled receptors associated with obesity and type 2 diabetes mellitus. Pharmacology & Therapeutics. 2021 Nov 22;108044.

268. Møller CL, Pedersen SB, Richelsen B, Conde-Frieboes KW, Raun K, Grove KL, et al. Melanocortin agonists stimulate lipolysis in human adipose tissue explants but not in adipocytes. BMC Res Notes [Internet]. 2015 Oct 12 [cited 2019 Oct 4];8. Available from: https://www.ncbi.nlm.nih.gov/pmc/articles/PMC4604100/

269. Hochgeschwender U, Costa JL, Reed P, Bui S, Brennan MB. Altered Glucose Homeostasis in Proopiomelanocortin-Null Mouse Mutants Lacking Central and Peripheral Melanocortin. Endocrinology. 2003 Dec 1;144(12):5194–202.

270. Maisto R, Gesualdo C, Trotta MC, Grieco P, Testa F, Simonelli F, et al. Melanocortin receptor agonists MCR 1-5 protect photoreceptors from high-glucose damage and restore antioxidant enzymes in primary retinal cell culture. J Cell Mol Med. 2017 May;21(5):968–74.

271. Tatro JB. Receptor Biology of the Melanocortins, a Family of Neuroimmunomodulatory Peptides. NIM. 1996;3(5):259–84.

272. Coll AP, Farooqi IS, Challis BG, Yeo GSH, O'Rahilly S. Proopiomelanocortin and Energy Balance: Insights from Human and Murine Genetics. J Clin Endocrinol Metab. 2004 Jun 1;89(6):2557–62.

273. Grieco P, Han G, Weinberg D, MacNeil T, Van der Ploeg LHT, Hruby VJ. Design and Synthesis of Highly Potent and Selective Melanotropin Analogues of SHU9119 Modified at Position 6. Biochemical and Biophysical Research Communications. 2002 Apr 12;292(4):1075–80.

274. Home, Resources, diabetes L with, Acknowledgement, FAQs, Contact, et al. IDF Diabetes Atlas | Tenth Edition [Internet]. [cited 2022 Jan 7]. Available from: https://diabetesatlas.org/

275. Holman RR, Paul SK, Bethel MA, Matthews DR, Neil HAW. 10-Year Follow-up of Intensive Glucose Control in Type 2 Diabetes [Internet]. http://dx.doi.org/10.1056/NEJMoa0806470. Massachusetts Medical Society; 2009 [cited 2022 Jan 7]. Available from: https://www.nejm.org/doi/10.1056/NEJMoa0806470

276. Ceriello A. Postprandial hyperglycemia and diabetes complications: is it time to treat? Diabetes. 2005 Jan;54(1):1–7.

277. American Diabetes Association Professional Practice Committee. 9. Pharmacologic Approaches to Glycemic Treatment: Standards of Medical Care in Diabetes—2022. Diabetes Care. 2021 Dec 16;45(Supplement_1):S125–43.

278. Fullerton B, Jeitler K, Seitz M, Horvath K, Berghold A, Siebenhofer A. Intensive glucose control versus conventional glucose control for type 1 diabetes mellitus. Cochrane Database Syst Rev. 2014 Feb 14;(2):CD009122.

279. Nolan CJ, Ruderman NB, Prentki M. Intensive insulin for type 2 diabetes: the risk of causing harm. The Lancet Diabetes & Endocrinology. 2013 Sep 1;1(1):9–10.

280. Nair AB, Jacob S. A simple practice guide for dose conversion between animals and human. J Basic Clin Pharm. 2016 Mar;7(2):27–31.

281. Reigner BG, Blesch K. Estimating the starting dose for entry into humans: principles and practice. Eur J Clin Pharmacol. 2002 Feb 1;57(12):835–45.

282. Bonadonna RC, Groop L, Kraemer N, Ferrannini E, Del Prato S, DeFronzo RA. Obesity and insulin resistance in humans: a dose-response study. Metabolism. 1990 May;39(5):452–9.

283. Knudtzon J. Alpha-melanocyte stimulating hormone increases plasma levels of glucagon and insulin in rabbits. Life Sci. 1984 Feb 6;34(6):547–54.